Royal Norwegian Council
for Scientific and Industrial Research
(NTNF)

NORSAR

(1)

NORSAR Scientific Report No. 2-89/90

Semiannual Technical Summary

1October 1989 — 31 March 1990

Kjeller, June 1990

UNCLASSIFIED
SECURITY CLASSIFICATION OF THIS PAGE

REPORT DOCUMENTATION PAGE

Form Approved OMB No. 0704-0188

1a. REPORT SECURITY CLASSIFICATION UNCLASSIFIED	1b. RESTRICTIVE MARKINGS NOT APPLICABLE
2a. SECURITY CLASSIFICATION AUTHORITY NOT APPLICABLE	3. DISTRIBUTION/AVAILABILITY OF REPORT APPROVED FOR PUBLIC RELEASE DISTRIBUTION UNLIMITED
2b. DECLASSIFICATION/DOWNGRADING SCHEDULE NOT APPLICABLE	
4. PERFORMING ORGANIZATION REPORT NUMBER(S) Scientific Rep. 2-89/90	5. MONITORING ORGANIZATION REPORT NUMBER(S) Scientific Rep. 2-89/90
6a. NAME OF PERFORMING ORGANIZATION NTNF/NORSAR 6b. OFFICE SYMBOL (If applicable)	7a. NAME OF MONITORING ORGANIZATION HQ/AFTAC/TTS
6c. ADDRESS (City, State, and ZIP Code) Post Box 51 N-2007 Kjeller, Norway	7b. ADDRESS (City, State, and ZIP Code) Patrick AFB, FL 32925-6001
8a. NAME OF FUNDING/SPONSORING ORGANIZATION Defence Advanced Research Projects Agency 8b. OFFICE SYMBOL (If applicable) NMRO	9. PROCUREMENT INSTRUMENT IDENTIFICATION NUMBER Contract No. F08606-89-C-0005
8c. ADDRESS (City, State, and ZIP Code) 1400 Wilson Blvd. Arlington, VA 22209-2308	10. SOURCE OF FUNDING NUMBERS PROGRAM ELEMENT NO.: R&D PROJECT NO.: NORSAR PHASE 3 TASK NO.: SOW TASK 5.0 WORK UNIT ACCESSION NO.: SEQUENCE No.003A2

11. TITLE (Include Security Classification)

SEMIANNUAL TECHNICAL SUMMARY, 1 OCTOBER 1989 - 31 MARCH 1990 (UNCLASSIFIED)

12. PERSONAL AUTHOR(S)
L.B. Loughran (ed.)

13a. TYPE OF REPORT	13b. TIME COVERED	14. DATE OF REPORT (Year, Month, Day)	15. PAGE COUNT
SCIENTIFIC SUMMARY	FROM 1 Oct 89 TO 31 Mar 90	June 1990	105

16. SUPPLEMENTARY NOTATION

NOT APPLICABLE

17. COSATI CODES			18. SUBJECT TERMS (Continue on reverse if necessary and identify by block number)
FIELD	GROUP	SUB-GROUP	
8	11		NORSAR, NORWEGIAN SEISMIC ARRAY

19. ABSTRACT (Continue on reverse if necessary and identify by block number)

(Please see reverse side)

20. DISTRIBUTION/AVAILABILITY OF ABSTRACT	21. ABSTRACT SECURITY CLASSIFICATION
☐ UNCLASSIFIED/UNLIMITED ☐ SAME AS RPT ☐ DTIC USERS	UNCLASSIFIED
22a. NAME OF RESPONSIBLE INDIVIDUAL MR. LEE BRIDGES	22b. TELEPHONE (Include Area Code) (407) 494-7765 22c. OFFICE SYMBOL AFTAC/TTS

DD Form 1473, JUN 86 — Previous editions are obsolete. — SECURITY CLASSIFICATION OF THIS PAGE

Abstract

This Semiannual Technical Summary describes the operation, maintenance and research activities at the Norwegian Seismic Array (NORSAR), the Norwegian Regional Seismic Array (NORESS) and the Arctic Regional Seismic Array (ARCESS) for the period 1 October 1989 – 31 March 1990. It also presents statistics from operation of the Intelligent Monitoring System (IMS). Under an agreement between NORSAR and the University of Helsinki, data from the Finnish Experimental Seismic Array (FINESA) are being recorded and processed at the NORSAR Data Center as well as in Helsinki, and results from the NORSAR processing of these data are reported.

The NORSAR Detection Processing system has been operated throughout the period with an average uptime of 91.8 as compared to 94.9 for the previous reporting period. A total of 1648 seismic events have been reported in the NORSAR monthly seismic bulletin. The performance of the continuous alarm system and the automatic bulletin transfer by telex to AFTAC has been satisfactory. Processing of requests for full NORSAR/NORESS data on magnetic tapes has progressed according to established schedules.

On-line detection processing and data recording at the NORSAR Data Processing Center (NDPC) of NORESS, ARCESS and FINESA data have been conducted throughout the period, with an average uptime of 96.9% for NORESS, 95.3% for ARCESS and 98.5% for FINESA. The Intelligent Monitoring System was installed at NORSAR in December 1989 and has been operated experimentally since 1 January 1990. Preliminary results of the IMS analysis are given.

There have been no modifications made to the NORSAR data acquisition system. The process of evaluating technical options for upgrading the array is continuing. A test of a full subarray acquisition system will be performed at the end of the next reporting period.

The routine detection processing of NORESS, ARCESS and FINESA is running satisfactorily on each of the arrays' SUN-3/280 data acquisition systems. The routine processing of FINESA data at NORSAR is similar to what is done in Helsinki.

Maintenance activities in the period comprise preventive/corrective maintenance in connection with all the NORSAR subarrays, NORESS and ARCESS. In addition, the maintenance center has been involved with modification of equipment for FINESA and preparatory work in connection with NORESS HF instrumentation. Other activities involved testing of the NORSAR communications systems.

During 14–17 February 1990 NORSAR hosted an international symposium

entitled "Regional Seismic Arrays and Nuclear Test Ban Verification".

The symposium demonstrated the considerable progress in the field of seismic monitoring during recent years. It particularly highlighted the technological advances in seismic instrumentation, data communication and computer processing, as exemplified by the development of advanced regional seismic arrays with very sophisticated automatic and interactive signal processing facilities. The presentations at the scientific symposium show that these technological advances are accompanied by considerable scientific progress, although much work remains in order to fully exploit the potential offered by regional arrays in a seismic monitoring context. The majority of the papers have been submitted for publication to the *Bulletin of the Seismological Society of America*, and will be published in a Special Issue of the *Bulletin*, scheduled to appear in the fall of 1990.

We have continued our work aimed at evaluating the stability of RMS Lg for yield estimation purposes. Data for Semipalatinsk explosions from the British station GAM in Garm, USSR, have been analyzed and compared to previously reported recordings at NORSAR, IRIS and CDSN stations. These studies confirm that for explosions at Semipalatinsk with good signal-to-noise ratio (>1.5), m_b(Lg) may be estimated at single stations with an accuracy (one standard deviation) of about 0.03 magnitude unit. It is noteworthy that this accuracy is consistently obtained for a variety of stations at very different azimuths and distances, even though the basic parameters remain exactly as originally proposed by Ringdal for NORSAR recordings (0.6–3.0 Hz bandpass filter, RMS window length of 2 minutes, centered at a time corresponding to a group velocity of 3.5 km/s). In particular, comparison of GAM and ARU data suggests that this consistency applies over a range of two full magnitude units.

A study is presented on integrated wavefield decomposition using three-component seismograms and array data. The array beam parameters are used to produce estimates of the P, SV and SH contributions as a function of time. This decomposition of the seismic wavefield by wavetype as a function of time not only has considerable benefits for the recognition of seismic phases, but also provides a domain in which the relative proportions of P, SV and SH can be compared directly, because free-surface amplification effects have been removed. This information on the current proportions of different wavetypes summarizes much of the propagation processes between source and receiver and therefore can be beneficial in attempts to discriminate between different source types.

A study on interpreting Lg azimuth anomalies observed at NORESS in terms of ray calculations is reported. Initial attempts to relate ray-calculated and observed azimuth anomalies have yielded somewhat inconsistent results,

but upon careful examination of the ray behavior it becomes evident that the nature of the Moho heterogeneity in the vicinity of NORESS is probably largely responsible. The complexity of the Moho saddle east of NORESS, its comparatively complicated geometry over a region of restricted spatial extent, results in ray diagrams which are very sensitive to source location and phase velocity. The study suggests that the Moho saddle, a feature which appears to be well defined and documented in a number of independent investigations, will play a significant role in distorting the wavefield and is probably responsible in large part for the Lg azimuth anomalies observed at NORESS from sources to the east.

A regionalized time-of-day analysis of six months of IAS data from the regional arrays NORESS and ARCESS has shown that about 97% of the more well-located events probably are of man-made origin. Based on the derived information about where and when the man-made events occur, contour maps (in magnitude) of associated capabilities for reporting natural earthquakes are provided, for different times or hourly intervals of the day. The magnitude limits vary from about 3.0 as a maximum in some mining areas and down to less than 1.0 for western and northern Norway offshore areas, where most of the man-made disturbances are still below the detection level.

The concept of threshold monitoring, introduced by Ringdal and Kværna, is a method of monitoring the seismic amplitude levels for the purpose of using this information to assess the largest size of events that might go undetected by a given network. In an effort to demonstrate the capabilities of this threshold monitoring concept, a preliminary version has been implemented into the Intelligent Monitoring System (IMS). Using recordings by the NORESS, ARCESS and FINESA arrays, the method has been applied for monitoring two selected target regions for a 24-hour interval: a mining site near the Finland-USSR border and the nuclear test site at Semipalatinsk. It is demonstrated that the implementation of the threshold monitoring method in the IMS system enables real-time operation. The displays provided by the threshold monitor appear to be very valuable in pointing out time intervals of particular interest, thus aiding the analyst in his work. The interesting intervals can be examined by different processing techniques to locate and identify the events. The examples in this study have demonstrated that the method can be applied both at regional and teleseismic distances. We note, however, that some additional research needs to be done to assess the potential bias in the upper magnitude limits when detected phases occur from events in the target region.

AFTAC Project Authorization	:	T/9141/B/PKP
ARPA Order No.	:	4138 AMD # 16
Program Code No.	:	0F10
Name of Contractor	:	Royal Norwegian Council for Scientific and Industrial Research
Effective Date of Contract	:	1 Oct 1988
Contract Expiration Date	:	30 Sep 1990
Project Manager	:	Frode Ringdal (06) 81 71 21
Title of Work	:	The Norwegian Seismic Array (NORSAR) Phase 3
Amount of Contract	:	$ 4,220,215
Contract Period Covered by Report	:	1 Oct 1989 - 31 Mar 1990

This research was supported by the Advanced Research Projects Agency of the Department of Defense and was monitored by AFTAC, Patrick AFB, FL 32925, under contract no. F08606-89-C-0005.

NORSAR Contribution No. 421

Contents

1 Summary

This Semiannual Technical Summary describes the operation, maintenance and research activities at the Norwegian Seismic Array (NORSAR), the Norwegian Regional Seismic Array (NORESS) and the Arctic Regional Seismic Array (ARCESS) for the period 1 October 1989 – 31 March 1990. It also presents statistics results from operation of the Intelligent Monitoring System (IMS). Under an agreement between NORSAR and the University of Helsinki, data from the Finnish Experimental Seismic Array (FINESA) are being recorded and processed at the NORSAR Data Center as well as in Helsinki, and results from the NORSAR processing of these data are reported.

The NORSAR Detection Processing system has been operated throughout the period with an average uptime of 91.8 as compared to 94.9 for the previous reporting period. A total of 1648 seismic events have been reported in the NORSAR monthly seismic bulletin. The performance of the continuous alarm system and the automatic bulletin transfer by telex to AFTAC has been satisfactory. Processing of requests for full NORSAR/NORESS data on magnetic tapes has progressed according to established schedules.

On-line detection processing and data recording at the NORSAR Data Center (NDPC) of NORESS, ARCESS and FINESA data have been conducted throughout the period, with an average uptime of 96.9% for NORESS, 95.3% for ARCESS and 98.5% for FINESA. The Intelligent Monitoring System was installed at NORSAR in December 1989 and has been operated experimentally since 1 January 1990. Preliminary results of the IMS analysis are given.

There have been no modifications made to the NORSAR data acquisition system. The process of evaluating technical options for upgrading the array is continuing. A test of a full subarray acquisition system will be performed at the end of the next reporting period.

The routine detection processing of NORESS, ARCESS and FINESA is running satisfactorily on each of the arrays' SUN-3/280 data acquisition systems. The routine processing of FINESA data at NORSAR is similar to what is done in Helsinki.

Maintenance activities in the period comprise preventive/corrective maintenance in connection with all the NORSAR subarrays, NORESS and ARCESS. In addition, the maintenance center has been involved with modification of equipment for FINESA and preparatory work in connection with NORESS HF instrumentation. Other activities involved testing of the NORSAR communications systems.

The research activity is summarized in Section 7. Section 7.1 presents a report from the symposium on "Regional Seismic Arrays and Nuclear Test Ban

Verification" which was held in Oslo, Norway, 14–17 February. An analysis of data from the British station GAM near Garm, USSR, for Soviet nuclear explosions is presented in Section 7.2. A study of wavefield decomposition for three-component seismograms is given in Section 7.3. Section 7.4 discusses a ray-based interpretation of Lg azimuth anomalies at NORESS. A study of earthquake reporting capabilities in Fennoscandia inferred from IAS data is given in Section 7.5, while Section 7.6 discusses application of the threshold monitoring method introduced by Ringdal and Kværna.

2 NORSAR Operation

2.1 Detection Processor (DP) Operation

There have been 103 breaks in the otherwise continuous operation of the NORSAR online system within the current 6-month reporting interval. The uptime percentage for the period is 91.8 as compared to 94.9 for the previous period.

Fig. 2.1.1 and the accompanying Table 2.1.1 both show the daily DP downtime for the days between 1 October 1989 and 31 March 1990. The monthly recording times and percentages are given in Table 2.1.2.

The breaks can be grouped as follows:

a)	Hardware failure	39
b)	Stops related to program work or error	2
c)	Hardware maintenance stops	18
d)	Power jumps and breaks	0
e)	TOD error correction	31
f)	Communication lines	14

The total downtime for the period was 338 hours and 33 minutes. The mean-time-between-failures (MTBF) was 1.6 days, as compared to 1.9 for the previous period.

J. Torstveit

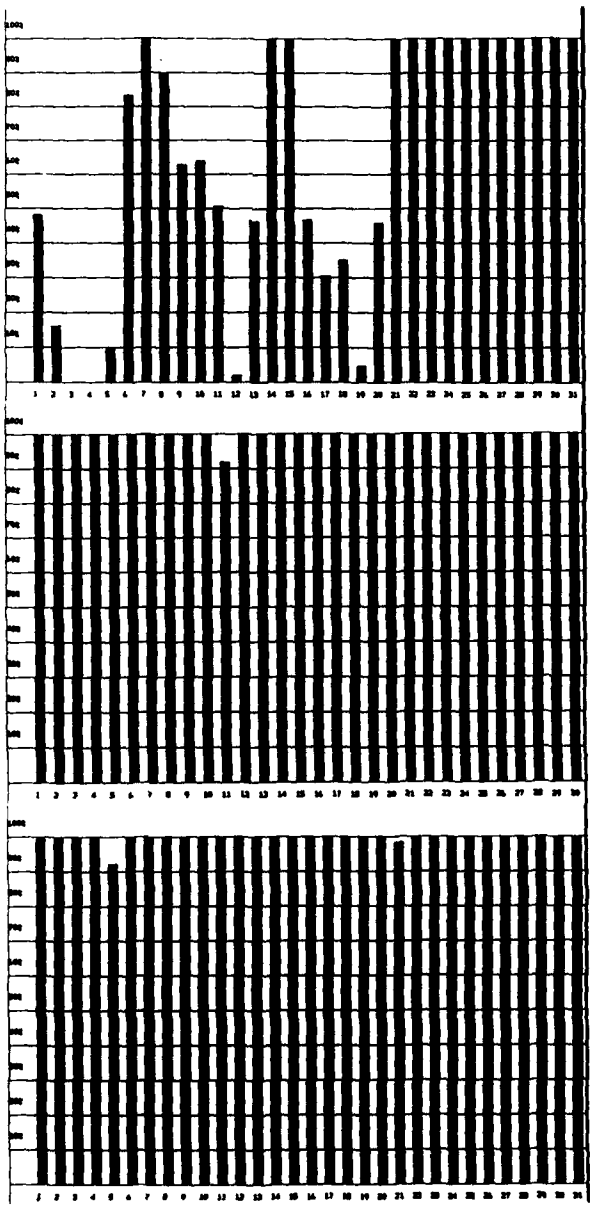

Fig. 2.1.1 Detection Processor downtime for October (top), November (middle) and December (bottom) 1989.

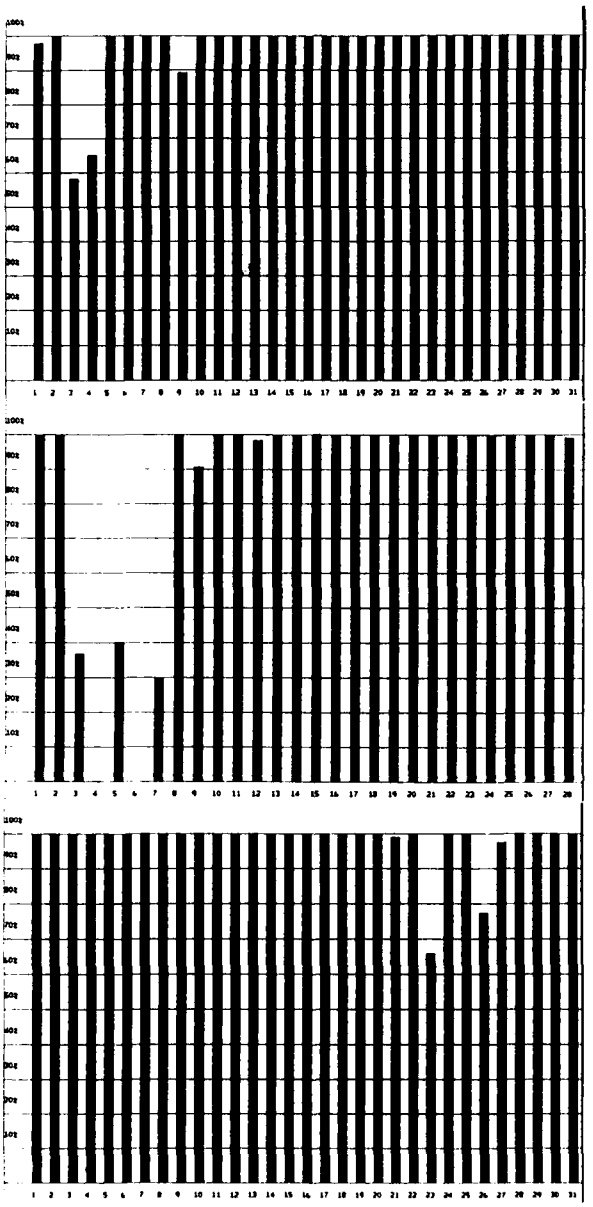

Fig. 2.1.1 Detection Processor downtime for January (top), February (middle) and March (bottom) 1990.

LIST OF BREAKS IN DP PROCESSING THE LAST HALF-YEAR

DAY	START		STOP		COMMENTS.....
274	5	43	9	10	MODCOMP FAILURE
274	11	5	12	9	MODCOMP FAILURE
274	14	20	17	50	MODCOMP FAILURE
274	19	17	19	58	MODCOMP FAILURE
274	20	21	24	0	MODCOMP FAILURE
275	0	0	7	10	MODCOMP FAILURE
275	8	9	10	46	MODCOMP FAILURE
275	10	53	11	21	MODCOMP FAILURE
275	13	50	14	47	MODCOMP FAILURE
275	15	5	24	0	MODCOMP FAILURE
276	0	0	24	0	MODCOMP FAILURE
277	0	0	24	0	MODCOMP FAILURE
278	0	0	13	5	MODCOMP FAILURE
278	14	23	22	45	MODCOMP FAILURE
278	23	45	24	0	MODCOMP FAILURE
279	0	0	0	40	MODCOMP FAILURE
279	8	48	11	55	MODCOMP FAILURE
279	12	34	12	45	MODCOMP FAILURE
281	6	14	7	41	MODCOMP FAILURE
281	8	20	8	40	MODCOMP FAILURE
281	20	31	21	11	MODCOMP FAILURE
282	3	28	6	47	MODCOMP FAILURE
282	12	54	13	52	CE MAINTENANCE
282	14	41	14	58	MODCOMP FAILURE
282	16	9	17	7	MODCOMP FAILURE
282	19	58	20	29	MODCOMP FAILURE
282	21	8	24	0	MODCOMP FAILURE
283	0	0	6	16	MODCOMP FAILURE
283	9	14	9	32	CE MAINTENANCE
283	11	2	11	21	MODCOMP FAILURE
283	13	27	13	40	MODCOMP FAILURE
283	14	7	14	23	CE MAINTENANCE
283	16	15	16	44	CE MAINTENANCE
283	17	0	17	20	MODCOMP FAILURE
283	20	58	21	26	MODCOMP FAILURE
284	0	16	6	16	MODCOMP FAILURE
284	8	30	8	37	MODCOMP FAILURE
284	9	46	10	16	CE MAINTENANCE
284	10	34	13	35	MODCOMP FAILURE
284	13	15	14	18	MODCOMP FAILURE
284	22	16	24	0	MODCOMP FAILURE
285	0	0	6	21	MODCOMP FAILURE
285	6	50	24	0	CE MAINTENANCE
286	0	0	12	52	CE MAINTENANCE
289	0	22	10	59	MODCOMP FAILURE
289	16	12	16	38	MODCOMP FAILURE
289	22	16	24	0	MODCOMP FAILURE
290	0	0	7	17	MODCOMP FAILURE
290	10	21	11	31	MODCOMP FAILURE
290	12	20	13	42	CE MAINTENANCE
290	15	0	15	43	CE MAINTENANCE
290	15	0	15	43	CE MAINTENANCE
291	0	0	6	25	MODCOMP FAILURE
291	7	25	7	32	MODCOMP FAILURE
291	8	34	9	19	MODCOMP FAILURE
291	10	12	12	0	MODCOMP FAILURE
291	12	46	13	4	MODCOMP FAILURE
291	17	48	24	0	MODCOMP FAILURE
292	0	0	6	20	MODCOMP FAILURE
292	7	27	24	0	CE MAINTENANCE
293	0	0	12	58	CE MAINTENANCE

DAY	START		STOP		COMMENTS.....
299	7	1	7	3	TOD RETARED 22MS
304	7	1	7	3	TOD RETARED 20MS
313	7	1	7	3	TOD RETARED 20MS
315	13	16	14	16	CE MAINTENANCE MODC
315	14	45	15	42	CE MAINTENANCE MODC
319	7	0	7	2	TOD RETARED 23MS
325	8	0	8	2	TOD RETARED 13MS
326	7	0	7	2	TOD RETARED 12MS
326	10	28	10	30	CE MAINTENANCE 02B
327	11	51	11	53	LINE FAILURE
332	7	0	7	2	TOD RETARED 14MS
332	14	44	14	46	LINE FAILURE
333	11	47	11	49	LINE FAILURE
335	7	53	7	55	LINE FAILURE
335	8	54	8	57	LINE FAILURE
339	7	40	7	42	TOD RETARED 22MS
339	7	42	9	31	HARDWARE FAILURE
347	7	41	7	43	TOD RETARED 22MS
347	14	33	14	35	LINE FAILURE
347	12	2	12	4	LINE FAILURE
355	7	4	7	6	TOD RETARED 23MS
355	12	47	13	7	CE MAINTENANCE
362	10	3	10	5	LINE FAILURE
1	13	35	14	0	SYSTEM WORK (NEW YEAR)
1	14	28	14	33	SYSTEM WORK (NEW YEAR)
2	7	25	7	27	TOD RETARED 90MS
3	6	30	16	30	LINE FAILURE
4	10	18	18	39	LINE FAILURE
5	7	1	7	3	TOD RETARED 13MS
9	13	10	15	45	LINE FAILURE
10	14	15	14	19	CE MAINTENANCE
18	8	51	8	53	LINE FAILURE
23	7	1	7	3	TOD RETARED 22MS
29	7	2	7	4	TOD RETARED 23MS
34	8	50	24	0	LINE FAILURE
35	0	0	24	0	LINE FAILURE
36	0	0	10	0	LINE FAILURE
36	19	40	24	0	TOD FAILURE
37	0	0	24	0	TOD FAILURE
38	0	0	16	48	TOD FAILURE
39	12	30	12	34	TOD RETARED 10MS
40	7	35	9	49	MAINTENANCE DISK
43	6	32	6	42	TOD FAILURE
43	9	31	9	43	MAINTENANCE TOD
44	7	10	7	12	TOD RETARED 12MS
46	10	6	10	8	LINE FAILURE
47	7	1	7	3	TOD RETARED 12MS
58	7	2	7	4	TOD RETARED 23MS
59	8	18	8	25	TOD FAILURE
59	14	45	14	48	TOD FAILURE
66	7	1	7	3	TOD RETARED 23MS
72	7	2	7	5	TOD RETARED 46MS
80	7	0	7	3	TOD RETARED 23MS
80	10	40	10	46	TOD FAILURE
80	11	3	11	6	TOD FAILURE
82	7	0	15	10	MODCOMP FAILURE
85	6	11	11	36	MODCOMP FAILURE
86	9	44	10	8	TOD FAILURE
86	10	55	11	5	TOD FAILURE
88	7	47	7	49	TOD RETARED 3MS

Table 2.1.1 Daily DP downtime in the period 1 October 1989 - 31 March 1990.

Month	DP Uptime Hours	DP Uptime %	No. of DP Breaks	No. of Days with Breaks	DP MTBF* (days)
OCT 89	493.53	66.3	50	19	0.3
NOV 89	717.75	99.7	11	8	2.5
DEC 89	741.57	99.7	10	6	3.4
JAN 90	722.20	97.1	11	10	2.5
FEB 90	574.73	85.5	12	13	1.8
MAR 90	729.63	98.1	10	7	2.8
		91.1	104	63	1.6

*Mean-time-between-failures = total uptime/no. of up intervals.

Table 2.1.2 Online system performance, 1 October 1989 – 31 March 1990.

2.2 Array communications

General

Table 2.2.1 reflects the performance of the communications system throughout the reporting period.

TM-data continued the fault finding procedure on the Modcomp computer in October, also the CPU microcodes were analyzed.

A new Modcomp rack equipped with new boards (except for 2 memory boards and a number of CPU PROM chips) was installed. Also this initiative failed. New PROMs were programmed and installed (23 Oct). Since that date the system has been reliable.

We have in the period also had a large number of breaks in the data stream between the subarrays and NDPC. Not only single subarrays have been affected, but also groups of/or all subarrays have been affected simultaneously.

02C was affected in October (week 40), probably caused by NTA trouble. 06C outages occurred four times in October (weeks 40, 42, 43 and 44) due to stuck CTV equipment.

In November a new break in the data stream from 02B occurred (21 Nov). The SLEM Digital Unit (DCU) was replaced. Also 02C was affected (28 Nov) in connection with scheduled NTA cable work. The final operation, splicing of the communications cable, went wrong and resulted in a break towards the CTV for 3 days.

7 December was the start of a bad period as far as communications was concerned. NTA/Lillestrøm, in cooperation with NTA/Hamar changes to another carrier system, in order to increase the capacity between Lillestrøm and Hamar. After this change the NORSAR communications system became less reliable. All systems were involved, separately and simultaneously, but the systems also operated well over several days.

The communications system instability continued in January. Due to the special character of the error pattern, it was difficult to locate the source for the trouble. Individual end-to-end subarray communications tests during bad periods did not reveal errors. A coax carrier system common to all systems functioned well until 7 January, when a damaged coax carrier cable was located in Nittedal, affecting all subarrays. Apart from spikes on all systems 12 Jan and on 02C and 03C 10 Jan, the system's performance for the second part of January improved.

In spite of 2 damaged coax carrier cables located/repaired, we still had irregularities in February. The two last outages were caused by the Time

of Day Generator, supplying 2400 Hz to the NORSAR systems. Two cards were replaced in the TOD, and the situation changed radically with respect to overall system performance, although individual systems were affected by other problems (02C, 03C and 06C).

In March the Modcomp's disk system failed two times: 23 March when the Spindle Drive Motor failed, and 24 March when a disk "crash" occurred, causing a total outage of 13 hrs and 48 min.

Also the TOD, which has as its main task "time tagging" NORSAR data and clocking out the NORSAR commands (ICWs), has been less reliable than before. The oscillator is drifting and the 2400 Hz has been "jittery". We have made an appointment with a firm capable of handling delicate instruments such as the TOD.

The performance of the communications systems, including communications lines, carrier systems, modems, etc., was very satisfactory throughout March.

Detailed summary

October (weeks 40-44, -41), 2.10-5.11.89

Fault finding continued with the Modcomp by TM-data. CPU microcodes were analyzed, and irregularities were observed. A new Modcomp rack equipped with new boards (except for 2 memory boards and a certain number of PROM chips). Even then the system failed, and new PROMs were programmed and installed 23 October. The Modcomp system has been reliable after that change.

02C was down week 40 (5.35%), probably due to NTA trouble. 06C outages occurred week 40 (7.14%), week 42 (41.0%) and week 44 (12.5%) due to "stuck" CTV equipment.

November (weeks 45-48), 6.11-3.12.89

The Modcomp was reliable after repair and restart 23 October. 02B was affected 21 November due to a failing Digital Unit (DCU) in the CTV. 23 November the unit was replaced. Scheduled NTA cable work north of Lillehammer affected 02C 28 November. The operation involved cable cut and splicing afterwards. The latter operation failed, causing a 3-day outage towards the CTV.

December (weeks 49-52), 4.12-31.12.89

7 December NTA/Lillestrøm and NTA/Hamar in cooperation changed a certain carrier group in order to increase the capacity between Lillestrøm and Hamar. After this change the NORSAR communications system became less

reliable, and this situation continued through 31 December 1989. All the subarray communications systems were affected, both simultaneously and separately. The systems also operated satisfactorily over several days.

January (weeks 1-4), 1-28.1.90

The instability which started in December continued in January. It was difficult to locate/isolate the source of the trouble due to the special characteristics of the error pattern. Individual end-to-end tests during bad periods did not reveal irregularities/errors (01A, 02C, 03C and 02B between Lillestrøm and Hamar). However, symptoms could indicate a faulty coax carrier cable/system common to all NORSAR systems.

4 January a damaged coax cable was located in Lillestrøm in connection with construction work. After the repair we believed the problems were solved because everything functioned properly until 7 January. This time a damaged coax carrier cable was located in the Nittedal community, affecting all the subarrays. 2.5 hours later the channels carried by the coax had been transferred to a spare coax cable.

Apart from spikes on all channels 12 January, and 02C/03C 10 January, the system performance for the second part of January improved.

February (weeks 5-8), 29.1-25.2.90

Communications system instability continued in February, and the different sources of trouble these weeks are as follows:

- Damaged coax carrier cable Lillestrøm
- Coax carrier cable between Kongsvinger and Skarnes (reason not stated)
- Coax carrier cable Nittedal (gradual deterioration)
- Time of Day Generator (TOD)

The two last outages 5-6 February and 11-12 February were caused by the TOD; two cards were replaced.

After the repair the situation improved radically as far as overall system performance is concerned, although individual systems such as 02C, 03C and 06C have been affected by other problems.

March (weeks 9-13), 26.2-1.4.90

This period the Modcomp disk system failed two times. 23 March the Spindle Drive Motor stopped, causing an outage of 8 hrs 13 mins. The next

failure occurred 24 March, and this time we had a disk "crash", causing an outage of 5 hrs and 35 mins.

Also the Time Code Generator (TOD) has been less reliable. The oscillator is drifting, and the 2400 Hz clocking the NORSAR commands (IWUs) toward the CTV has been "jittery". The latter may have been caused by the same "noise spikes" which probably also causd the TOD seconds to "jump". We believe the noise spikes observed in the TOD were introduced by the recorder used during time checks. For these checks we have now hooked up a digital clock locked to a West German station.

Otherwise the performance of the communications lines, carrier systems, modems etc., have been most satisfactory throughout the month.

O.A. Hansen

Sub-arrays	Oct 89 (4) 2-8.10 & 16.10-5.11	Nov 89 (4) 6.11-3.12	Dec 89 (4) 4-31.12	Jan 90 (4) 1-28.1	Feb 90 (4) 29.1-25.2	Mar 90 (5) 26.2-1.4	Average 1/2 year
01A	*0.0040	0.0030	*0.500	*1.058	6)*0.937	0.013	0.419
01B	0.0004	0.0004	*0.430	*1.008	")*0.936	0.010	0.397
02B	0.0020	0.0340	*0.440	*1.059	")*0.926	0.008	0.411
02C	1)*0.0009	3)*0.0006	*0.447	*0.580	")*1.805	0.009	0.478
03C	0.0030	0.0020	*0.468	*0.815	")*2.696	0.008	0.615
04C	0.0030	0.0006	*0.462	*0.974	")*0.900	0.008	0.391
06C	2)* N/A	0.0008	4)*0.307	5)*0.160	")*1.187	0.012	7)*0.333
AVER	0.0020	0.0060	0.440	0.807	1.341	0.009	0.442
LESS	06C						

*See Section 2.2 regarding figures preceded by an asterisk.
Figures representing error rate (in per cent) preceded by a number 1), 2), etc., are related to legend below.

1) Average 3 weeks 42–44
2) Stuck CTV equipment
3) Average 3 weeks 45–47, scheduled cable work
4) Average 3 weeks
5) Average 2 weeks
6) Average 2 weeks
7) Average 5 months

Table 2.2.1 Communications performance. The numbers represent error rates in per cent based on total transmitted frames/week (1 October 1989 – 31 March 1990).

2.3 Event Detection operation

In Table 2.3.1 some monthly statistics of the Detection and Event Processor operation are given. The table lists the total number of detections (DPX) triggered by the on-line detector, the total number of detections processed by the automatic event processor (EPX) and the total number of events accepted after analyst review (teleseismic phases, core phases and total).

	Total	Total	Accepted events			
	DPX	EPX	P-phases	Core phases	Sum	Daily
Oct 89	8525	999	183	47	230	7.4
Nov 89	12575	1574	278	53	331	11.0
Dec 89	18948	2610	260	48	308	9.9
Jan 90	14624	1622	196	64	260	8.4
Feb 90	10050	1040	199	35	234	8.4
Mar 90	11750	1209	231	54	285	9.2
			1347	301	1648	9.1

Table 2.3.1. Detection and Event Processor statistics, 1 October 1989 – 31 March 1990.

B. Paulsen

3 Operation of regional arrays

3.1 Recording of NORESS data at NDPC, Kjeller

Table 3.1.1 lists the main outage times and reasons, and as can be seen the main reason for the outage is hardware failure at the HUB and line failure.

The average recording time was 96.9% as compared to 92.1% for the previous period.

Date	Time	Cause
2 Oct	1756-1844	Transmission line failure
7 Oct	0459-0906	Transmission line failure
17 Oct	2306-	Transmission line failure
18 Oct	-1253	Transmission line failure
25 Oct	0336-0408	Transmission line failure
25 Oct	0440-0628	Transmission line failure
2 Nov	2346-2358	Transmission line failure
12 Nov	2248-	Hardware failure HUB
13 Nov	-	Hardware failure HUB
14 Nov	-1149	Hardware failure HUB
22 Dec	1447-	Hardware failure HUB
23 Dec	-0806	Hardware failure HUB
24 Dec	0201-0603	Hardware failure HUB
28 Dec	0658-0808	Transmission line failure
3 Jan	1206-1227	Transmission line failure
4 Jan	1018-1843	Transmission line failure
5 Jan	1625-1904	Transmission line failure
5 Jan	2143-	Transmission line failure
6 Jan	-1019	Transmission line failure
11 Jan	2033-2108	Transmission line failure
12 Jan	0944-1119	Transmission line failure
16 Jan	0612-0617	Transmission line failure
18 Jan	0943-0954	Hardware failure NDPC
25 Jan	0758-0927	Transmission line test
31 Jan	1205-1212	Hardware failure NDPC
17 Feb	0114-0117	Transmission line failure
18 Feb	0909-0912	Transmission line failure
7 Mar	1300-	Transmission line test
8 Mar	-1335	Transmission line test

13 Mar	1045-1108	Hardware failure HUB
13 Mar	1606-1802	Hardware failure HUB
13 Mar	1956-2106	Hardware failure HUB
26 Mar	0712 0734	Hardware failure HUB
26 Mar	1750 1834	Hardware failure HUB
31 Mar	0640-0734	Power break HUB
31 Mar	2237-2334	Power break HUB

Table 3.1.1. Interruptions in NORESS recordings at NDPC, October 1989 - March 1990.

Monthly uptimes for the NORESS on-line data recording task, taking into account all factors (field installations, transmissions line, data center operation) affecting this task were as follows:

October	:	97.1%
November	:	94.8%
December	:	97.7%
January	:	96.2%
February	:	99.9%
March	:	95.9%

Fig. 3.1.1 shows the uptime for the data recording task, or equivalently, the availability of NORESS data in our tape archive, on a day-by-day basis, for the reporting period.

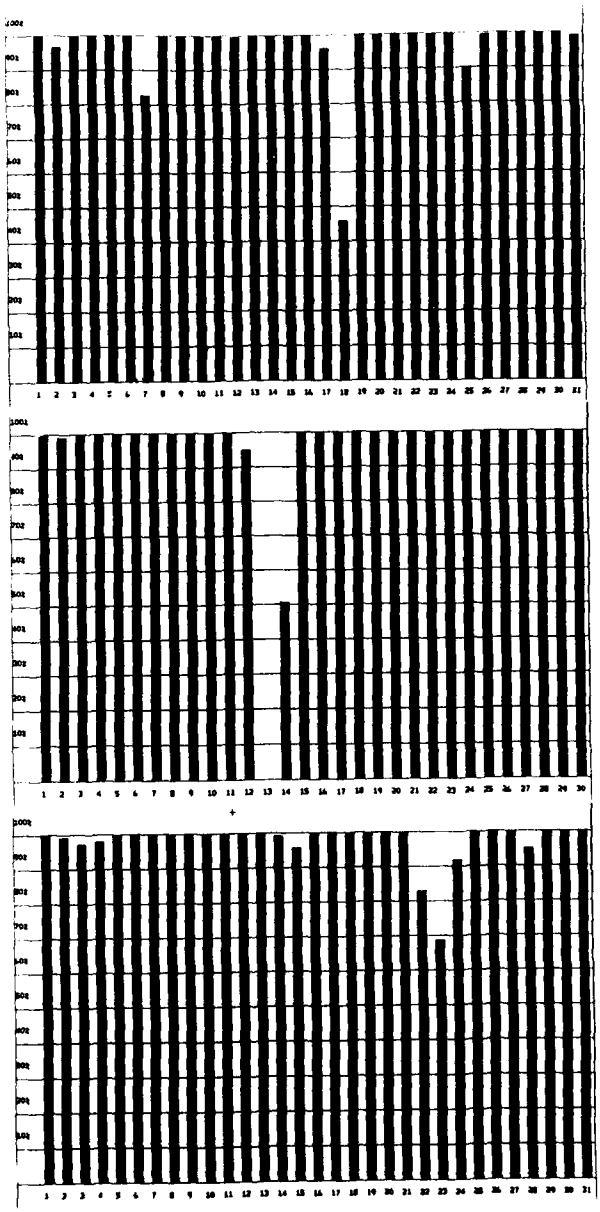

Fig. 3.1.1. NORESS data recording uptime for October (top), November (middle) and December (bottom) 1989.

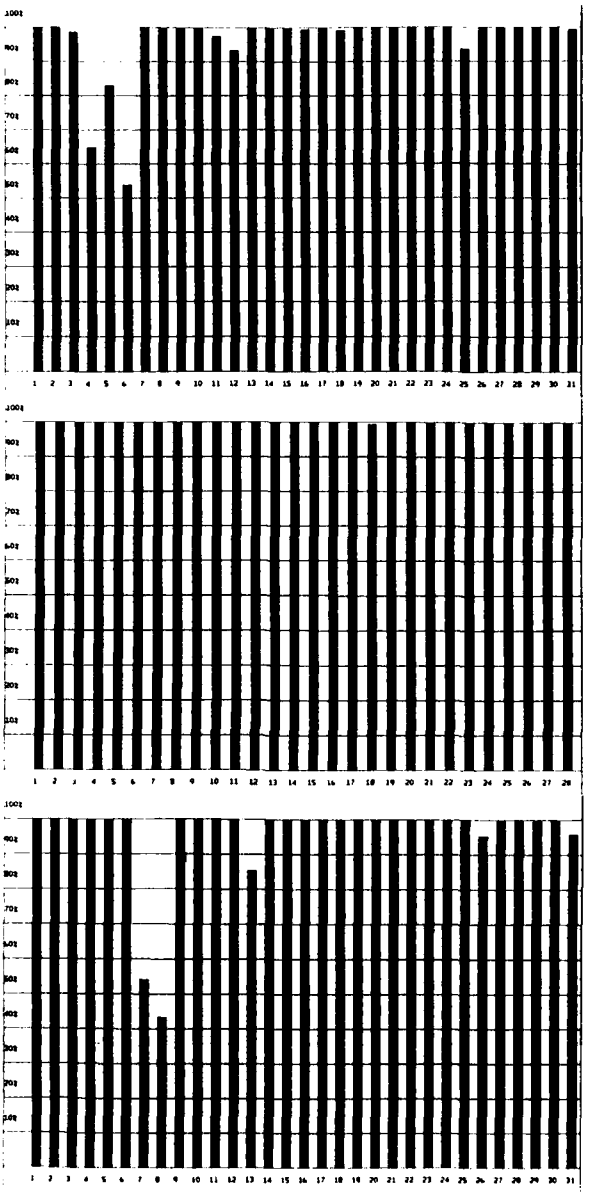

Fig. 3.1.1. NORESS data recording uptime for January (top), February (middle) and March (bottom) 1990.

3.2 Recording of ARCESS data at NDPC, Kjeller

The main reasons causing most of the ARCESS outage in the period are: Hardware failure at NDPC or HUB, transmission failure and power failure at HUB.

The long outage in March was caused by clock problems at HUB.

The average recording time was 95.3% as compared to 92.2% for the previous period.

Date	Time	Cause
10 Oct	0242-0658	Hardware failure at NDPC
12 Oct	0813-0828	Hardware maintenance at NDPC
13 Oct	0954-1002	Transmission line failure
3 Nov	1145-1158	Transmission line failure
20 Nov	0504-0549	Software failure at NDPC
28 Nov	1110-1124	Transmission line failure
9 Dec	0738-0825	Hardware failure at NDPC
24 Dec	0431-	Powerbreak HUB
25 Dec	-	Powerbreak HUB
26 Dec	-1027	Powerbreak HUB
29 Dec	0134-1707	Hardware failure at NDPC
29 Dec	2136-	Hardware failure at NDPC
30 Dec	-0610	Hardware failure at NDPC
4 Jan	2004-2218	Hardware failure at NDPC
9 Jan	0650-0946	Transmission line failure
12 Jan	2044-2057	Hardware failure at NDPC
14 Jan	0938-1006	Transmission line failure
23 Jan	1421-1443	Transmission line failure
28 Jan	1700-1800	Transmission line failure
9 Feb	0349-0407	Hardware failure at NDPC

15 Mar	2306-	Hardware failure at HUB
16 Mar	-	Hardware failure at HUB
17 Mar	-	Hardware failure at HUB
18 Mar	-	Hardware failure at HUB
19 Mar	-2200	Hardware failure at HUB
21 Mar	1431-1906	Powerbreak HUB
25 Mar	0800-1319	Powerbreak HUB
27 Mar	1630-1707	Hardware failure at NDPC

Table 3.2.1 The main interruptions in ARCESS recordings at NDPC, October 1989 – March 1990.

Monthly uptimes for the ARCESS on-line data recording task, taking into account all factors (field installations, transmissions line, data center operation) affecting this task were as follows:

October	:	99.3%
November	:	99.8%
December	:	89.4%
January	:	99.0%
February	:	99.9%
March	:	84.5%

Fig. 3.2.1 shows the uptime for the data recording task, or equivalently, the availability of ARCESS data in our tape archive, on a day-by-day basis, for the reporting period.

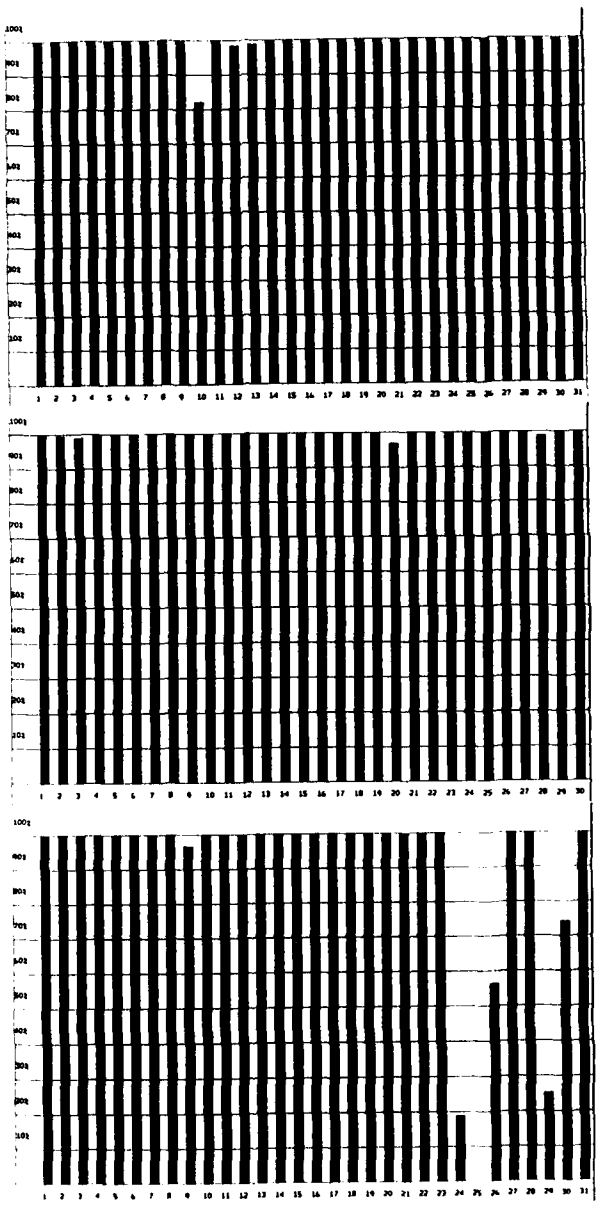

Fig. 3.2.1. ARCESS data recording uptime for October (top), November (middle) and December (bottom) 1989.

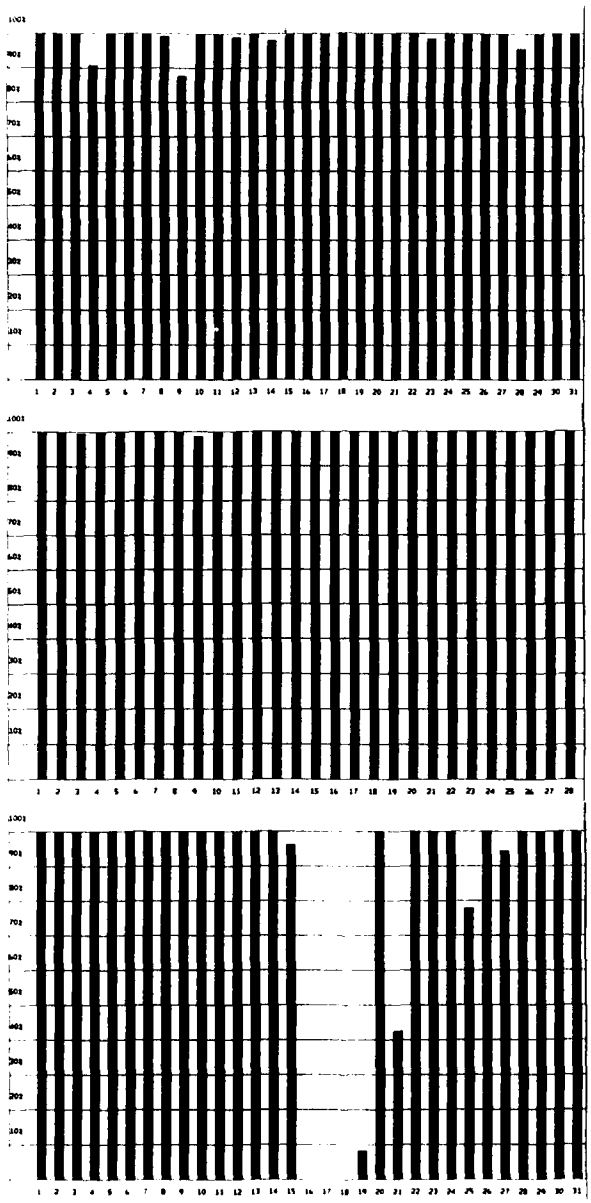

Fig. 3.2.1. ARCESS data recording uptime for January (top), February (middle) and March (bottom) 1990.

3.3 Recording of FINESA data at NDPC, Kjeller

Regular recording at NDPC, Kjeller, of data from the FINESA regional array in Finland started on 1 January 1990. A description of the FINESA system was given in our Semiannual Technical Summary for the period 1 April – 30 September 1989. The average recording time was 98.5%.

Date	Time	Cause
2 Jan	0622-0722	Hardware failure at NDPC
2 Jan	0753-0823	Transmission line failure
11 Jan	2033-2108	Transmission line failure
15 Jan	0759-	Transmission line failure
16 Jan	-1251	Transmission line failure
1 Feb	0002-0033	Transmission line failure

Table 3.3.1 The main interruptions in FINESA recordings at NDPC, January – March 1990.

Monthly uptimes for the FINESA on-line data recording task, taking into account all factors (field installations, transmissions line, data center operation) affecting this task were as follows:

January	:	95.8%
February	:	99.9%
March	:	99.9%

Fig. 3.3.1 shows the uptime for the data recording task, or equivalently, the availability of FINESA data in our tape archive, on a day-by-day basis, for the reporting period.

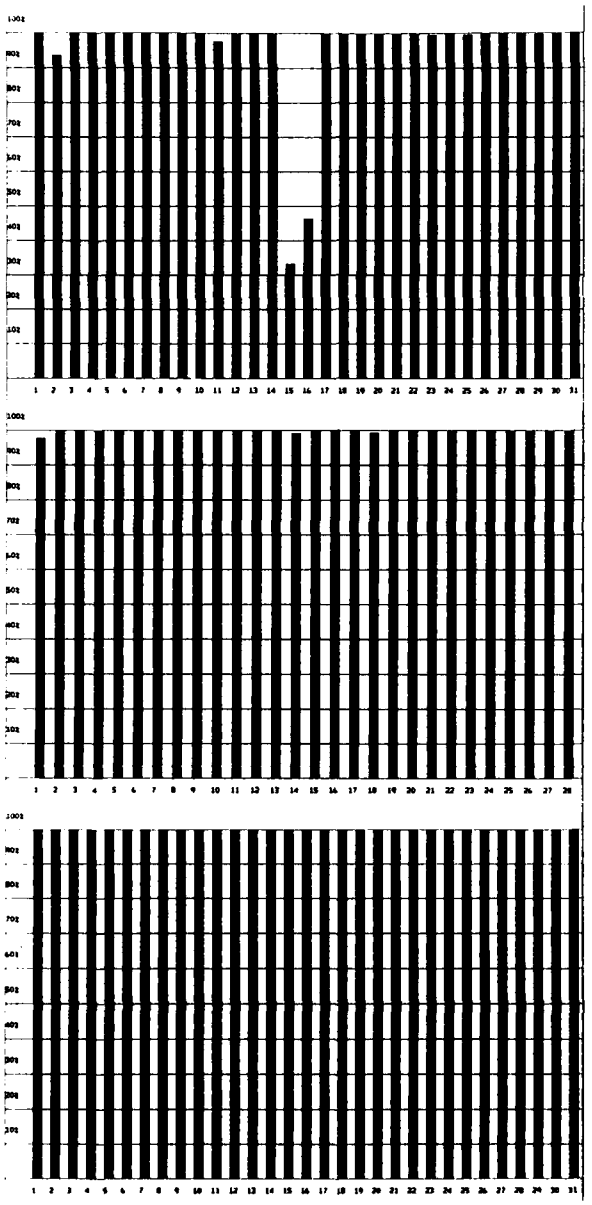

Fig. 3.3.1. FINESA data recording uptime for January (top), February (middle) and March (bottom) 1990.

3.4 Event detection operation

NORESS detections

The number of detections (phases) reported during day 274, 1989 through day 090, 1990 was 44113, giving an average of 244 detections per processed day (181 days processed).

Table 3.4.1 shows daily and hourly distribution of detections for NORESS.

Events automatically located by NORESS

During days 274, 1989 through 090, 1990, 2076 local and regional events were located by NORESS, based on automatic association of P- and S-type arrivals. This gives an average of 11.5 events per processed day (181 days processed). 67% of these events are within 300 km, and 88% of these events are within 1000 km.

ARCESS detections

The number of detections (phases) reported during day 274, 1989 through day 090, 1990 was 66702, giving an average of 375 detections per processed day (178 days processed).

Table 3.4.2 shows daily and hourly distribution of detections for ARCESS.

Events automatically located by ARCESS

During days 274, 1989, through 090, 1990, 3144 local and regional events were located by ARCESS, based on automatic association of P- and S-type arrivals. This gives an average of 16.9 events per processed day (178 days processed). 54% of these events are within 300 km, and 87% of these events are within 1000 km.

FINESA detections

The number of detections (phases) reported during day 327, 1989 through day 090, 1990 was 29240, giving an average of 290 detections per processed day (101 days processed).

Table 3.4.3 shows daily and hourly distribution of detections for FINESA.

Events automatically located by FINESA

During days 327, 1989, through 090, 1990, 2000 local and regional events were located by FINESA, based on automatic association of P- and S-type arrivals. This gives an average of 20.4 events per processed day (98 days processed). 74% of these events are within 300 km, and 89% of these events are within 1000 km.

J. Fyen

NRS .FKX Hourly distribution of detections

Day	00	01	02	03	04	05	06	07	08	09	10	11	12	13	14	15	16	17	18	19	20	21	22	23	Sum	Date	
274	9	1	1	8	1	7	10	11	5	7	12	4	9	9	4	7	13	6	11	4	2	1	1	0	143	Oct 01	Sunday
275	10	10	19	7	7	1	2	2	4	0	7	7	9	14	5	16	5	7	0	6	1	14	5	1	159	Oct 02	Monday
276	8	1	6	15	4	2	8	4	4	11	3	9	20	13	9	16	12	10	10	8	0	23	8	6	210	Oct 03	Tuesday
277	15	4	5	18	4	1	1	8	2	12	22	18	19	18	7	10	10	7	8	12	3	12	3	1	220	Oct 04	Wednesday
278	10	6	6	13	22	3	5	6	15	12	18	25	21	24	25	20	9	15	9	8	1	8	6	9	296	Oct 05	Thursday
279	8	13	3	12	4	7	7	5	3	13	14	11	16	6	11	12	8	11	16	8	4	8	0	3	203	Oct 06	Friday
280	9	7	2	8	2	0	0	0	0	1	1	1	2	1	3	15	10	19	17	17	10	1	0	1	127	Oct 07	Saturday
281	6	7	2	14	8	2	0	2	7	3	15	6	1	6	8	7	18	0	12	4	0	5	4	7	144	Oct 08	Sunday
282	10	15	0	4	0	4	4	9	5	4	5	10	15	11	9	20	26	16	14	11	4	16	2	4	218	Oct 09	Monday
283	7	4	5	14	8	6	5	7	0	10	12	10	11	16	10	9	8	17	8	5	5	6	0	1	184	Oct 10	Tuesday
284	12	8	5	14	7	1	13	12	4	4	15	12	12	8	38	14	8	8	8	11	1	11	2	0	228	Oct 11	Wednesday
285	10	11	5	13	5	1	5	2	1	8	8	8	22	15	22	8	10	11	7	8	1	16	6	6	209	Oct 12	Thursday
286	6	1	7	9	4	1	3	5	6	10	11	11	13	12	12	4	6	10	8	11	11	16	4	5	186	Oct 13	Friday
287	5	1	6	12	0	4	10	2	3	5	3	7	4	2	7	4	9	3	6	8	4	2	1	8	116	Oct 14	Saturday
288	3	3	2	1	5	2	1	4	9	3	1	4	2	4	5	1	14	1	12	2	1	6	0	10	96	Oct 15	Sunday
289	17	13	6	7	1	4	2	1	5	11	14	7	17	27	19	13	6	7	10	4	2	11	2	6	212	Oct 16	Monday
290	7	4	6	10	0	1	6	3	7	24	13	13	13	22	31	15	19	21	14	1	18	17	1	2	269	Oct 17	Tuesday
291	0	0	0	0	0	0	0	0	0	0	0	0	0	23	31	29	16	15	16	16	0	16	4	8	174	Oct 18	Wednesday
292	13	13	8	16	1	6	2	9	2	17	12	8	23	9	3	7	5	9	6	6	10	13	1	5	204	Oct 19	Thursday
293	7	5	9	11	1	4	8	14	4	2	8	20	18	15	5	15	7	14	7	15	2	19	0	1	211	Oct 20	Friday
294	8	2	8	18	3	6	12	2	8	13	1	8	5	3	3	3	0	2	1	1	5	5	1	3	121	Oct 21	Saturday
295	4	2	0	2	3	4	6	1	4	0	8	1	4	1	6	16	15	1	14	3	7	2	1	4	109	Oct 22	Sunday
296	10	3	3	7	2	1	5	6	6	4	12	15	4	16	17	7	3	8	5	15	5	12	0	3	169	Oct 23	Monday
297	9	6	2	16	2	3	2	14	5	1	6	6	16	32	11	20	8	9	13	9	2	9	1	4	206	Oct 24	Tuesday
298	16	5	4	2	2	5	3	3	11	14	10	12	19	12	27	11	6	10	5	13	15	9	0	9	223	Oct 25	Wednesday
299	5	4	6	8	2	0	2	4	8	24	5	8	13	16	4	14	10	17	5	12	2	11	9	3	192	Oct 26	Thursday
300	10	9	8	11	2	5	3	2	7	13	3	14	21	14	6	8	4	6	6	26	6	17	0	1	202	Oct 27	Friday
301	5	9	2	12	4	1	9	9	20	13	6	8	9	17	8	15	3	2	2	2	0	4	0	1	161	Oct 28	Saturday
302	4	4	6	11	1	18	2	9	4	7	4	12	6	3	2	3	11	4	9	15	4	3	1	14	157	Oct 29	Sunday
303	8	1	15	11	1	4	3	7	6	2	13	1	21	21	22	8	7	7	14	13	1	23	0	0	209	Oct 30	Monday
304	17	9	3	19	3	4	2	9	5	5	4	9	14	29	19	6	2	12	21	22	3	13	3	11	244	Oct 31	Tuesday
305	17	9	6	11	5	2	8	23	1	1	16	12	21	12	20	13	5	5	23	10	7	16	8	11	262	Nov 01	Wednesday
306	6	9	6	13	0	3	2	10	4	10	13	6	27	19	25	16	11	15	5	21	6	37	7	1	272	Nov 02	Thursday
307	7	9	4	15	1	3	3	6	11	24	16	16	5	16	7	4	4	9	14	14	17	3	2	1	211	Nov 03	Friday
308	11	1	3	16	4	0	10	20	4	3	13	15	13	11	4	6	4	3	24	10	14	9	11	5	214	Nov 04	Saturday
309	3	4	6	4	8	5	3	4	3	4	4	15	6	4	2	9	16	2	4	1	3	4	5	3	122	Nov 05	Sunday
310	11	9	1	21	5	3	14	10	10	5	23	1	10	26	13	9	0	7	10	9	2	16	2	4	221	Nov 06	Monday
311	8	8	3	17	2	4	8	13	9	10	11	9	13	19	8	11	2	12	11	10	8	10	0	5	211	Nov 07	Tuesday
312	6	10	1	8	0	5	10	23	4	6	9	17	13	11	19	20	11	11	10	11	20	7	5	14	251	Nov 08	Wednesday
313	7	12	2	15	5	8	4	9	0	4	5	4	8	17	23	14	3	5	12	8	2	11	3	4	185	Nov 09	Thursday
314	6	6	2	12	4	1	16	14	6	5	15	10	22	10	7	9	3	14	5	10	4	3	0	9	193	Nov 10	Friday
315	20	8	1	14	5	3	5	2	3	3	5	4	2	8	4	14	13	14	16	26	27	18	37	24	276	Nov 11	Saturday
316	33	23	38	37	35	39	37	34	41	21	26	35	27	33	27	33	25	23	38	29	28	30	18	0	710	Nov 12	Sunday
317	0	0	0	0	0	0	0	0	0	0	0	0	0	0	0	0	0	0	0	0	0	0	0	0	0	Nov 13	Monday
318	0	0	0	0	0	0	0	0	0	0	0	3	10	11	16	9	1	13	11	15	4	7	0	11	111	Nov 14	Tuesday
319	7	8	9	12	13	2	2	11	0	8	7	5	8	8	11	6	7	7	18	10	15	3	6	17	200	Nov 15	Wednesday
320	4	16	2	7	3	6	9	12	9	18	9	3	20	29	19	11	3	12	19	13	15	5	5	10	259	Nov 16	Thursday
321	6	8	3	9	12	9	7	7	6	4	5	10	14	21	9	10	12	9	12	12	3	18	3	8	217	Nov 17	Friday
322	7	1	2	23	5	8	5	7	4	11	3	16	11	5	6	5	8	10	4	3	8	9	5	5	171	Nov 18	Saturday
323	8	3	4	16	16	8	5	8	19	4	7	3	4	9	12	17	24	4	7	0	1	4	5	9	197	Nov 19	Sunday
324	9	7	1	18	8	2	5	8	4	5	6	13	10	17	16	14	0	10	11	10	1	16	1	6	198	Nov 20	Monday
325	7	3	13	16	5	2	1	10	6	10	10	24	15	23	31	9	4	9	10	13	9	21	2	2	255	Nov 21	Tuesday
326	10	3	2	4	1	4	3	7	3	2	12	15	19	12	8	7	2	8	11	8	9	8	2	13	173	Nov 22	Wednesday
327	2	10	5	8	3	0	8	8	6	12	12	9	25	10	24	17	10	7	14	14	6	9	7	4	230	Nov 23	Thursday
328	12	18	8	16	0	2	1	7	1	4	8	7	19	16	8	19	13	15	15	18	12	28	27	21	295	Nov 24	Friday
329	23	12	6	9	3	7	10	8	15	4	7	15	16	2	14	21	13	3	8	3	5	13	25	48	290	Nov 25	Saturday

Table 3.4.1 (Page 1 of 4)

NRS .FKX Hourly distribution of detections

Day	00	01	02	03	04	05	06	07	08	09	10	11	12	13	14	15	16	17	18	19	20	21	22	23	Sum	Date	
330	41	5	6	3	9	8	17	4	5	7	8	14	8	16	14	10	4	5	5	4	0	40	24	30	287	Nov 26	Sunday
331	6	13	65	64	40	20	7	2	8	5	7	1	16	11	13	3	12	16	16	7	7	5	6	20	370	Nov 27	Monday
332	29	9	34	40	33	21	19	15	10	8	4	8	21	53	36	35	31	41	37	10	16	6	0	5	521	Nov 28	Tuesday
333	9	9	8	10	3	0	10	7	6	13	16	7	6	20	15	31	33	32	33	28	21	38	32	41	428	Nov 29	Wednesday
334	50	32	21	28	44	55	41	28	23	10	21	9	19	19	27	36	60	56	65	65	51	51	45	40	896	Nov 30	Thursday
335	32	45	24	49	32	37	15	19	17	20	4	10	16	22	18	12	29	46	38	34	67	58	81	72	797	Dec 01	Friday
336	105	94	92	34	16	50	45	38	17	1	7	11	18	19	30	39	48	47	59	60	44	53	64	48	1039	Dec 02	Saturday
337	57	28	3	10	6	13	4	11	3	16	8	19	6	14	16	7	40	40	43	59	68	67	41	38	617	Dec 03	Sunday
338	37	8	0	6	1	0	16	12	8	7	13	15	10	18	17	16	9	15	32	7	11	39	67	50	414	Dec 04	Monday
339	61	42	38	41	37	3	2	7	5	0	9	17	27	31	17	10	3	5	3	11	15	21	48	44	497	Dec 05	Tuesday
340	40	11	5	16	5	11	5	5	10	6	16	12	18	13	10	2	2	4	4	6	3	3	3	10	220	Dec 06	Wednesday
341	7	7	8	13	16	9	15	10	9	5	4	19	18	30	24	13	6	4	10	6	2	14	6	10	265	Dec 07	Thursday
342	8	7	5	5	5	6	14	13	2	10	9	26	25	12	13	7	5	22	17	22	34	32	22	23	344	Dec 08	Friday
343	20	21	27	34	40	52	59	57	18	25	18	14	24	13	7	1	5	1	1	3	16	6	5	7	474	Dec 09	Saturday
344	5	13	8	9	14	10	5	12	4	10	2	6	3	11	22	35	15	8	23	19	13	14	12	10	283	Dec 10	Sunday
345	22	6	12	18	47	17	19	12	14	12	11	18	25	36	14	10	18	3	3	12	3	19	0	7	358	Dec 11	Monday
346	14	14	19	12	16	0	5	5	15	14	6	10	15	16	12	23	7	2	6	7	6	22	13	8	267	Dec 12	Tuesday
347	3	2	4	1	5	11	13	8	21	13	7	16	29	29	17	9	14	6	9	5	4	10	0	4	240	Dec 13	Wednesday
348	4	6	5	11	3	4	4	6	12	3	4	18	13	13	21	2	10	10	14	29	13	29	30	36	300	Dec 14	Thursday
349	42	39	24	41	32	23	15	4	9	17	25	34	54	11	13	9	9	14	18	26	11	18	7	5	500	Dec 15	Friday
350	2	7	9	3	6	8	2	8	8	14	16	9	10	4	6	14	10	9	10	5	9	7	6	8	190	Dec 16	Saturday
351	4	2	1	6	12	12	4	22	12	9	14	5	16	9	13	4	9	7	5	4	4	9	2	7	192	Dec 17	Sunday
352	12	2	4	4	11	3	1	16	5	2	10	6	7	23	13	6	3	12	4	3	3	11	3	2	166	Dec 18	Monday
353	2	8	2	5	1	2	13	12	13	20	15	14	16	19	16	8	3	9	9	3	3	18	13	18	242	Dec 19	Tuesday
354	31	34	25	34	32	26	22	17	16	10	13	26	29	28	19	22	13	21	20	15	22	20	11	15	521	Dec 20	Wednesday
355	12	5	6	12	13	10	3	11	17	12	13	20	21	20	20	10	7	12	4	3	10	19	0	5	265	Dec 21	Thursday
356	3	5	1	9	0	4	10	6	5	10	12	5	10	25	5	8	2	10	1	15	14	7	3	3	173	Dec 22	Friday
357	2	3	3	7	9	2	1	3	2	0	3	8	4	3	3	3	7	5	2	0	4	2	5	5	86	Dec 23	Saturday
358	8	7	4	5	4	1	4	1	7	7	1	1	7	7	5	6	7	3	5	10	8	3	4	1	116	Dec 24	Sunday
359	6	2	7	3	2	3	0	9	8	3	3	1	7	12	9	6	2	3	0	4	10	2	1	2	105	Dec 25	Monday F:rste
360	1	5	4	2	1	1	0	5	4	5	8	11	17	9	2	6	5	2	9	14	10	8	22	24	175	Dec 26	Tuesday Andre
361	19	31	26	37	16	16	21	22	5	5	6	11	17	15	8	4	1	22	13	2	9	8	8	9	331	Dec 27	Wednesday
362	23	26	30	20	15	17	20	0	19	18	22	20	19	28	24	18	15	20	16	11	33	26	37	42	519	Dec 28	Thursday
363	48	46	43	62	53	44	41	36	33	26	21	20	17	10	15	37	65	63	44	23	4	4	5	7	767	Dec 29	Friday
364	13	4	1	18	6	11	5	8	5	27	5	12	8	6	6	1	11	8	3	6	6	3	5	5	183	Dec 30	Saturday
365	8	9	7	15	27	53	43	58	78	57	49	68	96	100	107	103	96	104	123	118	91	25	4	0	1439	Dec 31	Sunday
1	6	8	9	12	7	11	5	6	4	12	7	6	11	8	10	5	16	10	16	15	5	8	9	9	215	Jan 01	Monday F:rste
2	15	30	23	38	42	65	52	62	75	52	40	24	34	37	78	121	124	102	90	92	56	37	10	13	1312	Jan 02	Tuesday
3	4	9	2	15	7	4	3	8	7	3	3	10	4	20	11	7	3	7	7	8	5	12	4	8	171	Jan 03	Wednesday
4	5	2	0	7	8	8	5	5	5	9	1	0	0	0	0	0	0	0	0	3	5	5	0	8	76	Jan 04	Thursday
5	5	6	4	5	5	2	7	4	7	8	13	8	14	6	14	0	44	34	0	11	7	10	0	0	214	Jan 05	Friday
6	0	0	0	0	0	0	0	0	0	0	2	14	8	6	2	1	7	2	12	11	9	9	8	8	99	Jan 06	Saturday
7	13	10	4	5	4	4	9	6	1	3	4	2	0	8	5	2	8	3	5	3	3	0	0	5	107	Jan 07	Sunday
8	7	4	6	6	4	2	6	4	7	2	9	12	17	17	7	5	7	2	5	8	17	17	17	16	204	Jan 08	Monday
9	15	9	2	5	4	8	0	4	3	16	9	5	11	21	6	13	1	5	5	14	0	4	2	0	162	Jan 09	Tuesday
10	1	0	0	13	3	8	10	1	5	5	9	8	14	15	20	1	8	7	1	3	5	6	2	2	147	Jan 10	Wednesday
11	1	0	2	4	8	7	2	1	1	8	6	10	5	20	19	5	3	6	6	8	3	8	0	3	136	Jan 11	Thursday
12	2	2	3	13	5	2	9	8	9	8	0	7	12	9	10	11	2	8	6	6	7	1	2	3	145	Jan 12	Friday
13	3	3	3	22	0	7	7	2	3	2	8	4	5	4	6	4	6	6	7	6	12	11	5	27	163	Jan 13	Saturday
14	48	29	17	14	12	4	8	20	15	10	9	0	11	4	10	11	9	6	7	6	3	14	4	5	276	Jan 14	Sunday
15	4	4	1	9	7	10	11	9	4	5	3	10	19	8	6	5	1	3	4	4	3	4	0	4	138	Jan 15	Monday
16	7	3	1	4	2	0	2	12	17	3	5	9	12	26	22	14	10	9	4	16	24	18	16	18	254	Jan 16	Tuesday
17	4	7	4	8	4	0	10	3	3	3	10	7	13	17	26	5	1	3	1	1	1	2	2	2	137	Jan 17	Wednesday
18	1	0	1	1	0	0	25	16	14	6	26	24	21	26	20	6	1	3	5	6	11	10	11	11	245	Jan 18	Thursday
19	21	36	31	55	33	26	28	25	11	21	21	15	13	13	6	12	7	6	0	5	7	7	4	8	411	Jan 19	Friday
20	8	13	8	6	2	1	4	3	2	1	7	4	6	2	4	1	2	2	2	2	4	3	1	0	88	Jan 20	Saturday

Table 3.4.1 (Page 2 of 4)

NRS .FKX Hourly distribution of detections

Day	00	01	02	03	04	05	06	07	08	09	10	11	12	13	14	15	16	17	18	19	20	21	22	23	Sum	Date
21	1	4	3	2	3	1	8	7	8	0	2	2	3	3	2	9	12	12	11	6	9	12	9	5	134	Jan 21 Sunday
22	6	7	5	11	12	5	5	8	10	8	7	11	15	14	16	7	7	8	3	5	2	7	2	2	183	Jan 22 Monday
23	1	4	4	10	0	1	6	10	8	9	23	33	21	22	13	9	2	6	2	5	4	4	0	3	200	Jan 23 Tuesday
24	1	6	2	3	9	5	9	11	17	19	26	17	25	31	41	2	10	6	4	8	2	9	0	4	267	Jan 24 Wednesday
25	5	17	18	25	12	7	17	17	0	9	20	23	18	25	34	12	7	4	8	6	9	7	0	3	303	Jan 25 Thursday
26	4	3	6	11	4	3	8	22	14	7	18	19	9	1	7	3	7	2	2	1	1	10	12	10	184	Jan 26 Friday
27	6	4	3	7	5	3	6	6	2	13	6	9	7	10	4	6	7	7	4	3	2	2	3	4	129	Jan 27 Saturday
28	9	13	7	5	9	7	3	4	2	5	7	11	2	3	7	5	8	4	8	1	6	3	2	6	137	Jan 28 Sunday
29	3	1	11	7	1	1	5	1	7	4	4	14	26	18	8	8	2	2	12	3	6	6	4	2	156	Jan 29 Monday
30	4	2	2	16	0	3	6	15	12	11	35	19	16	20	29	6	4	2	4	11	2	6	5	3	233	Jan 30 Tuesday
31	2	4	3	4	3	0	5	18	8	12	21	19	16	30	25	13	3	2	6	4	11	7	2	3	221	Jan 31 Wednesday
32	7	3	9	10	5	1	5	17	9	18	20	35	16	14	17	2	2	8	10	4	3	9	5	2	231	Feb 01 Thursday
33	5	4	3	2	2	3	6	25	19	25	26	26	9	15	10	7	1	5	3	7	2	6	0	5	216	Feb 02 Friday
34	2	2	2	9	5	3	3	3	2	11	4	4	2	4	4	6	5	3	4	3	3	2	9	4	99	Feb 03 Saturday
35	6	16	14	7	1	4	9	4	18	6	5	7	10	1	6	9	9	3	15	1	5	2	1	5	164	Feb 04 Sunday
36	7	3	1	5	0	13	6	2	6	22	5	3	8	9	14	8	3	6	5	5	3	13	5	5	157	Feb 05 Monday
37	4	3	2	11	1	2	5	8	2	10	1	2	8	6	15	9	2	8	5	5	3	8	4	5	129	Feb 06 Tuesday
38	7	4	6	6	4	3	4	2	11	7	8	6	13	22	9	12	5	1	1	6	6	3	4	4	154	Feb 07 Wednesday
39	2	4	0	8	4	3	0	12	10	10	7	10	7	15	20	6	10	19	8	13	7	6	1	0	182	Feb 08 Thursday
40	7	19	15	14	13	0	8	6	10	64	37	74	13	9	13	7	11	12	10	6	6	14	7	6	381	Feb 09 Friday
41	11	2	2	10	6	5	4	8	3	2	1	6	6	3	2	5	1	2	2	4	4	1	6	6	102	Feb 10 Saturday
42	2	7	2	3	5	7	4	12	3	2	4	1	5	11	8	7	11	10	3	4	2	2	8	4	127	Feb 11 Sunday
43	3	5	4	8	1	1	2	5	5	5	4	10	30	55	9	10	6	5	9	19	17	9	4	7	233	Feb 12 Monday
44	5	4	1	6	4	4	3	2	4	14	5	9	14	17	20	11	7	5	7	8	4	13	1	1	169	Feb 13 Tuesday
45	16	6	6	6	0	1	4	5	8	5	9	15	10	12	8	14	8	8	7	8	7	3	1	2	169	Feb 14 Wednesday
46	7	6	8	15	3	8	1	5	5	35	1	4	9	12	20	6	2	4	5	20	6	14	8	13	217	Feb 15 Thursday
47	12	5	4	12	4	5	7	4	8	11	3	18	23	16	6	4	6	8	9	15	17	8	4	6	215	Feb 16 Friday
48	9	8	12	18	5	3	10	5	5	33	76	72	89	115	120	121	134	120	105	72	6	4	1	3	1146	Feb 17 Saturday
49	4	3	8	9	4	8	6	14	4	6	11	3	8	8	6	4	21	7	17	2	6	0	5	4	168	Feb 18 Sunday
50	8	4	2	7	2	9	13	19	4	43	15	20	15	19	18	8	4	7	9	1	0	7	7	5	246	Feb 19 Monday
51	3	2	2	4	5	1	8	13	5	8	10	13	5	7	16	7	5	6	5	6	11	1	4	5	152	Feb 20 Tuesday
52	7	3	4	11	2	3	3	6	4	8	8	11	17	8	12	10	6	7	12	4	4	10	3	3	166	Feb 21 Wednesday
53	3	6	1	13	1	0	5	7	6	59	151	105	31	25	4	13	5	10	7	9	3	6	10	7	487	Feb 22 Thursday
54	6	6	7	7	2	3	4	4	5	82	100	8	20	8	7	18	11	14	14	13	5	8	1	10	363	Feb 23 Friday
55	10	3	1	4	6	3	5	5	4	5	1	11	5	11	7	10	9	5	3	18	7	4	2	1	140	Feb 24 Saturday
56	3	7	3	10	3	7	7	5	6	4	12	8	5	3	5	3	14	2	10	1	3	4	1	9	135	Feb 25 Sunday
57	4	7	4	11	2	1	0	1	8	10	5	10	4	8	11	6	4	8	17	9	13	8	3	5	159	Feb 26 Monday
58	6	3	5	10	4	2	1	1	4	8	13	4	6	18	12	16	2	6	6	4	3	9	4	1	148	Feb 27 Tuesday
59	5	4	3	11	2	2	1	3	0	7	12	6	15	10	15	6	4	8	13	4	9	8	7	8	163	Feb 28 Wednesday
60	10	8	11	12	6	3	9	8	6	7	9	12	8	14	32	6	3	6	9	6	1	15	5	7	213	Mar 01 Thursday
61	5	11	2	8	2	4	3	5	13	4	9	9	14	11	10	8	9	1	9	3	4	5	4	5	158	Mar 02 Friday
62	2	5	5	15	26	16	15	6	14	6	8	10	15	18	14	7	17	7	6	3	6	2	3	11	237	Mar 03 Saturday
63	10	2	4	0	4	3	5	2	0	3	1	7	9	8	5	12	5	7	2	6	13	8	1	6	123	Mar 04 Sunday
64	1	5	4	5	1	1	3	1	8	17	3	3	10	4	1	3	9	6	7	2	10	12	3	8	127	Mar 05 Monday
65	8	2	4	7	1	2	0	11	3	4	7	13	10	10	8	13	7	8	21	11	8	24	3	12	197	Mar 06 Tuesday
66	14	7	16	16	15	8	9	8	8	13	11	9	1	0	0	0	0	0	0	0	0	0	0	0	135	Mar 07 Wednesday
67	0	0	0	0	0	0	0	0	0	0	0	0	0	2	19	3	5	4	11	8	3	7	2	3	67	Mar 08 Thursday
68	13	0	2	8	4	5	9	2	1	8	10	14	12	9	5	1	2	9	4	8	1	14	3	0	144	Mar 09 Friday
69	14	2	5	10	9	2	7	9	1	3	8	6	10	3	1	2	6	6	1	4	5	2	4	1	121	Mar 10 Saturday
70	2	5	9	7	4	4	12	1	7	4	7	6	11	10	10	6	10	9	3	1	2	3	8	1	142	Mar 11 Sunday
71	4	2	5	5	1	2	3	1	4	9	7	6	7	11	17	15	3	8	4	7	4	2	3	4	134	Mar 12 Monday
72	12	3	2	9	3	4	14	8	5	15	13	15	22	14	21	9	0	0	4	12	0	12	5	10	212	Mar 13 Tuesday
73	11	14	12	12	5	3	18	25	10	17	18	11	17	24	29	47	6	13	3	11	2	14	4	2	328	Mar 14 Wednesday
74	6	3	11	9	1	11	9	11	13	4	6	8	20	10	14	15	1	6	8	4	9	1	1	1	189	Mar 15 Thursday
75	5	3	2	7	7	4	3	6	2	6	8	9	22	16	3	6	7	3	6	8	2	13	3	1	152	Mar 16 Friday
76	10	2	1	8	1	9	0	0	0	0	0	0	0	3	4	3	6	7	6	2	1	2	2	0	67	Mar 17 Saturday

Table 3.4.1 (Page 3 of 4)

NRS .FKX Hourly distribution of detections

Day	00	01	02	03	04	05	06	07	08	09	10	11	12	13	14	15	16	17	18	19	20	21	22	23	Sum	Date
77	2	1	5	2	0	0	0	0	0	2	4	6	6	7	6	9	5	2	7	1	0	0	0	2	67	Mar 18 Sunday
78	12	4	7	14	2	5	7	4	4	7	7	6	9	10	7	5	2	11	10	7	11	2	1	6	160	Mar 19 Monday
79	3	8	3	2	6	2	4	7	5	11	11	12	4	16	7	4	2	10	9	10	15	1	6	4	162	Mar 20 Tuesday
80	5	3	3	15	3	2	3	10	3	6	6	4	9	9	21	10	5	15	14	11	3	10	8	6	184	Mar 21 Wednesday
81	8	4	7	8	2	0	1	5	8	6	4	6	8	12	8	7	2	4	11	9	3	20	3	4	150	Mar 22 Thursday
82	5	8	6	9	3	3	2	3	8	6	6	6	8	10	4	2	5	14	11	11	3	22	1	1	157	Mar 23 Friday
83	12	1	1	11	2	5	2	2	3	1	4	2	2	0	8	5	3	3	5	4	4	3	2	2	87	Mar 24 Saturday
84	4	9	3	5	0	5	3	4	2	2	5	1	5	10	14	16	10	16	6	2	2	3	3	7	137	Mar 25 Sunday
85	1	4	12	5	6	3	3	0	0	0	0	0	0	0	0	0	0	0	0	0	0	0	0	0	34	Mar 26 Monday
86	0	6	21	11	7	4	8	6	11	5	15	17	0	0	0	0	0	0	0	0	0	0	0	0	111	Mar 27 Tuesday
87	6	11	9	10	5	10	2	8	13	10	8	17	26	10	0	11	11	15	29	3	22	1	12	13	262	Mar 28 Wednesday
88	2	15	19	2	12	4	7	6	9	3	6	16	14	5	7	3	24	8	23	5	16	0	2	11	219	Mar 29 Thursday
89	11	6	24	3	4	4	3	3	9	6	10	8	13	12	3	0	6	8	15	1	13	2	6	2	172	Mar 30 Friday
90	5	8	16	5	15	8	1	0	0	0	0	0	0	0	0	0	1	1	6	5	5	12	0	0	88	Mar 31 Saturday
NRS	00	01	02	03	04	05	06	07	08	09	10	11	12	13	14	15	16	17	18	19	20	21	22	23		
Sum	1536	1870	2161	1416	1243	1332	1625	1417	1837	1421	2169	2044	2666	2472	2104	2509	1992	1907	1951	2128	2012	1570	1494	1237	44113	Total sum
181	10	8	8	12	7	7	8	9	8	10	11	12	14	15	14	12	11	11	12	11	9	11	7	8	244	Total average
126	10	9	8	13	7	6	8	9	8	11	13	13	15	16	15	11	9	11	11	11	8	12	7	8	248	Average workdays
55	11	8	7	10	7	9	8	9	8	8	8	10	11	11	11	12	14	11	14	11	10	9	7	8	233	Average weekends

Table 3.4.1 Daily and hourly distribution of NORESS detections. For each day is shown number of detections within each hour of the day and number of detections for that day. The end statistics give total number of detections distributed for each hour and the total sum of detections during the period. The averages show number of processed days, hourly distribution and average per processed day. (Page 4 of 4)

ARC .FKX Hourly distribution of detections

Day	00	01	02	03	04	05	06	07	08	09	10	11	12	13	14	15	16	17	18	19	20	21	22	23	Sum	Date		
330	15	9	15	3	13	4	14	0	11	9	6	2	3	11	8	20	10	9	7	10	10	13	4	7	6	12	15	984	Nov 26	Sunday	
331	4	8	10	5	7	8	15	9	8	17	10	18	26	10	12	9	6	23	8	12	13	10	12	16	276	Nov 27	Monday	
332	4	7	8	1	7	10	12	5	14	7	14	10	40	52	13	25	5	10	2	12	16	6	10	12	302	Nov 28	Tuesday	
333	5	9	5	5	1	3	18	5	3	26	15	17	17	20	11	15	9	6	13	10	13	5	10	16	257	Nov 29	Wednesday	
334	4	0	4	5	7	11	9	20	3	12	7	14	32	17	10	9	8	9	3	6	15	6	8	15	234	Nov 30	Thursday	
335	2	5	6	4	2	11	4	10	16	18	15	23	37	18	13	17	16	19	9	10	9	6	12	9	291	Dec 01	Friday	
336	4	4	4	5	3	8	4	3	4	7	2	18	4	3	7	5	6	4	7	8	12	2	8	12	144	Dec 02	Saturday	
337	5	4	2	3	2	5	7	7	9	26	15	34	19	10	17	9	2	4	10	17	13	21	19	19	279	Dec 03	Sunday	
338	29	39	25	25	19	7	6	12	9	8	11	27	30	36	19	14	13	4	7	0	2	3	3	11	359	Dec 04	Monday	
339	0	5	7	5	6	6	4	7	5	11	9	12	11	10	9	21	19	11	12	24	31	39	45	46	355	Dec 05	Tuesday	
340	54	62	61	76	83	66	47	54	59	55	64	61	63	46	18	19	9	4	6	11	10	4	12	8	952	Dec 06	Wednesday	
341	5	5	8	4	1	13	8	10	12	4	8	9	25	24	5	9	8	12	8	5	6	4	9	15	217	Dec 07	Thursday	
342	9	9	13	6	5	6	7	4	9	11	22	28	35	31	22	12	12	16	17	10	23	9	14	22	352	Dec 08	Friday	
343	18	8	8	8	11	10	18	15	5	4	15	24	27	13	8	11	17	11	10	14	14	8	3	15	295	Dec 09	Saturday	
344	5	8	8	10	8	5	2	15	6	7	1	9	12	11	6	16	21	13	10	21	11	32	24	30	291	Dec 10	Sunday	
345	26	31	27	44	36	33	42	57	50	57	42	36	26	27	32	24	35	17	20	12	16	10	21	26	747	Dec 11	Monday	
346	22	24	30	33	35	37	33	43	53	63	66	63	72	57	76	72	56	67	49	46	46	52	55	77	1227	Dec 12	Tuesday	
347	55	66	51	28	41	29	24	32	33	22	22	18	41	51	44	38	39	40	35	29	22	34	50	55	899	Dec 13	Wednesday	
348	53	59	53	45	40	11	14	10	13	12	21	27	34	25	26	35	36	36	45	42	41	50	29	25	782	Dec 14	Thursday	
349	18	13	21	34	45	44	45	51	49	50	45	55	75	58	30	23	19	11	26	56	36	19	20	19	862	Dec 15	Friday	
350	13	19	11	11	15	3	17	21	10	10	36	23	23	10	20	14	16	9	10	8	8	11	21	19	358	Dec 16	Saturday	
351	8	8	6	9	12	15	18	16	8	8	17	15	11	6	12	10	9	16	16	22	19	18	14	27	320	Dec 17	Sunday	
352	32	35	34	35	14	16	9	8	13	5	10	16	37	19	17	11	15	10	12	5	25	7	7	18	410	Dec 18	Monday	
353	7	14	6	5	2	4	9	17	14	20	27	16	16	17	8	17	7	9	18	11	13	11	7	19	294	Dec 19	Tuesday	
354	32	19	12	25	27	13	15	18	15	19	19	21	38	13	25	16	8	17	9	11	8	3	12	13	408	Dec 20	Wednesday	
355	11	4	4	5	4	4	3	12	6	13	9	21	23	14	12	8	11	20	16	15	10	14	10	18	267	Dec 21	Thursday	
356	8	4	15	8	6	6	4	12	7	13	24	27	29	19	10	5	10	10	10	13	11	11	22	20	304	Dec 22	Friday	
357	9	13	3	1	0	0	0	0	0	0	0	0	0	0	0	0	0	0	0	15	19	16	24	38	138	Dec 23	Saturday	
358	27	23	18	19	11	0	0	0	0	0	0	0	0	0	0	0	0	0	0	0	0	0	0	0	98	Dec 24	Sunday	
359	0	0	0	0	0	0	0	0	0	0	0	0	0	0	0	0	0	0	0	0	0	0	0	0	0	Dec 25	Monday	F:rste
360	0	0	0	0	0	0	0	0	0	0	6	17	11	10	6	11	10	7	12	10	6	5	2	5	118	Dec 26	Tuesday	Andre
361	2	4	3	4	4	3	8	13	3	11	11	8	19	10	12	14	9	9	10	8	15	8	15	21	224	Dec 27	Wednesday	
362	4	11	6	12	11	13	23	22	16	22	25	23	15	15	17	12	7	6	6	10	6	9	10	17	318	Dec 28	Thursday	
363	8	1	0	0	0	0	0	0	0	0	0	0	0	0	0	0	0	7	6	3	6	5	0	0	36	Dec 29	Friday	
364	0	0	0	0	0	0	7	10	10	12	9	13	18	10	4	5	13	8	5	7	8	8	5	19	171	Dec 30	Saturday	
365	7	12	9	5	11	2	2	2	10	3	1	8	4	7	6	5	3	6	6	6	6	4	6	8	139	Dec 31	Sunday	
1	6	3	6	2	2	2	5	5	9	6	7	9	5	8	9	18	12	8	9	9	12	8	8	8	176	Jan 01	Monday	F:rste
2	6	12	8	8	5	4	7	8	6	8	9	7	14	17	10	13	15	18	10	16	35	28	19	33	316	Jan 02	Tuesday	
3	21	20	13	9	14	11	9	12	10	17	14	20	19	13	6	9	7	17	4	10	9	3	22	15	304	Jan 03	Wednesday	
4	4	10	13	6	9	14	11	8	7	7	22	9	28	13	7	8	6	15	15	4	0	0	9	20	245	Jan 04	Thursday	
5	5	5	4	4	5	5	6	18	16	9	6	17	29	17	10	14	15	4	16	6	9	7	11	11	249	Jan 05	Friday	
6	5	9	2	11	3	0	0	2	9	6	8	25	10	12	8	11	11	10	17	11	14	8	6	7	205	Jan 06	Saturday	
7	6	7	9	2	2	7	15	10	2	7	15	20	3	5	5	4	12	12	3	16	8	8	7	15	200	Jan 07	Sunday	
8	11	3	16	5	9	8	12	15	15	5	14	16	17	17	8	13	9	12	6	8	26	4	8	24	281	Jan 08	Monday	
9	8	3	10	10	11	10	6	0	0	0	0	17	25	19	13	23	12	7	13	15	3	7	8	20	240	Jan 09	Tuesday	
10	3	1	4	9	5	3	16	12	4	34	18	19	29	18	3	4	12	17	5	6	6	5	18	17	268	Jan 10	Wednesday	
11	3	7	7	4	4	6	11	9	11	19	11	19	14	19	7	3	16	4	10	7	18	11	11	15	246	Jan 11	Thursday	
12	10	4	8	12	8	6	21	12	7	12	16	29	24	25	9	16	10	6	7	8	5	7	7	16	285	Jan 12	Friday	
13	4	12	8	12	4	9	7	8	6	7	13	25	11	18	5	8	3	10	10	17	11	13	6	18	245	Jan 13	Saturday	
14	9	7	3	15	16	12	4	4	3	4	7	7	4	5	5	5	3	12	10	9	10	19	9	11	193	Jan 14	Sunday	
15	9	2	4	5	9	13	14	3	9	12	21	13	27	9	10	14	14	10	5	6	8	5	9	21	252	Jan 15	Monday	
16	5	7	5	4	5	13	6	15	16	20	13	20	23	24	9	16	7	6	17	10	20	11	13	18	303	Jan 16	Tuesday	
17	13	10	12	13	7	11	18	20	20	16	16	19	33	20	19	9	8	11	4	11	11	6	21	25	353	Jan 17	Wednesday	
18	9	7	9	9	6	16	11	7	4	21	10	31	40	17	13	12	9	1	21	12	19	7	14	31	336	Jan 18	Thursday	
19	10	21	14	7	12	5	6	13	12	25	29	15	41	15	16	11	13	12	12	10	13	12	15	18	357	Jan 19	Friday	
20	15	21	11	12	8	4	16	8	11	18	24	11	19	10	5	15	7	20	6	5	6	6	5	13	276	Jan 20	Saturday	

Table 3.4.2 (Page 1 of 4)

ARC .FKX Hourly distribution of detections

Day	00	01	02	03	04	05	06	07	08	09	10	11	12	13	14	15	16	17	18	19	20	21	22	23	Sum	Date	
21	4	7	17	7	8	6	9	13	12	5	14	14	2	9	5	10	9	17	7	6	13	13	9	17	233	Jan 21	Sunday
22	5	3	6	3	4	14	18	5	17	10	9	9	16	28	16	17	13	17	22	9	14	12	16	22	305	Jan 22	Monday
23	3	1	4	10	5	4	8	14	15	7	15	14	32	20	8	15	13	13	9	9	16	14	20	14	283	Jan 23	Tuesday
24	16	13	9	10	9	14	14	17	15	16	22	23	32	21	16	16	14	6	18	9	17	12	11	21	371	Jan 24	Wednesday
25	19	7	7	17	17	17	15	13	22	37	19	18	19	15	13	14	15	14	8	6	14	26	21	20	393	Jan 25	Thursday
26	6	10	6	8	6	9	6	17	9	11	21	7	29	14	20	6	25	11	15	18	9	7	11	12	293	Jan 26	Friday
27	5	12	11	8	8	8	12	10	7	5	16	19	11	13	7	6	15	8	7	12	12	2	9	18	241	Jan 27	Saturday
28	11	7	9	2	10	3	6	4	8	11	11	12	8	8	2	7	8	0	23	7	12	5	6	21	201	Jan 28	Sunday
29	12	2	9	7	4	1	2	12	12	9	5	17	22	13	18	14	10	15	9	7	15	23	6	19	263	Jan 29	Monday
30	6	6	3	14	7	10	19	20	52	87	57	45	36	19	24	19	17	13	20	25	13	20	27	22	581	Jan 30	Tuesday
31	16	16	18	22	10	4	10	58	37	58	22	11	52	63	21	14	15	13	14	9	6	3	11	19	522	Jan 31	Wednesday
32	8	7	10	10	18	15	5	31	14	8	18	22	21	18	12	11	8	10	25	7	10	16	15	8	327	Feb 01	Thursday
33	9	6	8	5	8	6	8	10	18	21	41	30	53	31	9	17	11	17	14	13	8	7	14	9	373	Feb 02	Friday
34	3	6	7	7	10	5	7	6	3	23	23	19	17	37	19	14	7	1	7	3	7	4	6	14	255	Feb 03	Saturday
35	6	5	10	8	5	2	9	5	11	12	8	8	10	6	3	4	17	18	6	10	12	5	6	13	199	Feb 04	Sunday
36	7	2	18	12	5	21	12	19	11	12	10	9	21	15	15	12	8	13	23	9	7	12	12	17	302	Feb 05	Monday
37	8	3	6	7	7	5	12	10	9	8	14	12	18	21	6	6	7	13	4	5	10	1	15	17	224	Feb 06	Tuesday
38	2	3	6	7	3	4	11	27	66	78	65	61	75	25	72	32	68	82	51	18	13	15	19	15	818	Feb 07	Wednesday
39	3	6	7	7	2	8	10	27	37	24	16	26	23	8	13	12	13	11	4	8	13	13	5	13	309	Feb 08	Thursday
40	4	13	19	9	12	6	4	6	12	27	11	11	31	13	13	5	10	16	8	3	9	8	16	17	283	Feb 09	Friday
41	14	11	8	14	22	14	10	12	4	17	12	33	37	29	1	6	11	16	3	5	13	5	2	20	319	Feb 10	Saturday
42	5	8	4	1	6	17	2	14	13	7	5	18	9	8	9	5	9	16	5	30	10	3	11	10	225	Feb 11	Sunday
43	12	3	7	10	8	13	9	13	14	12	12	12	26	22	14	14	9	11	11	6	9	5	13	20	285	Feb 12	Monday
44	16	4	4	6	6	8	16	5	8	11	6	14	21	26	8	10	10	24	6	11	8	7	5	14	254	Feb 13	Tuesday
45	7	8	3	5	11	9	17	26	13	11	21	18	19	23	25	5	9	5	29	12	8	10	19	10	323	Feb 14	Wednesday
46	7	9	4	12	14	10	22	14	10	17	27	21	23	20	13	14	9	18	8	20	11	7	11	21	342	Feb 15	Thursday
47	13	8	9	9	6	12	16	14	18	15	21	17	40	31	17	14	15	12	19	25	13	26	13	15	398	Feb 16	Friday
48	5	18	13	14	8	6	17	6	17	14	14	41	29	21	17	11	14	9	14	15	6	15	6	16	346	Feb 17	Saturday
49	6	6	4	14	11	12	5	5	9	10	14	7	17	9	8	19	9	15	16	15	18	7	9	11	256	Feb 18	Sunday
50	13	4	5	9	7	20	26	24	14	15	11	22	28	10	26	12	8	12	16	5	17	11	23	16	354	Feb 19	Monday
51	8	7	6	5	7	10	14	22	26	20	19	23	25	23	17	8	10	13	8	6	6	7	12	8	310	Feb 20	Tuesday
52	6	5	2	10	5	6	7	12	13	16	5	4	12	21	4	4	5	15	16	13	10	4	16	21	232	Feb 21	Wednesday
53	12	5	7	8	15	7	11	7	10	15	20	12	34	17	21	17	26	23	12	10	11	8	17	26	351	Feb 22	Thursday
54	18	28	20	24	13	16	25	13	18	21	22	15	48	22	9	12	7	6	19	6	13	12	11	18	416	Feb 23	Friday
55	12	14	3	4	2	4	7	5	13	17	13	33	22	9	14	11	11	10	15	12	5	8	3	12	259	Feb 24	Saturday
56	3	15	18	27	25	40	20	14	7	13	5	7	10	8	5	14	11	14	12	6	23	28	28	36	389	Feb 25	Sunday
57	13	17	18	55	44	34	21	29	41	20	18	23	18	14	18	11	4	18	12	13	17	9	12	14	493	Feb 26	Monday
58	31	27	42	30	28	33	37	22	11	15	25	28	19	12	11	10	17	3	9	9	17	8	17	16	477	Feb 27	Tuesday
59	4	5	4	5	8	3	12	11	16	13	9	30	35	20	15	10	13	6	9	5	5	7	14	9	268	Feb 28	Wednesday
60	9	4	9	6	3	2	5	9	7	13	15	15	20	19	12	14	9	5	13	35	47	57	61	63	452	Mar 01	Thursday
61	46	47	18	8	5	5	13	7	16	14	21	16	26	12	4	6	13	4	11	6	9	9	13	17	346	Mar 02	Friday
62	10	20	18	5	10	14	14	17	14	4	18	18	25	13	25	19	30	49	61	72	76	75	68	71	746	Mar 03	Saturday
63	58	62	58	49	46	29	18	17	14	11	7	10	8	6	6	11	8	12	19	22	35	29	44	43	622	Mar 04	Sunday
64	14	9	6	12	10	8	6	10	18	13	9	16	19	17	6	19	20	16	13	13	23	25	16	24	342	Mar 05	Monday
65	13	11	8	13	4	5	9	16	10	13	17	21	14	16	17	13	8	11	7	8	4	7	21	20	286	Mar 06	Tuesday
66	13	14	25	17	29	16	8	13	18	15	24	29	33	20	16	13	46	40	39	45	56	59	51	62	701	Mar 07	Wednesday
67	55	54	64	75	71	80	71	63	61	46	29	65	38	37	61	44	48	27	23	16	20	9	11	21	1089	Mar 08	Thursday
68	4	7	7	9	5	8	6	8	15	13	21	18	28	19	13	22	4	20	15	10	8	19	12	9	300	Mar 09	Friday
69	10	3	11	12	4	6	7	4	7	9	9	4	9	7	8	3	7	11	5	3	8	8	3	10	168	Mar 10	Saturday
70	6	7	9	2	8	4	4	2	11	6	7	5	6	8	22	9	10	8	8	6	10	4	12	18	192	Mar 11	Sunday
71	11	21	34	25	32	34	32	26	23	10	17	10	25	15	20	15	19	6	6	6	3	4	7	17	418	Mar 12	Monday
72	15	8	4	7	11	3	6	9	11	22	13	7	14	15	8	18	28	11	9	9	19	27	19	20	313	Mar 13	Tuesday
73	6	15	21	19	17	15	23	15	15	20	83	24	44	21	41	42	29	41	17	12	11	15	7	17	570	Mar 14	Wednesday
74	8	9	8	5	15	16	4	13	35	24	36	19	50	60	21	27	92	23	11	13	9	13	15	0	526	Mar 15	Thursday
75	0	0	0	0	0	0	0	0	0	0	0	0	0	0	0	0	0	0	0	0	0	0	0	0	0	Mar 16	Friday
76	0	0	0	0	0	0	0	0	0	0	0	0	0	0	0	0	0	0	0	0	0	0	0	0	0	Mar 17	Saturday

Table 3.4.2 (Page 2 of 4)

ARC .FKX Hourly distribution of detections

Day	00	01	02	03	04	05	06	07	08	09	10	11	12	13	14	15	16	17	18	19	20	21	22	23	Sum	Date	
274	2	4	3	5	2	6	5	4	9	8	9	12	13	13	14	8	15	19	2	12	12	7	2	20	206	Oct 01	Sunday
275	4	5	3	7	14	9	16	3	9	6	14	20	40	16	18	25	8	11	9	12	2	8	24	25	308	Oct 02	Monday
276	1	1	9	23	21	19	22	11	14	22	16	36	34	18	23	26	6	7	6	7	10	5	10	22	369	Oct 03	Tuesday
277	9	6	3	7	17	4	9	24	8	4	22	28	28	15	14	15	4	18	19	15	13	7	19	24	332	Oct 04	Wednesday
278	7	9	13	12	2	9	20	34	22	9	13	43	23	18	26	20	16	11	18	24	10	13	13	6	391	Oct 05	Thursday
279	4	7	8	20	27	13	8	29	24	37	30	31	45	11	19	24	9	8	24	10	3	12	16	23	442	Oct 06	Friday
280	14	21	7	4	4	13	19	20	18	27	27	9	20	15	34	36	25	21	18	18	17	7	9	17	420	Oct 07	Saturday
281	20	17	14	21	39	11	3	5	24	6	43	21	17	21	33	44	44	56	21	19	25	11	24	55	594	Oct 08	Sunday
282	166	59	4	7	2	9	14	9	17	21	15	12	25	22	9	18	21	7	14	4	5	1	22	15	498	Oct 09	Monday
283	4	8	5	0	0	0	0	15	16	20	8	17	23	29	8	38	20	4	12	9	9	4	12	16	277	Oct 10	Tuesday
284	4	3	5	1	8	3	12	28	22	23	46	59	33	19	17	21	18	10	13	17	14	9	12	13	410	Oct 11	Wednesday
285	3	15	6	4	2	5	17	15	8	53	30	49	92	44	34	32	29	14	17	5	12	17	10	16	529	Oct 12	Thursday
286	10	15	3	5	8	4	44	62	39	16	22	27	48	18	16	24	19	14	23	19	19	18	10	20	503	Oct 13	Friday
287	17	3	14	20	129	138	40	23	13	17	26	19	53	88	115	75	83	60	19	10	17	12	15	21	1027	Oct 14	Saturday
288	9	8	5	9	28	25	14	12	12	7	9	25	20	8	16	9	15	4	15	8	12	26	9	21	326	Oct 15	Sunday
289	19	12	14	5	9	25	18	19	23	17	21	9	25	17	24	25	18	16	44	30	13	16	17	34	470	Oct 16	Monday
290	18	17	20	17	17	16	11	3	12	13	12	31	33	17	26	25	7	8	20	7	12	6	19	25	392	Oct 17	Tuesday
291	10	14	6	6	17	11	11	35	19	9	30	20	45	18	33	31	24	19	32	26	32	5	17	20	490	Oct 18	Wednesday
292	4	8	8	4	9	15	10	13	18	24	27	32	16	21	28	19	17	12	20	16	7	8	14	12	362	Oct 19	Thursday
293	6	4	2	15	5	5	21	32	29	17	37	32	40	30	19	19	13	9	18	15	11	4	14	15	412	Oct 20	Friday
294	10	10	6	9	12	5	11	6	11	19	23	26	25	8	16	11	11	4	5	7	2	6	2	14	259	Oct 21	Saturday
295	9	4	2	2	5	1	7	2	5	8	7	5	4	10	8	8	5	6	9	5	16	10	11	15	164	Oct 22	Sunday
296	8	5	4	7	8	6	5	10	22	10	21	17	20	31	8	10	9	4	3	8	14	10	9	22	271	Oct 23	Monday
297	11	5	7	8	11	5	9	9	12	11	10	16	13	30	16	15	19	17	10	8	9	5	7	16	279	Oct 24	Tuesday
298	12	8	3	4	7	2	7	12	14	14	11	28	32	15	16	18	5	11	6	9	19	10	11	15	289	Oct 25	Wednesday
299	7	5	5	10	7	10	5	9	13	10	8	17	10	23	37	7	13	23	7	6	13	11	22	17	295	Oct 26	Thursday
300	6	14	12	8	5	3	13	8	18	32	17	15	33	12	19	26	3	11	14	10	15	16	21	21	352	Oct 27	Friday
301	7	15	12	15	10	8	21	23	9	8	13	23	41	23	27	12	14	7	18	12	11	8	20	26	383	Oct 28	Saturday
302	15	14	14	24	26	40	16	13	14	7	4	21	30	20	14	13	21	27	30	46	63	46	54	54	626	Oct 29	Sunday
303	22	13	24	20	6	29	9	7	15	25	39	36	29	18	14	14	26	10	18	22	18	9	24	34	481	Oct 30	Monday
304	29	18	8	5	9	6	12	11	25	17	19	27	19	23	30	24	16	17	7	25	15	8	13	21	404	Oct 31	Tuesday
305	7	6	11	3	6	0	10	24	16	15	17	25	27	25	14	8	11	9	23	18	15	10	17	21	338	Nov 01	Wednesday
306	3	6	9	13	3	4	5	15	13	21	26	14	25	19	15	16	26	16	18	10	8	6	15	12	318	Nov 02	Thursday
307	3	3	8	4	5	7	8	19	44	18	13	19	21	35	24	17	14	7	3	12	11	7	7	7	316	Nov 03	Friday
308	7	1	4	7	5	2	10	15	9	11	32	24	22	8	10	7	4	6	36	9	18	10	10	9	276	Nov 04	Saturday
309	3	13	23	21	14	7	8	8	3	9	4	11	7	11	6	6	13	5	15	24	11	7	7	16	252	Nov 05	Sunday
310	7	5	20	6	8	7	18	6	17	17	8	11	28	25	12	12	2	5	10	13	19	15	9	16	296	Nov 06	Monday
311	3	2	2	4	3	9	4	6	18	9	12	13	15	18	16	16	16	44	26	16	13	15	17	22	319	Nov 07	Tuesday
312	24	17	8	7	6	5	13	14	5	21	6	18	15	13	15	11	10	19	10	13	9	6	17	17	299	Nov 08	Wednesday
313	8	5	2	5	2	6	6	6	24	7	19	19	32	23	20	12	17	8	26	7	6	13	18	7	298	Nov 09	Thursday
314	3	2	6	6	4	6	23	14	26	8	23	21	21	13	19	18	19	11	3	8	11	21	13	27	326	Nov 10	Friday
315	4	4	4	12	3	4	1	19	17	22	5	24	34	13	14	24	8	2	10	7	9	14	10	19	283	Nov 11	Saturday
316	9	3	2	7	10	3	4	8	5	0	4	5	4	22	3	7	9	8	9	8	25	18	9	7	189	Nov 12	Sunday
317	8	4	22	57	18	11	18	14	40	6	84	99	164	22	6	12	31	18	136	64	241	58	154	126	1296	Nov 13	Monday
318	136	86	72	62	54	100	148	95	79	58	90	167	41	97	89	78	91	29	48	61	10	17	15	18	1741	Nov 14	Tuesday
319	7	15	35	29	50	67	10	6	6	19	15	16	18	3	17	11	13	20	12	15	7	8	8	6	413	Nov 15	Wednesday
320	3	8	3	9	5	7	12	11	10	10	15	14	25	23	15	8	13	6	12	7	11	12	13	8	260	Nov 16	Thursday
321	2	3	5	4	25	12	7	17	30	15	13	26	23	19	14	16	10	19	22	8	7	2	9	11	319	Nov 17	Friday
322	6	2	1	6	7	7	10	8	1	16	5	10	30	9	16	9	17	10	6	7	12	6	3	9	213	Nov 18	Saturday
323	2	12	2	3	11	9	9	2	1	4	7	18	6	8	10	11	7	13	8	11	10	14	21	19	218	Nov 19	Sunday
324	20	19	12	16	15	3	13	14	11	14	17	19	18	26	26	18	9	12	6	8	22	8	22	16	364	Nov 20	Monday
325	5	7	14	11	7	12	12	6	16	18	17	33	27	24	23	9	14	13	8	8	16	13	20	36	369	Nov 21	Tuesday
326	25	26	24	7	10	3	4	14	13	17	20	11	26	31	22	34	31	43	65	71	65	79	91	74	806	Nov 22	Wednesday
327	61	45	41	50	55	54	74	81	81	79	76	63	55	38	32	33	47	50	29	27	16	11	9	16	1123	Nov 23	Thursday
328	10	6	5	14	10	10	10	15	13	11	21	12	51	26	10	18	9	8	9	7	7	9	10	14	315	Nov 24	Friday
329	7	7	9	4	1	3	11	9	22	9	14	18	23	17	23	20	28	15	12	9	20	75	128	153	637	Nov 25	Saturday

Table 3.4.2 (Page 3 of 4)

ARC .FKX Hourly distribution of detections

Day	00	01	02	03	04	05	06	07	08	09	10	11	12	13	14	15	16	17	18	19	20	21	22	23	Sum	Date
77	0	0	0	0	0	0	0	0	0	0	0	0	0	0	0	0	0	0	0	0	0	0	0	0	0	Mar 18 Sunday
78	0	0	0	0	0	0	0	0	0	0	0	0	0	0	0	0	0	0	0	0	0	0	11	15	26	Mar 19 Monday
79	19	9	7	9	3	8	10	9	25	17	19	21	36	11	46	11	17	15	17	9	12	7	38	36	411	Mar 20 Tuesday
80	36	43	53	54	61	47	32	22	14	19	9	18	34	20	7	0	0	0	0	0	3	5	15	10	502	Mar 21 Wednesday
81	13	4	12	4	3	3	13	6	16	14	15	17	31	28	12	0	0	0	0	0	0	0	0	0	191	Mar 22 Thursday
82	0	0	0	0	0	0	0	8	17	15	18	23	24	22	11	10	10	6	11	8	11	9	7	26	236	Mar 23 Friday
83	11	2	7	2	9	3	13	14	9	10	8	26	35	26	18	15	16	11	2	13	16	7	8	10	291	Mar 24 Saturday
84	7	15	19	21	6	21	14	6	0	0	0	0	0	0	22	1	0	0	0	0	0	0	0	0	132	Mar 25 Sunday
85	0	0	3	3	15	22	21	34	24	31	15	30	18	11	12	7	16	12	13	10	14	5	15	10	341	Mar 26 Monday
86	14	17	16	4	10	7	11	8	7	8	23	13	11	14	12	13	6	2	9	7	6	10	13	4	245	Mar 27 Tuesday
87	2	6	5	7	10	10	4	12	1	8	14	14	10	9	8	11	11	10	5	4	7	9	11	10	198	Mar 28 Wednesday
88	17	15	19	19	21	15	14	15	6	15	29	25	10	18	10	5	15	8	19	17	4	12	11	11	350	Mar 29 Thursday
89	9	3	8	3	11	9	1	4	15	8	5	20	26	4	3	6	6	4	2	6	6	4	15	3	181	Mar 30 Friday
90	6	4	4	2	3	8	11	8	7	9	25	8	14	4	15	4	6	7	13	10	24	23	35	21	271	Mar 31 Saturday
PRS	00	01	02	03	04	05	06	07	08	09	10	11	12	13	14	15	16	17	18	19	20	21	22	23		
Sum	2257	2289	2304	2634	2895	3797	3413	2683	2447	2355	2376	3631														
	2421	2195	2368	2403	2763	3276	4600	2935	2671	2580	2482	2927													66702	Total sum
178	14	13	12	13	13	13	14	15	16	16	18	21	26	19	16	15	15	14	14	13	14	13	16	20	375	Total average
126	14	13	13	13	13	13	15	17	18	19	21	24	30	22	18	16	16	14	16	13	14	13	17	20	402	Average workdays
52	12	13	11	12	14	13	10	9	9	9	12	16	16	13	13	12	13	12	12	13	15	14	15	21	309	Average weekends

Table 3.4.2 Daily and hourly distribution of ARCESS detections. For each day is shown number of detections within each hour of the day and number of detections for that day. The end statistics give total number of detections distributed for each hour and the total sum of detections during the period. The averages show number of processed days, hourly distribution and average per processed day. (Page 4 of 4)

FIN .FKX Hourly distribution of detections

Day	00	01	02	03	04	05	06	07	08	09	10	11	12	13	14	15	16	17	18	19	20	21	22	23	Sum	Date	
327	0	0	0	0	0	0	0	0	0	0	0	0	61	0	0	0	0	0	0	0	0	0	0	0	61	Nov 23	Thursday
328	0	0	0	0	0	0	0	0	0	0	0	0	0	0	0	0	0	0	0	0	0	0	0	0	0	Nov 24	Friday
329	0	0	0	0	0	0	0	0	0	0	0	0	0	0	0	0	0	0	0	0	0	0	0	0	0	Nov 25	Saturday
330	0	0	0	0	0	0	0	0	0	0	0	0	0	0	0	0	0	0	0	0	0	0	0	0	0	Nov 26	Sunday
331	0	0	0	0	0	0	0	0	8	12	18	22	39	23	37	63	7	0	0	0	0	0	0	0	229	Nov 27	Monday
332	0	0	0	0	0	0	0	0	0	0	0	0	0	0	0	0	0	0	0	0	0	0	0	10	10	Nov 28	Tuesday
333	11	11	11	7	6	5	8	5	3	19	16	20	23	4	0	0	0	0	0	0	0	0	0	0	149	Nov 29	Wednesday
334	5	7	7	9	10	1	3	6	5	16	16	23	39	26	27	21	17	14	13	22	66	26	40	15	434	Nov 30	Thursday
335	10	42	43	4	22	34	13	13	14	17	16	25	30	14	5	28	35	47	58	54	11	94	83	69	781	Dec 01	Friday
336	20	8	11	8	13	19	16	11	28	17	3	21	30	19	30	28	19	23	19	24	26	24	38	27	482	Dec 02	Saturday
337	18	38	31	40	59	39	13	22	14	28	19	34	37	33	32	26	30	24	25	17	19	12	12	54	676	Dec 03	Sunday
338	33	16	7	3	7	13	32	24	15	30	40	20	38	12	21	13	42	52	22	38	15	6	13	56	568	Dec 04	Monday
339	21	75	76	11	8	20	9	12	10	0	5	11	39	44	69	34	44	47	15	44	62	56	6	15	733	Dec 05	Tuesday
340	12	5	36	91	63	6	9	7	19	27	22	22	34	26	11	3	3	7	2	7	7	8	6	6	439	Dec 06	Wednesday
341	5	4	3	4	10	1	4	5	23	22	17	39	58	53	35	18	8	11	6	6	32	58	49	46	517	Dec 07	Thursday
342	50	30	16	5	11	2	8	4	6	18	20	31	25	13	8	18	16	13	10	14	17	7	12	19	373	Dec 08	Friday
343	9	12	8	5	10	12	24	36	25	34	22	21	39	38	30	56	46	15	2	0	0	0	0	0	444	Dec 09	Saturday
344	0	0	0	0	0	0	0	0	0	0	0	0	0	0	0	0	0	0	0	0	0	0	0	0	0	Dec 10	Sunday
345	0	0	0	0	0	0	0	0	0	0	0	0	0	0	0	0	0	0	0	0	0	0	0	0	0	Dec 11	Monday
346	0	0	0	0	0	0	0	0	0	0	0	0	0	0	0	0	0	0	0	0	0	0	0	0	0	Dec 12	Tuesday
347	0	0	0	0	0	0	0	0	0	0	0	0	0	0	0	0	0	0	0	0	0	0	0	0	0	Dec 13	Wednesday
348	0	0	0	0	0	0	0	0	0	0	0	0	0	0	0	0	0	0	0	0	0	0	0	0	0	Dec 14	Thursday
349	0	0	0	0	0	0	0	0	0	0	0	0	0	0	0	0	0	0	0	0	0	0	0	0	0	Dec 15	Friday
350	0	0	0	0	0	0	0	0	0	0	0	0	0	0	0	0	0	0	0	0	0	0	0	0	0	Dec 16	Saturday
351	0	0	0	0	0	0	0	0	0	0	0	0	0	0	0	0	0	0	0	0	0	0	0	0	0	Dec 17	Sunday
352	0	0	0	0	0	0	0	0	0	0	0	0	0	0	0	0	0	0	0	0	0	0	0	0	0	Dec 18	Monday
353	0	0	0	0	0	0	0	0	0	0	0	0	0	0	0	0	0	0	0	0	0	0	0	0	0	Dec 19	Tuesday
354	0	0	0	0	0	0	0	0	0	0	0	0	0	0	0	0	0	0	0	0	0	0	0	0	0	Dec 20	Wednesday
355	0	0	0	0	0	0	0	0	0	0	0	0	0	0	0	0	0	0	0	0	0	0	0	0	0	Dec 21	Thursday
356	0	0	0	0	0	0	0	0	0	0	0	0	0	0	0	0	0	0	0	0	0	0	0	0	0	Dec 22	Friday
357	0	0	0	0	0	0	0	0	0	0	0	0	0	0	0	0	0	0	0	0	0	0	0	0	0	Dec 23	Saturday
358	0	0	0	0	0	0	0	0	0	0	0	0	0	0	0	0	0	0	0	0	0	0	0	0	0	Dec 24	Sunday
359	0	0	0	0	0	0	0	0	0	0	0	0	0	0	0	0	0	0	0	0	0	0	0	0	0	Dec 25	Monday F:rste
360	0	0	0	0	0	0	0	0	0	0	0	0	0	0	0	0	0	0	0	0	0	0	0	0	0	Dec 26	Tuesday Andre
361	0	0	0	0	0	0	0	0	0	0	0	0	0	0	0	0	0	0	0	0	0	0	0	0	0	Dec 27	Wednesday
362	0	0	0	0	0	0	0	0	0	0	0	0	0	0	0	0	0	0	0	0	0	0	0	0	0	Dec 28	Thursday
363	0	0	0	0	0	0	0	0	0	0	0	0	0	0	0	0	0	0	0	0	0	0	0	0	0	Dec 29	Friday
364	0	0	0	0	0	0	0	0	0	0	0	0	0	0	0	0	0	0	0	0	0	0	0	0	0	Dec 30	Saturday
365	0	0	0	0	0	0	0	0	0	0	0	0	0	0	0	0	0	0	0	0	0	0	0	0	0	Dec 31	Sunday
1	0	0	0	0	0	0	0	0	0	0	0	0	0	0	0	0	0	0	0	0	0	0	0	0	0	Jan 01	Monday F:rste
2	0	0	0	0	0	0	0	0	0	0	0	0	0	0	0	0	0	0	0	0	0	0	0	0	0	Jan 02	Tuesday
3	0	0	0	0	0	0	0	0	0	0	0	0	0	0	0	0	0	0	0	0	0	0	0	0	0	Jan 03	Wednesday
4	0	0	0	0	0	0	0	0	0	0	0	0	36	33	19	12	5	14	19	18	12	12	11	18	209	Jan 04	Thursday
5	11	20	16	10	15	5	5	14	18	30	43	33	38	16	24	20	7	11	28	6	14	15	8	14	421	Jan 05	Friday
6	10	5	4	11	14	4	5	7	24	18	35	47	41	19	11	11	4	4	11	6	6	13	4	8	322	Jan 06	Saturday
7	2	3	3	0	5	5	22	7	0	0	0	0	0	0	0	0	0	0	0	0	0	0	0	0	47	Jan 07	Sunday
8	0	0	0	0	0	0	0	9	13	38	26	38	44	39	20	17	6	11	10	24	10	13	5	11	334	Jan 08	Monday
9	16	9	19	11	13	13	8	3	9	51	29	22	52	25	27	31	41	23	12	21	11	9	15	3	473	Jan 09	Tuesday
10	4	10	8	18	14	3	11	7	15	6	28	23	44	31	8	8	14	13	7	13	10	15	15	7	332	Jan 10	Wednesday
11	8	9	9	4	17	6	8	28	10	23	34	36	33	36	12	7	6	10	13	17	12	20	20	8	386	Jan 11	Thursday
12	13	12	12	23	27	18	19	19	4	43	40	61	39	42	42	45	44	52	33	20	23	36	68	28	763	Jan 12	Friday
13	17	14	7	18	11	48	43	8	23	9	19	8	32	33	11	23	26	12	6	8	28	24	8	14	450	Jan 13	Saturday
14	5	11	7	16	21	21	22	16	20	27	28	35	5	1	5	5	5	14	8	10	13	33	20	8	356	Jan 14	Sunday
15	13	5	6	8	7	4	6	8	0	0	0	0	0	0	0	0	0	0	0	0	0	0	0	0	57	Jan 15	Monday
16	0	0	0	0	0	0	0	0	0	0	0	0	5	12	12	9	7	6	13	10	15	4	5	8	106	Jan 16	Tuesday
17	8	4	8	4	7	4	7	1	12	6	15	21	17	29	9	4	5	8	37	37	49	27	3	4	326	Jan 17	Wednesday

Table 3.4.3 (Page 1 of 3)

FIN .FKX Hourly distribution of detections

Day	00	01	02	03	04	05	06	07	08	09	10	11	12	13	14	15	16	17	18	19	20	21	22	23	Sum	Date
18	1	2	9	5	5	2	5	8	3	19	14	24	27	25	4	9	7	8	8	7	8	12	7	5	224	Jan 18 Thursday
19	8	10	5	6	6	4	2	6	4	15	20	16	34	24	18	9	10	9	8	11	15	4	7	12	263	Jan 19 Friday
20	9	17	14	10	5	7	2	7	8	4	7	8	10	5	6	3	2	1	2	1	4	5	5	2	144	Jan 20 Saturday
21	1	3	4	1	5	6	3	6	7	9	5	4	6	5	5	2	5	10	6	4	17	8	13	5	140	Jan 21 Sunday
22	9	11	8	6	3	2	8	7	11	13	20	17	24	15	21	6	7	13	4	2	2	5	4	7	225	Jan 22 Monday
23	9	9	4	13	5	4	4	2	6	13	8	19	27	25	16	11	7	4	4	5	13	8	8	6	230	Jan 23 Tuesday
24	3	7	3	6	11	7	1	5	5	9	15	18	37	17	10	6	5	7	14	10	5	4	1	9	215	Jan 24 Wednesday
25	1	5	6	3	3	3	10	7	6	16	10	11	29	15	8	8	4	1	5	3	4	11	5	2	176	Jan 25 Thursday
26	3	6	6	6	4	5	2	1	13	13	21	24	34	19	13	3	3	7	7	10	5	8	6	9	228	Jan 26 Friday
27	8	5	7	5	11	9	5	23	28	40	27	15	11	5	1	5	5	5	3	5	3	4	3	5	238	Jan 27 Saturday
28	4	6	2	3	3	10	11	7	5	3	5	10	0	6	3	2	3	6	5	2	9	7	8	8	128	Jan 28 Sunday
29	8	7	5	6	3	3	4	1	4	13	7	17	27	26	14	9	5	9	9	5	9	9	5	2	207	Jan 29 Monday
30	4	2	2	4	0	1	4	3	6	8	14	16	34	50	15	18	5	5	4	8	9	1	2	5	220	Jan 30 Tuesday
31	6	6	14	3	6	3	2	14	1	18	25	10	28	21	11	5	6	3	5	6	10	5	5	6	219	Jan 31 Wednesday
32	5	3	11	6	3	4	3	3	12	14	14	29	19	8	17	6	3	6	13	9	5	8	5	8	214	Feb 01 Thursday
33	7	5	3	4	4	0	1	4	8	13	10	14	31	18	9	4	5	4	9	5	6	18	27	30	239	Feb 02 Friday
34	12	8	9	6	6	7	6	5	16	9	5	7	1	5	30	33	16	5	13	12	9	12	4	13	249	Feb 03 Saturday
35	40	41	26	29	35	5	12	6	5	23	15	11	9	10	9	15	17	5	8	4	8	5	2	5	345	Feb 04 Sunday
36	6	2	1	1	3	8	3	10	9	13	8	15	22	26	15	9	11	6	4	9	7	11	15	6	220	Feb 05 Monday
37	7	3	6	6	6	1	7	4	6	16	14	27	28	13	8	12	7	2	2	9	6	8	8	6	212	Feb 06 Tuesday
38	7	2	4	5	1	1	3	7	6	15	9	11	24	32	23	3	10	4	12	5	7	14	13	14	232	Feb 07 Wednesday
39	20	28	18	15	13	8	3	12	14	8	20	24	24	23	20	10	4	4	7	7	12	6	12	8	320	Feb 08 Thursday
40	6	13	8	14	10	4	3	4	4	22	12	21	39	20	14	8	13	18	18	9	20	30	26	20	356	Feb 09 Friday
41	25	39	19	9	19	5	3	5	2	2	4	10	11	6	5	7	38	18	24	14	22	28	37	23	375	Feb 10 Saturday
42	33	46	78	55	34	30	18	8	20	18	18	19	15	25	30	36	14	8	22	15	15	36	20	7	620	Feb 11 Sunday
43	11	14	5	4	3	2	2	4	5	7	6	18	34	16	10	11	5	6	6	6	5	4	4	9	197	Feb 12 Monday
44	12	6	5	1	6	3	7	3	13	15	12	17	30	7	8	10	14	8	6	13	19	8	9	6	238	Feb 13 Tuesday
45	11	10	12	17	14	4	3	5	13	5	24	7	32	16	10	22	4	4	5	3	2	5	3	4	235	Feb 14 Wednesday
46	4	4	9	14	6	4	0	1	9	23	18	15	20	20	5	17	3	1	0	10	6	5	6	2	202	Feb 15 Thursday
47	5	4	2	4	4	0	9	2	9	13	21	18	32	17	4	11	2	4	8	3	6	12	2	8	200	Feb 16 Friday
48	10	14	8	7	4	7	6	5	7	3	8	9	11	7	8	9	9	9	7	8	11	7	4	7	185	Feb 17 Saturday
49	7	6	12	9	10	7	6	3	10	2	6	10	12	7	6	13	8	4	14	11	3	6	7	5	184	Feb 18 Sunday
50	10	11	6	9	6	10	6	6	10	10	13	19	32	12	17	9	3	5	3	7	7	10	13	5	239	Feb 19 Monday
51	1	8	10	8	8	3	5	10	4	16	9	16	21	19	13	6	2	4	7	15	26	36	22	36	305	Feb 20 Tuesday
52	32	23	20	11	6	24	12	3	4	13	12	11	36	8	12	7	5	4	8	6	8	3	4	5	277	Feb 21 Wednesday
53	9	7	2	7	6	3	5	15	23	14	17	15	30	27	17	4	2	11	3	5	16	11	6	14	269	Feb 22 Thursday
54	7	9	5	3	1	2	4	4	8	27	21	25	30	19	9	7	9	9	8	3	5	4	3	5	227	Feb 23 Friday
55	4	4	8	3	9	3	7	4	4	0	6	11	14	5	4	7	8	9	21	10	3	4	0	2	150	Feb 24 Saturday
56	7	23	1	7	3	8	3	2	5	10	9	4	9	5	4	8	7	2	4	4	7	4	6	7	149	Feb 25 Sunday
57	14	9	12	9	11	9	10	6	6	9	11	16	23	23	7	11	6	2	8	9	11	8	12	4	246	Feb 26 Monday
58	10	13	12	8	5	7	2	4	5	14	13	17	21	18	25	21	28	43	35	21	21	12	8	7	370	Feb 27 Tuesday
59	1	4	14	17	20	8	3	8	7	10	11	21	27	18	7	15	5	0	1	6	5	8	7	7	230	Feb 28 Wednesday
60	7	3	10	2	7	1	3	7	13	10	9	16	30	17	7	18	4	3	2	8	5	7	7	14	210	Mar 01 Thursday
61	5	7	18	10	6	4	2	4	12	14	12	23	18	18	11	4	4	10	15	12	7	10	10	11	247	Mar 02 Friday
62	4	8	15	14	20	17	28	13	12	5	16	5	19	11	18	34	65	82	70	71	80	61	47	45	760	Mar 03 Saturday
63	42	43	66	70	39	36	16	9	15	6	6	11	15	8	5	10	6	7	8	14	14	14	14	15	489	Mar 04 Sunday
64	15	10	7	11	4	2	6	3	6	10	7	24	30	19	12	10	12	11	8	8	12	17	8	17	269	Mar 05 Monday
65	8	8	14	7	8	4	12	2	9	15	19	27	31	30	12	20	14	21	8	10	7	9	3	16	314	Mar 06 Tuesday
66	6	11	17	10	11	2	4	4	10	19	25	23	32	6	10	8	5	10	14	27	19	16	23	15	327	Mar 07 Wednesday
67	23	26	16	14	4	4	7	8	9	6	8	11	13	5	8	9	6	6	8	8	7	5	10	12	233	Mar 08 Thursday
68	5	6	7	5	4	2	2	3	3	3	11	14	19	4	1	3	8	9	8	5	8	8	10	9	157	Mar 09 Friday
69	8	10	13	8	6	9	4	3	6	6	16	10	9	6	6	8	5	5	9	9	9	4	11	7	187	Mar 10 Saturday
70	8	6	17	11	11	13	11	3	5	11	6	16	19	9	15	3	4	5	9	3	6	9	25	11	236	Mar 11 Sunday
71	13	5	8	9	6	4	7	4	5	9	9	16	19	21	21	13	7	8	4	3	7	11	8	12	229	Mar 12 Monday
72	12	7	4	3	6	2	5	3	11	9	18	19	16	20	10	19	9	7	10	4	0	0	0	0	194	Mar 13 Tuesday
73	0	0	0	0	0	0	0	0	0	0	0	0	0	0	3	18	12	5	7	7	0	9	7	3	71	Mar 14 Wednesday

Table 3.4.3 (Page 2 of 3)

FIN .FKX Hourly distribution of detections

Day	00	01	02	03	04	05	06	07	08	09	10	11	12	13	14	15	16	17	18	19	20	21	22	23	Sum	Date
74	11	7	5	10	5	5	2	5	10	6	16	19	26	22	16	12	5	7	6	7	3	3	5	1	214	Mar 15 Thursday
75	10	6	9	7	5	6	2	2	9	16	12	15	39	20	8	5	7	3	9	6	3	2	4	4	209	Mar 16 Friday
76	1	9	2	2	3	4	4	5	5	10	13	5	11	5	6	2	3	0	2	3	3	1	4	4	107	Mar 17 Saturday
77	2	2	8	5	4	3	7	9	9	6	6	4	*12*	4	5	5	5	7	7	8	5	*14*	*16*	*10*	*163*	*Mar 18 Sunday*
78	10	3	6	8	2	10	3	5	9	14	9	12	19	14	11	10	4	11	10	2	4	8	16	9	209	Mar 19 Monday
79	23	17	16	10	3	2	1	6	4	15	13	12	21	18	10	6	7	3	5	4	5	10	9	11	231	Mar 20 Tuesday
80	4	7	9	9	1	2	4	4	5	5	15	16	20	24	20	11	10	12	9	10	12	11	8	5	233	Mar 21 Wednesday
81	9	7	7	15	8	14	9	7	6	16	15	17	36	22	21	7	8	3	3	3	3	5	4	7	252	Mar 22 Thursday
82	9	3	7	4	4	6	3	4	8	8	10	19	28	36	20	10	9	4	4	9	10	12	2	4	233	Mar 23 Friday
83	11	16	31	26	18	7	6	9	8	9	4	10	11	6	3	8	9	5	1	6	4	3	8	15	234	Mar 24 Saturday
84	9	9	15	4	10	7	9	14	4	10	7	9	8	7	14	12	12	9	7	9	11	8	9	5	218	Mar 25 Sunday
85	4	10	7	12	8	6	3	12	8	15	14	24	15	4	18	7	8	6	14	18	16	20	27	26	302	Mar 26 Monday
86	30	34	28	28	24	12	3	11	13	13	18	19	12	9	6	6	1	8	11	18	14	16	18	17	369	Mar 27 Tuesday
87	22	23	21	19	6	9	5	7	8	14	31	22	28	9	13	7	7	4	3	4	5	8	21	15	311	Mar 28 Wednesday
88	16	21	24	17	11	10	8	11	12	17	19	42	15	8	9	5	14	7	7	11	8	5	7	11	315	Mar 29 Thursday
89	11	4	16	5	0	4	8	49	15	17	37	65	26	5	18	24	19	12	11	8	13	25	23	14	429	Mar 30 Friday
90	35	40	32	25	19	32	41	37	29	37	51	64	46	35	32	33	34	17	4	4	9	9	1	2	668	Mar 31 Saturday
FIN	00	01	02	03	04	05	06	07	08	09	10	11	12	13	14	15	16	17	18	19	20	21	22	23		
Sum	1173	1055	765	785	1379	1848	1731	1274	1031	1052	1266	1151	1071	1218	959	735	947	1507	2486	1365	1092	1022	1158	1170	29240	Total sum
101	11	12	12	10	9	8	7	8	9	14	15	18	25	17	14	13	11	10	10	10	11	13	12	11	290	Total average
127	6	6	6	5	4	3	3	4	5	8	9	11	16	11	8	7	5	6	6	6	6	7	7	7	161	Average workdays
55	7	8	8	7	7	7	6	5	6	6	7	8	8	6	6	7	7	6	6	5	6	6	6	6	159	Average weekends

Table 3.4.3 Daily and hourly distribution of FINESA detections. For each day is shown number of detections within each hour of the day and number of detections for that day. The end statistics give total number of detections distributed for each hour and the total sum of detections during the period. The averages show number of processed days, hourly distribution and average per processed day. (Page 3 of 3)

3.5 IMS operation

The Intelligent Monitoring System (IMS) was installed at NORSAR in December 1989 and has been operated experimentally since 1 January 1990 for automatic processing of multiple-array data. The current version of IMS processes data from the two-array network consisting of NORESS and ARCESS. Future upgrades of IMS will allow data from additional arrays and single stations to be incorporated.

Table 3.5.1 gives a summary of phase detections and processed regional events by IMS during its first three months of operation at NORSAR. From top to bottom, the table gives the total number of detections by the IMS, the detections that are associated with regional events declared by the IMS, the number of detections that are not associated with such events, the number of regional events declared by the IMS, the number of such events rejected by the analyst, the number of events accepted by the analyst, the number of events accepted by the analyst without any changes, and finally the number of events accepted after some sort of modification by the analyst. This last category is divided into three classes: Events where phases (not detected by the IMS) have been added by the analyst, events for which the phase assignments by the IMS have been changed or one or more phase detections have been removed, and events for which the changes by the analyst have amounted to retiming the phases only.

B.Kr. Hokland
U. Baadshaug
S. Mykkeltveit

	Jan 90	Feb 90	Mar 90	total
Phase detections	15421	15313	15012	45746
- Associated phases	2043	2485	2244	6772
- Unassociated phases	13378	12828	12768	38974
Events declared	1131	1174	982	3287
- Rejected events	403	355	234	992
- Accepted events	728	819	748	2295
Unchanged events	261	127	124	512
Modified events	467	692	624	1783
Phases added	39	49	64	152
Phases changed or removed	318	437	379	1134
Retiming only	110	206	181	497

Table 3.5.1. IMS phase detections and events summary.

4 Improvements and modifications

4.1 NORSAR

NORSAR Data acquisition

No modification has been done to the NORSAR data acquisition system.

The process of evaluating technical options for upgrading the array is continuing. The requirement is to find digitizer units that will fit into existing seismometer vaults, and that may use existing buried cables for DC power and data transmission to each subarray center. So far it seems to be possible to use the Nanometric RD3 digitizers at the seismometer with help of small batteries. These digitizers give 24-bit dynamic range using 16-bit resolution and automatic gain ranging (comparable to NORESS). Digitizers with 24-bit resolution are also available, but the power requirement for most existing units is currently beyond the supported level at the seismometer site.

Continued research will be done to find 24-bit resolution digitizers with satisfactory power consumption.

Data center operation, communication with subarrays, and subarray processing systems in connection with the upgrade appear to pose few problems, as many of the NORESS/FINESA/GERESS/Hagfors concepts may be used.

A test of a full subarray acquisition system will be performed at the end of the next reporting period.

NORSAR Detection processing

The NORSAR detection processor has been running satisfactorily on the IBM 4341/4381 computers during this reporting period.

Detection statistics are given in section 2.

NORSAR Event processing

There are no changes in the routine processing of NORSAR events, using the IBM system. Full event processing on the SUN system is not yet implemented. Processing of the large NORSAR array requires a data base of time delay corrections to get the benefit of using the array for locating teleseismic events. The current time delay correction data base on IBM is not easy to convert to SUN/unix installations. In light of a future upgrade of the system, a research task would be to build a new time delay correction data base for the NORSAR array, with a design that may be used for any type of array and computer system.

4.2 Regional arrays

Detection processing

The routine detection processing of the regional arrays is running satisfactorily on each of the arrays' SUN-3/280 acquisition systems. The same program is used for NORESS/ARCESS/ FINESA, but with different recipes. The beam table for NORESS/ARCESS may be found in NORSAR Sci. Rep. No. 1-89/90. The beam deployment for FINESA is given in Table 4.2.1.

Event processing. Phase estimation

This process applies F-K and polarization analysis to each detection in order to determine phase velocity, azimuth and type of phase.

The processing makes use of the EP program, and may be performed on any of the SUN workstations.

Plot and epicenter determination

A description of single array event processing has been given in NORSAR Sci. Rep. No. 2-88/89.

The processing makes use of the EP program, and may be performed on any of the SUN workstations. Different recipes are used for each array, as the rules for associating phases are somewhat different. In particular, the relation between Sn, Lg and Rg in terms of amplitudes is quite different for the three arrays.

The main output is event parameters and plots of single sensor and beam traces for each regional and teleseismic event. These plots are useful both for assessing processing performance and in monitoring array data quality.

The routine processing of FINESA data at NORSAR is similar to what is done in Helsinki.

Automatic single array event bulletins are available, but the solutions are not routinely reviewed, as this is the task for the IMS system.

4.3 GSETT-2 experiments

EP recipes for extracting NORESS/ARCESS events and producing level 1 and level 2 data files have been developed.

The EP program reads phase information from the automatic (or reviewed) bulletins, accesses the necessary seismometer data, forms array beams, and produces level 2 data files.

J. Fyen

BEAM	Velocity	Azimuth	Filter band	Threshold		Configuration
C011	99999.9	0.0	0.50 - 1.50	4.20	7	A1 C
C021	99999.9	0.0	1.0 - 3.0	4.20	7	A1 C
C031	99999.9	0.0	1.50 - 3.50	4.20	7	A1 C
C032	11.0	30.0	1.50 - 3.50	4.20	7	A1 C
C033	11.0	90.0	1.50 - 3.50	4.20	7	A1 C
C034	11.0	150.0	1.50 - 3.50	4.20	7	A1 C
C035	11.0	210.0	1.50 - 3.50	4.20	7	A1 C
C036	11.0	270.0	1.50 - 3.50	4.20	7	A1 C
C037	11.0	330.0	1.50 - 3.50	4.20	7	A1 C
C038	15.0	80.0	1.50 - 3.50	3.70	7	A1 C
C039	10.0	20.0	1.50 - 3.50	3.70	7	A1 C
C041	99999.9	0.0	2.0 - 4.0	4.20	7	A1 C
C042	10.20	30.0	2.0 - 4.0	4.20	7	A1 C
C043	10.20	90.0	2.0 - 4.0	4.20	7	A1 C
C044	10.20	150.0	2.0 - 4.0	4.20	7	A1 C
C045	10.20	210.0	2.0 - 4.0	4.20	7	A1 C
C046	10.20	270.0	2.0 - 4.0	4.20	7	A1 C
C047	10.20	330.0	2.0 - 4.0	4.20	7	A1 C
C048	15.0	80.0	2.0 - 4.0	3.70	7	A1 C
C049	10.0	20.0	2.0 - 4.0	3.70	7	A1 C
C051	99999.9	0.0	2.50 - 4.50	4.20	12	B1 BC
C052	8.90	30.0	2.50 - 4.50	4.20	12	B1 BC
C053	8.90	90.0	2.50 - 4.50	4.20	12	B1 BC
C054	8.90	150.0	2.50 - 4.50	4.20	12	B1 BC
C055	8.90	210.0	2.50 - 4.50	4.20	12	B1 BC
C056	8.90	270.0	2.50 - 4.50	4.20	12	B1 BC
C057	8.90	330.0	2.50 - 4.50	4.20	12	B1 BC
C058	15.0	80.0	2.50 - 4.50	3.70	12	B1 BC
C061	99999.9	0.0	3.0 - 5.0	4.20	12	B1 BC
C062	10.50	30.0	3.0 - 5.0	4.20	12	B1 BC
C063	10.50	90.0	3.0 - 5.0	4.20	12	B1 BC
C064	10.50	150.0	3.0 - 5.0	4.20	12	B1 BC
C065	10.50	210.0	3.0 - 5.0	4.20	12	B1 BC
C066	10.50	270.0	3.0 - 5.0	4.20	12	B1 BC
C067	10.50	330.0	3.0 - 5.0	4.20	12	B1 BC
C068	15.0	80.0	3.0 - 5.0	3.70	12	B1 BC
C071	99999.9	0.0	3.50 - 5.50	4.20	15	A1 ABC
C072	11.10	30.0	3.50 - 5.50	4.20	15	A1 ABC
C073	11.10	90.0	3.50 - 5.50	4.20	15	A1 ABC
C074	11.10	150.0	3.50 - 5.50	4.20	15	A1 ABC
C075	11.10	210.0	3.50 - 5.50	4.20	15	A1 ABC

C076	11.10	270.0	3.50 - 5.50	4.20	15	A1 ABC
C077	11.10	330.0	3.50 - 5.50	4.20	15	A1 ABC
C081	99999.9	0.0	4.0 - 8.0	4.20	15	A1 ABC
C082	9.50	30.0	4.0 - 8.0	4.20	15	A1 ABC
C083	9.50	90.0	4.0 - 8.0	4.20	15	A1 ABC
C084	9.50	150.0	4.0 - 8.0	4.20	15	A1 ABC
C085	9.50	210.0	4.0 - 8.0	4.20	15	A1 ABC
C086	9.50	270.0	4.0 - 8.0	4.20	15	A1 ABC
C087	9.50	330.0	4.0 - 8.0	4.20	15	A1 ABC
C091	99999.9	0.0	5.0 - 10.0	4.70	15	A1 ABC
C092	10.50	30.0	5.0 - 10.0	4.70	15	A1 ABC
C093	10.50	90.0	5.0 - 10.0	4.70	15	A1 ABC
C094	10.50	150.0	5.0 - 10.0	4.70	15	A1 ABC
C095	10.50	210.0	5.0 - 10.0	4.70	15	A1 ABC
C096	10.50	270.0	5.0 - 10.0	4.70	15	A1 ABC
C097	10.50	330.0	5.0 - 10.0	4.70	15	A1 ABC
C101	99999.9	0.0	8.0 - 16.0	4.70	9	A1 AB
C102	9.90	30.0	8.0 - 16.0	4.70	9	A1 AB
C103	9.90	90.0	8.0 - 16.0	4.70	9	A1 AB
C104	9.90	150.0	8.0 - 16.0	4.70	9	A1 AB
C105	9.90	210.0	8.0 - 16.0	4.70	9	A1 AB
C106	9.90	270.0	8.0 - 16.0	4.70	9	A1 AB
C107	9.90	330.0	8.0 - 16.0	4.70	9	A1 AB
CI01	99999.9	0.0	0.50 - 1.50	2.50	7	A1 C
CI02	99999.9	0.0	1.0 - 2.0	2.50	7	A1 C
CI03	99999.9	0.0	1.50 - 2.50	2.50	7	A1 C
CI04	99999.9	0.0	2.0 - 4.0	2.10	7	A1 C
CI05	99999.9	0.0	3.50 - 5.50	2.10	7	A1 C
CI06	99999.9	0.0	5.0 - 10.0	2.50	7	A1 C

Table 4.2.1. FINESA beam table. The table shows the name of the beam, velocity (km/sec), azimuth (degrees), filter band (Hz), STA/LTA threshold, and configuration. The configuration is described with number of sensors and A,B or C-rings, with center A1 or B1. CI01 - CI06 are incoherent beams.

5 Maintenance Activities

5.1 Activities in the field and at the Maintenance Center

This section summarizes the activities in the field, at the Maintenance Center (NMC) Hamar and NDPC activities related to monitoring and control of the NORSAR, NORESS and ARCESS arrays.

Activities comprise preventive/corrective maintenance in connection with all the NORSAR subarrays, NORESS and ARCESS. In addition, NMC has been involved in modification of equipment (FINESA) and preparatory work in connection with HF instrumentation (NORESS). Other activities are related to testing the NORSAR communications systems.

NORSAR

In the NORSAR array, spike complaints have been investigated, SP/LP channel gain adjusted, LP seismometer parameters corrected, SLEMs have been replaced, batteries and transmitters replaced at the telemetry stations, and communications lines have been tested, including modems and level checks.

NORESS

The NORESS array has been visited in connection with preparing vault C2 for HF instrumentation instead of A0. Hub 69 cards (I/F) have been replaced, and the Hub power supply repaired. NORESS has been visited in connection with communication trouble, all equipment in vault C2 was removed as a precaution, ADC card replacements were done.

ARCESS

ARCESS activities comprise resetting of the "white box", replacement of GPS synchronized clock (satellite clock), and replacement of fiber optic transmitters.

Details are presented in Table 5.1.

Subarray/ area	Task	Date
NORSAR:		
01A	SA visited in connection with spike complaints	18 Oct
06C	All SP channel gains adjusted.	18 Oct
NORESS:	Vault C2 made ready in order prepare this vault for HF instrumentation instead of A0	4–6 Oct
	Hub 69 card (I/F card) repaired due to a bad line driver	18 Oct
FINESA:	Field maintenance	week 48
NMC:	General work, incl. the FINESA acquisition system equipment	Oct
NDPC:	Daily check of data and comm. systems NORSAR, NORESS, ARCESS and FINESA.	Oct
	Weekly calibration of SP/LP instruments.	
	Continuous measurement of Mass Position and Free Period	
	Adjustment of Mass Position and Free Period when outside tolerances	
NORSAR:		
06C	Adjusted SP/LP instruments.	9 Nov
02B	Visit in connection with degraded data.	22 Nov
04C/06C	Adjustment of SP/LP instruments.	23 Nov
02B	Replaced Digital Unit (DCU)	24 Nov
01B/02C	Adjustment of SP/LP instruments.	27 Nov
03C	Adjustment of SP/LP instruments.	30 Nov
NORESS:	Hub reset.	21 Nov
FINESA:	Installation of a new data acquisition system.	13–16 Nov
NDPC:	Daily check of data and comm. systems NORSAR, NORESS, ARCESS and FINESA.	Nov
	Weekly calibration of SP/LP instruments.	
	Continuous measurement of Mass Position and Free Period	
	Adjustment of Mass Position and Free Period when outside tolerances	

Table 5.1 Activities in the field and the NORSAR Maintenance Center, including NDPC activities related to the NORSAR array, 1 October 1989 - 31 March 1990.

Subarray/ area	Task	Date
NORSAR:		
02B(tel)	Replaced batteries at stations 1, 5 and 6.	1,4,7,8
	Replaced transmitter at 1 and 5.	9,12 and 18 Dec
01A	Line test and SP/LP adjustment.	6 Dec
NORESS:	Hub power supply repaired.	24 Dec
ARCESS:	NORSAR's local contact visited the site and reset the "white box".	
FINESA:	Data acquisition unit returned from Finland and modified with respect to hardware and software	14 Dec
NDPC:	Daily check of data and comm. systems NORSAR, NORESS, ARCESS and FINESA. Weekly calibration of SP/LP instruments. Continuous measurement of Mass Position and Free Period Adjustment of Mass Position and Free Period when outside tolerances	Dec
NORSAR:		
01A,06C	Communications test.	3 Jan 1990
NORESS:	Visit in connection with communications trouble	6 Jan
FINESA:	Faulty cable located between B2 and C5. Replaced amplifier (C6).	30-31 Jan
NDPC:	Daily check of data and comm. systems NORSAR, NORESS, ARCESS and FINESA. Weekly calibration of SP/LP instruments. Continuous measurement of Mass Position and Free Period Adjustment of Mass Position and Free Period when outside tolerances	Jan
NORSAR:		
01A	Line and communications tests.	7 Feb
06C	Line and communications tests.	7 Feb
06C	NTA/Hamar was advised to check the line level toward the CTV. As a result, the level was raised by 5 dBm.	15 Feb
02B(tel)	A new battery was installed at the receiving station.	9 Feb

Table 5.1 (cont.)

Subarray/ area	Task	Date
NORESS:	As a precaution, all equipment in the vault C2 was disconnected and removed.	23 Feb
NDPC:	Daily check of data and comm. systems NORSAR, NORESS, ARCESS and FINESA.	Feb
	Weekly calibration of SP/LP instruments.	
	Continuous measurement of Mass Position and Free Period	
	Adjustment of Mass Position and Free Period when outside tolerances	
NORSAR:		
02B(tel)	Replaced station 4 battery.	12 Mar
ARCESS:	Replaced GPS synchronized clock (satellite clock) with a 4F-DC Radio Clock.	19–23 Mar
	Replaced fiber optic transmission at remote site D6.	
	Replaced fiber optic transmission at Hub site B3.	
NDPC:	Daily check of data and comm. systems NORSAR, NORESS, ARCESS and FINESA.	Mar
	Weekly calibration of SP/LP instruments.	
	Continuous measurement of Mass Position and Free Period	
	Adjustment of Mass Position and Free Period when outside tolerances	

Table 5.1 (cont.)

5.2 Array status

As of 31 Mar 1990 the following NORSAR channels deviated from tolerances.

01A 01 8 Hz filter
    02 8 Hz filter
    04 30 dB attenuator
02C 04 Spikes

O.A. Hansen

6 Documentation developed

Dahle, A., H. Bungum and L.B. Kvamme: Attenuation models inferred from intraplate earthquake recordings. *Earthq. Eng. and Structural Dynamics*, in press.

Hansen, R.A., F. Ringdal and P.G. Richards: The stability of RMS Lg measurements and their potential for accurate yields of Soviet underground nuclear explosions. Submitted *Bull. Seism. Soc. Am.*, Special Issue.

Kushnir, A., V.M. Lapshin, V.I. Pinsky and J. Fyen: Statistically optimal event detection using small array data. Submitted *Bull. Seism. Soc. Am.*, Special Issue.

Mykkeltveit, S., F. Ringdal, T. Kværna and R.W. Alewine: Application of regional arrays in seismic verification research. Submitted *Bull. Seism. Soc. Am.*, Special Issue.

Ringdal, F.: Teleseismic event detection using the NORESS array, with special reference to low-yield Semipalatinsk explosions. Submitted *Bull. Seism. Soc. Am.*, Special Issue.

Semiannual Tech. Summary, 1 Oct 1989 - 31 March 1990, NORSAR Sci. Rep. No. 1-89/90, Kjeller, Norway.

Ødegaard, E., D.J. Doornbos and T. Kværna: Surface topographic effects at arrays and 3-component stations. Submitted *Bull. Seism. Soc. Am.*, Special Issue.

L.B. Loughran

7 Summary of Technical Reports / Papers Published

7.1 Report from the symposium on "Regional Seismic Arrays and Nuclear Test Ban Verification" in Oslo, Norway, 14–17 February 1990

During 14–17 February 1990 NORSAR hosted an international symposium entitled "Regional Seismic Arrays and Nuclear Test Ban Verification". The symposium was attended by 76 scientists and representatives from 21 countries, including a large number of seismologists participating in the work of the Conference on Disarmament's Group of Scientific Experts (GSE) in Geneva.

The purpose of the symposium was to assess the state-of-the-art of research on regional seismic arrays and associated topics. In particular, the symposium focused upon the advanced regional arrays NORESS and ARCESS in Norway and their associated data processing facilities, in the light of the potential of such arrays to provide a much improved monitoring capability for a future comprehensive nuclear test ban treaty. During a three-day scientific symposium, a number of presentations were given on topics relevant to this issue. A special session was devoted to summarizing the experience and discussing further plans for the on-going international GSE experiment (GSETT-2).

In this paper, we give a brief review of some of the results presented during the scientific symposium. A list of all the presentations is provided in an appendix, and the numbers in brackets refer to this list. The majority of the papers have been submitted for publication to the *Bulletin of the Seismological Society of America*, and will be published in a Special Issue of the *Bulletin*, scheduled to appear in the fall of 1990.

Development of regional arrays

Reviews of recent developments with regard to regional seismic arrays are presented for NORESS and ARCESS in Norway [1], GERESS in the Federal Republic of Germany [2] and FINESA in Finland [3]. Paper [1] summarizes the design considerations leading to the establishment of the first regional array, NORESS, and describes how the success of this new array concept motivated the deployment of additional arrays of this type. The paper documents the basic signal processing techniques used in real-time data analysis for regional arrays, and demonstrates the excellent detection performance of such arrays at regional distances (less than 2000 km). It is shown that NORESS and ARCESS are capable of detecting seismic events of magnitude 2.5 with 90 per cent probability, if these events occur within 1000 km distance, whereas global teleseismic networks have much higher event detection thresholds. The FINESA array is also documented to have an excellent performance [3], and

together, these three arrays are capable of locating weak seismic events in Fennoscandia very accurately (typically to within 10–20 km). The GERESS array currently under development shows many of the same excellent features [2], and will contribute further to an excellent regional coverage of large parts of Northern Europe.

Processing of data from a network of regional arrays

Recent technological advances have allowed very sophisticated processing techniques to be applied in detecting, locating and identifying seismic events using a network of seismic arrays and single stations, and this is highlighted by the development of the Intelligent Monitoring System (IMS) [4],[5]. Two of the goals for this system are (1) to demonstrate the monitoring performance and capability of the system for small events at regional distances and (2) to explore the promise of an expert-systems approach for providing improved monitoring performance as experience accumulates. The first operational version, described in [4], processes data from NORESS and ARCESS, whereas later versions will be expanded to networks including both arrays and single stations. The IMS is ambitious in exploring and integrating many new computer technologies, and the validity of the concept is documented in an evaluation of its initial operational performance [5].

Signal analysis methods

A number of presentations addressed methods for processing seismic signals recorded by arrays as well as three-component stations. It was demonstrated that both types of stations can provide information very useful in phase identification, azimuth estimation and estimating the apparent velocity of detected phases. From theoretical considerations as well as from experimental comparison [12],[26],[14] arrays are shown to be superior in this regard at low signal-to-noise ratios, although the precision e.g. of azimuth estimates is influenced by a number of factors, including phase type, frequency of the signal and systematic bias caused by earth heterogeneities [14],[18], [26]. A very promising approach, discussed in [17] is that of joint analysis of 3-component and array data.

Signal detection methods are discussed in several papers. In [11], a system for on-line detection and signal analysis is presented as applied to a Soviet 3-component station in Kazakhstan. In [13], a detection technique is described using NORESS array and 3-component data. A statistical approach, using adaptive techniques, to detection processing and estimation is presented in [7] for array data and [15] for 3-component data. A new approach to obtain precise relative location estimates of seismic events, using high frequency recordings, is presented in [25].

Source identification

Traditionally, seismic discrimination research has focused on distinguishing between earthquakes and underground nuclear explosions. Under a Comprehensive Test Ban Treaty, emphasis will be on detecting and identifying *weak* seismic events, and a third category, large chemical explosions for industrial purposes (e.g. mining work) will become important to consider. In [10], a very promising method is applied to NORESS data to discriminate between earthquakes and ripple-fired quarry blasts (mining events consisting of several explosions closely grouped in space and time). Using spectral characteristics of the signals, an "automatic" discriminant is proposed computing the likelihood that ripple firing occurred in each given case.

In [8], a novel approach making use of artificial neural networks is used to develop a classification procedure between earthquakes and mining explosions. Also in this approach, the spectral characteristics of the signals form the basis for the discriminants. The neural network appears to improve in particular the classification of outliers in the population, and reduce the number of uncertain events. Application of neural networks in improving seismic processing performance is also addressed in [9].

Of considerable interest for source identification is also the method proposed in [16], applying transfer functions to transform e.g. between recordings of presumed single explosions and ripple-fired explosions, and also between recordings at different NORESS sensors for a given event. This gives promise to improve the coherence of seismic phases recorded at an array, with ensuing implications for improved source parameter estimation. In [6], a case-based reasoning approach to event identification is discussed, and a waveform envelope matching technique is applied to a set of Western Norway earthquakes and explosions.

Detection thresholds and in-country networks

While regional arrays were originally designed to enhance the capabilities for detecting and characterizing weak seismic events at regional distances, they have also been found very effective in the teleseismic distance range. As an example, published yields of Soviet underground nuclear explosions at Semipalatinsk have been used to evaluate the NORESS detection threshold, in terms of explosive yield for events at this test site [21]. The threshold for detection at NORESS is estimated to be as low as 0.1 kt, assuming full coupling and normal noise conditions. It is pointed out that NORESS has particularly favorable conditions for detecting small events from this test site, and that the seismic identification threshold necessarily will be higher than the detection threshold.

Data from new Global Seismic Network stations in the Soviet Union, installed as a cooperative project between American and Soviet scientists, have

been applied in several studies to address problems relevant to an in-country monitoring network. Seismic noise levels at these stations are analyzed in [19], and found to be higher than at NORESS in the band 1-20 Hz, with maximum difference ranging from 7 to 25 dB, depending on the station. However, significant noise reduction can be achieved by borehole deployment.

Using data from stations in the USSR, the frequency-dependent attenuation of regional seismic phases has been studied in [22]. Attenuation characteristics are found to be similar to those observed in Scandinavia, but with an absolute Pn amplitude almost a factor of 2 higher in eastern Kazakhstan for a fixed Lg magnitude.

Recordings of Semipalatinsk nuclear explosions at the new Global Seismic Network stations in the Soviet Union, together with data from stations in China have been analyzed in [20] and it is shown that RMS Lg can be measured at widely separated stations with a remarkable degree of consistency. The standard deviation of the differences between pairs of stations is as low as 0.03–0.04 in logarithmic units, and reliable measurements may be made at magnitude (m_b) down to about 4.0 for stations situated about 1500 km away from Semipalatinsk. The importance of this observation in terms of supplying yield estimates for nuclear explosions down to and even below one kiloton is pointed out.

Earth structure, wave propagation, scattering

Several of the papers were devoted to studies of general problems in seismology and geophysics, in areas relevant to the seismic monitoring issue. The structure of the crust and upper mantle in parts of Northern Eurasia is addressed in papers [23], [24], [27] and [29], with the three latter papers specifically making use of regional array data. Seismic wave propagation and scattering are addressed in a number of papers, e.g. [13], [26], [28], [29], [30].

Conclusion

The Oslo symposium demonstrated the considerable progress in the field of seismic monitoring during recent years. It particularly highlighted the technological advances in seismic instrumentation, data communication and computer processing, as exemplified by the development of advanced regional seismic arrays with very sophisticated automatic and interactive signal processing facilities. The presentations at the scientific symposium show that these technological advances are accompanied by considerable scientific progress, although much work remains in order to fully exploit the potential offered by regional arrays in a seismic monitoring context.

F. Ringdal
S. Mykkeltveit

Appendix

List of scientific presentations given during the 1990 Oslo Symposium on Regional Seismic Arrays and Nuclear Test Ban Verification

References

[1] Svein Mykkeltveit[1], Frode Ringdal[1] and Ralph W. Alewine[2] — [1] NORSAR, Norway, and [2] DARPA, USA: "Application of Regional Arrays in Seismic Verification Research"

[2] Hans Peter Harjes — Ruhr Univ., Fed. Rep. of Germany: "Design and Siting of a New Regional Array in Central Europe"

[3] Marja Uski — University of Helsinki, Finland: "The Upgraded FINESA Array and Experiences of Data Analysis"

[4] Thomas C. Bache[1], James Wang[1], Robert M. Fung[2], Cris Kobryn[1] and Jeffrey Given[1] — [1] Science Applications International Corp., USA, and [2] Advanced Decision Systems, USA: "The Intelligent Monitoring System"

[5] Steven Bratt, Henry Swanger, Richard Stead and Floriana Ryall — Science Applications International Corp., USA: "Results from the Intelligent Monitoring System"

[6] Douglas Baumgardt and Gregory Young — ENSCO, Inc., USA: "Regional Seismic Waveform Patterns and Case-based Event Identification using Regional Arrays"

[7] A. Kushnir, V. Laphsin, V. Pinsky and V. Pisarenko — Inst. of Physics of the Earth, USSR: "Statistical Procedures for Seismic Signal Detection and Estimation by using Small Array Data"

[8] Paul Dysart[1] and Jay Pulli[2] — [1] Science Applications International Corp., USA, and [2] Radix Systems, Inc., USA: "Regional Seismic Event Classification at the NORESS Array: Seismological Measurements and the Use of Trained Neural Networks"

[9] Kenneth Anderson — BBN, USA: "Automatic Improvement of Seismic Array Performance"

[10] Michael J. Hedlin, J. Bernard Minster and John A. Orcutt — Scripps Inst. of Oceanography, UCSD, USA: "An 'Automatic' Means to Discriminate between Earthquakes and Quarry Blasts"

[11] O.K. Kedrov and V.M. Ovtchinnikov — Inst. of Earth Physics, USSR: "An On-Line Analysis System for Three-Component Seismic Data: Method and Preliminary Results"

[12] David B. Harris — Lawrence Livermore National Laboratory, USA: "A Comparison of the Direction Estimation Performance of High-Frequency Seismic Arrays and Three-Component Stations"

[13] B.O. Ruud, E.S. Husebye and S.C. Bannister — University of Oslo, Norway: " NORESS Recording — Joint 3C and Array Analysis"

[14] Anne Suteau-Henson — Science Applications International Corp., USA: "Estimating Azimuth and Slowness from Three-Component and Array Stations"

[15] A. Kushnir, V. Pinsky, V. Pisarenko and I. Savin — Institute of Physics of the Earth, USSR: "Wavelet Decomposition and Parameter Estimation Using 3-Component Seismograms"

[16] Zoltan A. Der[1] and Robert H. Shumway[2] — [1] ENSCO, Inc., USA, and [2] University of California at Davis, USA: "Coherent Array Processing of Regional Seismic Data for Ripple Fire Patterns, Source Mechanisms and Source Azimuths"

[17] D.C. Jepsen and B.L.N. Kennett — Australian National University, Canberra, Australia: "Three-component Array Analysis of Regional Seismograms"

[18] Dorthe Bame, Marianne C. Walck and Kathie L. Hiebert-Dodd — Sandia National Laboratory: "Azimuth Estimation Capabilities of the NORESS Regional Seismic Array"

[19] Holly K. Given — Scripps Inst. of Oceanography, UCSD, USA: "Broadband Seismic Noise and Detection Experiments at IRIS/IDA Stations in the USSR"

[20] Roger A. Hansen[1], Frode Ringdal[1] and Paul G. Richards[2] — [1] NORSAR, Norway, and [2] Lamont-Doherty Geological Observatory, USA: "The Stability of RMS Lg Measurements, and their Potential for Accurate Estimation of the Yields of Soviet Underground Nuclear Explosions"

[21] Frode Ringdal — NORSAR, Norway: "Teleseismic Event Detection using the Small-Aperture NORESS and ARCESS Arrays"

[22] Thomas Sereno — Science Applications International Corp., USA: "Frequency-Dependent Attenuation in Eastern Kazakhstan and Implications for Seismic Detection Thresholds in the Soviet Union"

[23] A. Egorkin — International Inst. of Earthquake Prediction, USSR: "New Methods of Seismic Surface Wave Data Processing and its Application for the Study of the North Eurasian Shelf Structure"

[24] Vladimir Ryaboy — Science Applications International Corp., USA: "Upper Mantle Structure along a Profile from Oslo (NORESS) to Helsinki to Leningrad, based on Explosion Seismology"

[25] Hans Israelsson — Science Applications International Corp., USA: "Studies Using Seismic High Frequency Data"

[26] Erik Ødegaard[1], Durk Doornbos[1] and Tormod Kværna[2] — [1] University of Oslo, Norway, and [2] NORSAR, Norway: "Topographic Effects on Arrays and Three-Component Stations"

[27] Kristin Vogfjord and Charles Langston — Penn State Univ., USA: "Analysis of Regional Events Recorded at NORESS"

[28] I. Gupta, C.S. Lynnes and R.A. Wagner — Teledyne Geotech, USA: "F-K Analysis of NORESS Array and Single-Station Data to Identify Sources of Near-Receiver and Near-Source Scattering"

[29] Douglas Baumgardt — ENSCO, Inc., USA: "Investigation of Teleseismic Lg Blockage and Scattering using the NORESS and ARCESS Regional Arrays"

[30] Anton Dainty and M. Nafi Toksoz — Earth Resources Lab., MIT, USA: "Array Analysis of Seismic Scattering"

7.2 Analysis of data from the British station GAM near Garm, USSR for Soviet nuclear explosions

This contribution is a follow-up to earlier work (Ringdal and Marshall, 1989; Hansen *et al*, 1989; and Hansen and Ringdal, 1989) aimed at evaluating the stability of seismic Lg magnitudes for yield estimation purposes. In particular, these efforts have involved analyzing available Lg data from Soviet nuclear explosions at the Shagan River, Semipalatinsk test site, and conducting comparative analyses of Lg and P recordings at various seismograph stations.

Hansen *et al* (1989) analyzed data recorded at four digital stations installed by IRIS in the Soviet Union, and found an excellent correspondence between Lg measurements at these stations and the NORSAR M(Lg) estimates published by Ringdal and Marshall (1989). Furthermore, they noted the very high Lg signal-to-noise ratio observed at the IRIS stations, in particular ARU and GAR, and concluded that reliable Lg measurements at these stations would be possible for explosions as small as $m_b = 4.0$, assuming normal noise conditions.

Hansen and Ringdal (1989) extended the analysis to data from the China Digital Seismograph Network (CDSN), which is operated by the USGS in cooperation with the State Seismological Bureau, Beijing. Two of the CDSN stations, WMQ in Urumqi and HIA in Hailar, have particularly good Lg propagation paths from Semipalatinsk, and they based their analysis on data from these two stations.

In this paper, we extend the analysis to data from a broad-band seismic station, GAM, installed very near the IRIS station near Garm, USSR (The BSVRP Working Group, (1989)). This data supplements the previously sparse data from GAR and allows the comparison of two closely separated seismic stations.

Fig. 7.2.1 shows the locations of several stations in the USSR and China in relation to the test site, as well as locations of the NORSAR. (The GAM station and GAR IRIS station are located at the same place on the map and indicated only by the GAR symbol.) The station GAM at a distance of about 1380 km shows excellent Lg recordings of Semipalatinsk explosions, as illustrated by the examples in Fig. 7.2.2.

In the analysis of GAM Lg recordings, we have employed the exact same procedure as described for IRIS data by Hansen *et al* (1989), and the details will not be repeated here. Data from a total of 6 Shagan River explosions, dating back to 1988, were provided to us for this analysis by the BSVRP Group in Britain. Table 7.2.1 lists these events along with the estimated parameters.

Fig. 7.2.3 shows a comparison of GAM and NORSAR log RMS (Lg) estimates for these 6 events. The slope of the plot is 0.92, and the orthogonal

standard deviation of the differences between the two stations is only 0.035 units. This is essentially the same scatter found earlier by Hansen *et al* (1989) when comparing data from NORSAR and the Soviet station ARU, and confirms the excellent stability of the RMS Lg estimates.

As a contrast to these well recorded events, Fig. 7.2.4 illustrates the capabilities of the GAM station to record an m_b(P) 3.8 event from the Shagan River test site on day 270 (September 26) of 1988. (This magnitude is based on the NORSAR m_b(P) of 4.3 with an assumed regional correction of 0.5 units for comparison to world wide m_b estimates and therefore must be considered somewhat uncertain). The unfiltered broad band trace at GAM essentially shows no signal for this event, however the band pass filtered trace clearly shows energy arriving that can be identified as Lg with a signal to noise ratio of about 2. (Similar SNR was obtained by Hansen *et al* (1989) for the recording at ARU for this event.) This SNR is near the lower limit of about 1.5 for allowing reliable RMS Lg estimates at a single site.

Fig. 7.2.5 illustrates the stability of the RMS Lg amplitudes by comparing GAM and ARU. These stations are chosen as they are the only pair for which we have Lg recordings of the m_b(P) 3.8 event shown in Fig. 7.2.4 and so illustrate the stability of measurement covering a span of two full magnitude units. Here we again have a slope of very nearly one still with an orthogonal standard deviation of only 0.026 logarithmic units (i.e. magnitude units).

Fig. 7.2.6 compares the signal-to-noise ratios (SNR) (defined as RMS Lg signal to pre-P RMS noise in the 0.6 to 3.0 Hz band) for stations at various distances, using 5 large explosions. The range in magnitude (m_b) is from 5.2 for the event on day 317 of 1988 to 6.1 for the JVE event on day 258 of 1988. The event on day 317 indicates the minimum for which RMS Lg was measured at NORSAR at a distance of about 4200 km with a signal to noise ratio of about 1.1. For this same event a signal to noise ratio of about 30 is observable at ARU and GAR at a distance of about 1500 km and about 80 at WMQ at a distance of 950 km. Again, the event at day 258 of 1988 in Fig. 7.2.6 (shown with the open circle around a plus sign) shows an SNR gain of nearly 100 between NORSAR with an SNR of 3.5 and WMQ with an SNR of 331. (It should be noted that the low SNR for this event at ARU is due to the fact that this event was only recorded on the low gain channel which does not adequately resolve the background noise.) It can be seen that the SNR for GAM fits nicely to the trend as a function of distance, and actually is slightly better than for GAR for all common events.

In conclusion, our studies confirm that Lg magnitude estimates of Semipalatinsk explosions are remarkably consistent between stations widely distributed in epicentral distance and azimuth. It thus appears that a single station with good signal-to-noise ratio can provide m_b(Lg) measurements with an

accuracy (one standard deviation) of about 0.03 magnitude units. Therefore, Lg signals appear to provide an excellent basis for supplying estimates of the yields of nuclear explosions even down to below one kiloton, when such signals are recorded at high-quality digital *in-country* seismic stations, and when calibrated by access to independent (non-seismic) yield information for a few nuclear explosions at the test sites of interest. For a review of previous studies of Lg amplitudes and a more detailed account of this work see Hansen *et al* (1990).

R.A. Hansen

References

The BSVRP Working Group (1989): The British Seismic Verification Research Project (BSVRP), *Q. J. R. Astr. Soc.*, 30, 311-324.

Hansen, R.A., F. Ringdal and P.G. Richards (1989): Analysis of IRIS data for Soviet nuclear explosions, *NORSAR Semiannual Tech. Summary, 1 Oct 1988 - 31 Mar 1989*, NORSAR Sci. Rep. 2-88/89.

Hansen, R.A. and F. Ringdal (1989): Analysis of data from the China Digital Seismograph Network (CDSN) for Soviet nuclear explosions, *NORSAR Semiannual Tech. Summary, 1 Apr 1989 - 30 Sep 1989*, NORSAR Sci. Rep. 1-89/90.

Hansen, R.A., F. Ringdal and P.G. Richards (1990): The Stability of RMS Lg Measurements, and Their Potential for Accurate Estimation of the Yields of Soviet Underground Nuclear Explosions. Manuscript accepted by *Bull. Seism. Soc. Am.*.

Ringdal, F. and P.D. Marshall (1989): Yield determination of Soviet underground nuclear explosions at the Shagan River Test Site, *NORSAR Semiannual Tech. Summary, 1 Oct 1988 - 31 Mar 1989*, NORSAR Sci. Rep. 2-88/89.

No.	Date	m_b	GAM Lg
1	88258	6.03	3.184
2	88270	3.8	1.196
3	88317	5.20	2.521
4	88352	5.80	3.034
5	89022	6.0	3.161
6	89043	5.90	2.923

Table 7.2.1 Magnitudes (m_b) and log RMS Lg values at GAM for 6 explosions analyzed in this study.

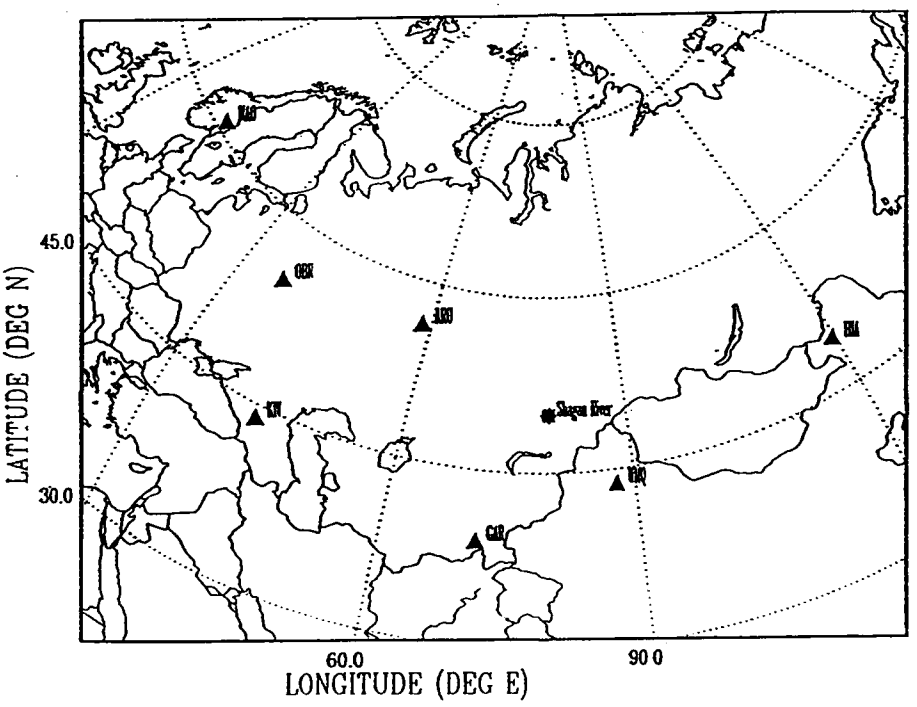

Fig. 7.2.1 Map indicating the locations of the Shagan River Test Site, the IRIS and British stations in the USSR, the NORSAR array in Norway and the stations WMQ and HIA in China. The NORESS array is collocated near the NORSAR array, and the station GAM is collocated near the GAR station.

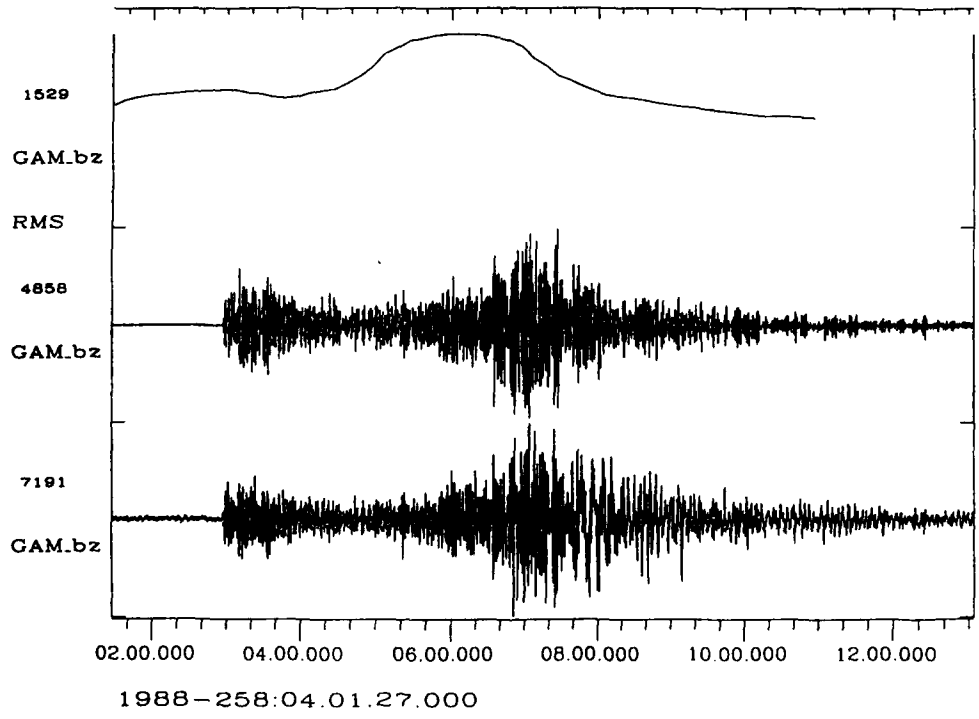

Fig. 7.2.2 Example of recordings from a Soviet nuclear explosion (14 Sept 1988) at the station GAM. For each of the three components we show the unfiltered trace (bottom), the filtered trace (0.6–3.0 Hz) and the 120-second window RMS measure (top) as a function of time.

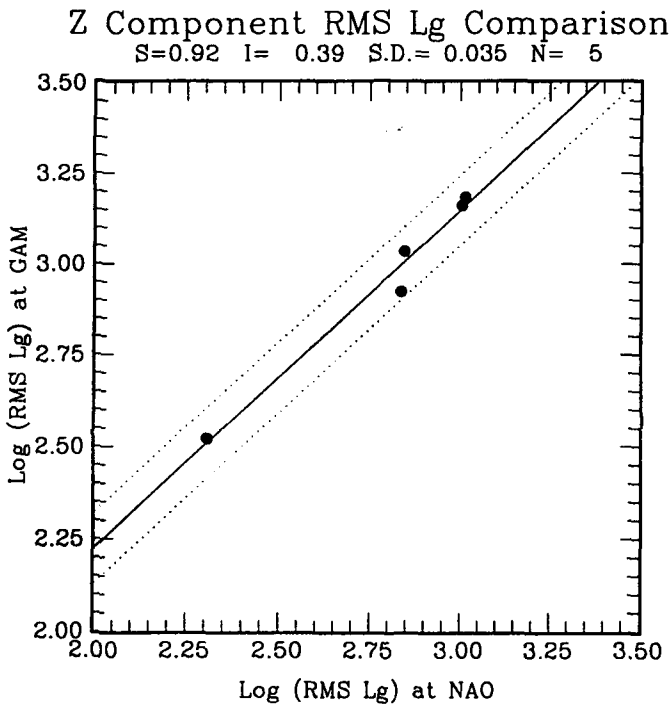

Fig. 7.2.3 Comparison of log RMS Lg measurements obtained at GAM and NORSAR. The standard deviation of the differences is 0.035 orthogonal to the line. The dotted lines correspond to plus or minus two standard deviations.

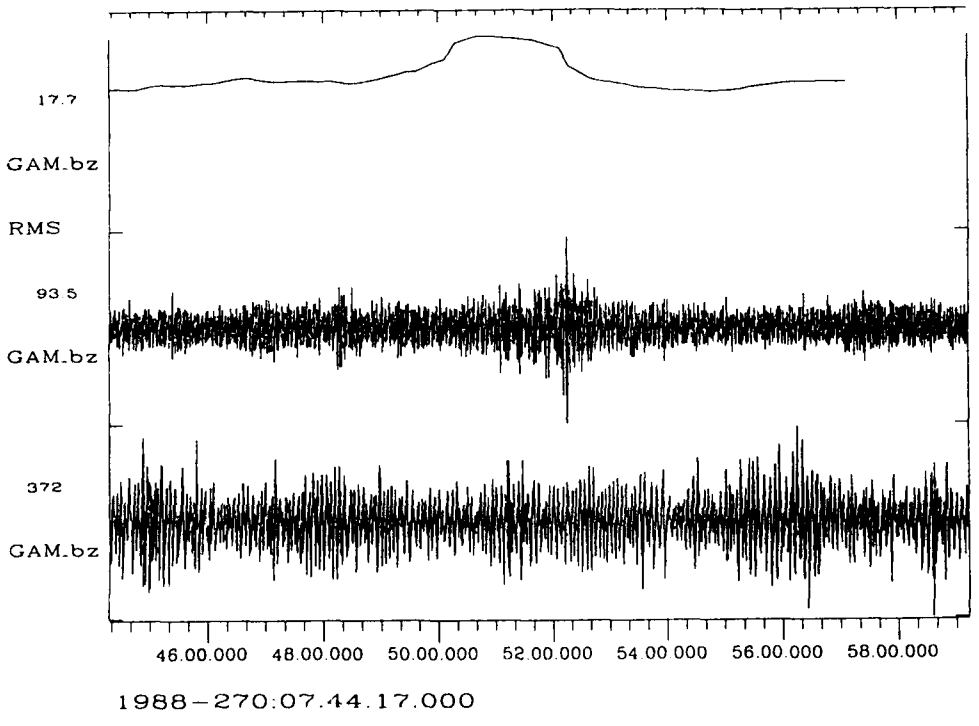

Fig. 7.2.4 The GAM vertical component seismogram from the m_b 3.8 explosion on September 26, 1988. The lower trace is the unfiltered seismogram, the middle trace is the band pass filtered seismogram between 0.6 Hz and 3.0 Hz, and the upper trace is the RMS amplitude as a function of time.

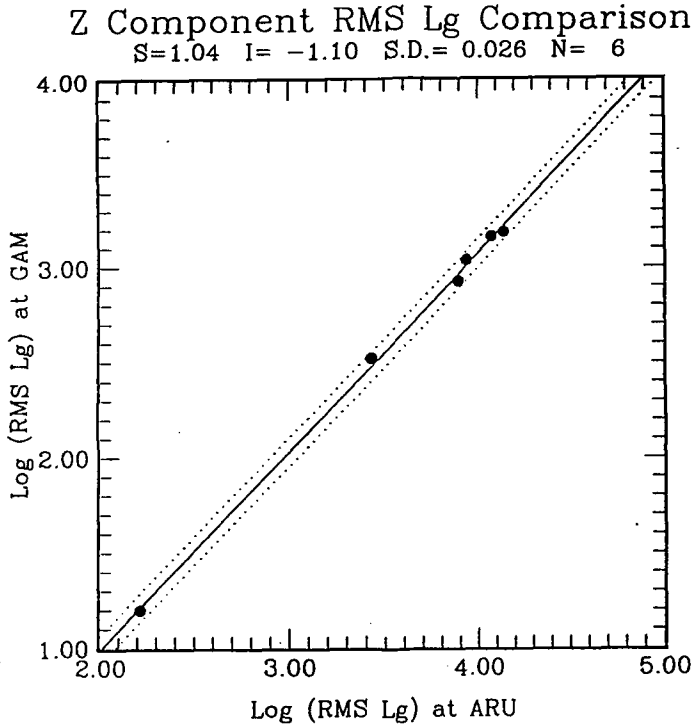

Fig. 7.2.5 Comparison of log RMS Lg measurements at ARU and GAM. The slope of the line is 1.04 and the standard deviation of the misfit of the line to the data is 0.026 orthogonal to the line. The dotted lines correspond to plus or minus two standard deviations. Note the remarkable stability of measurement between the two stations over two full magnitude units.

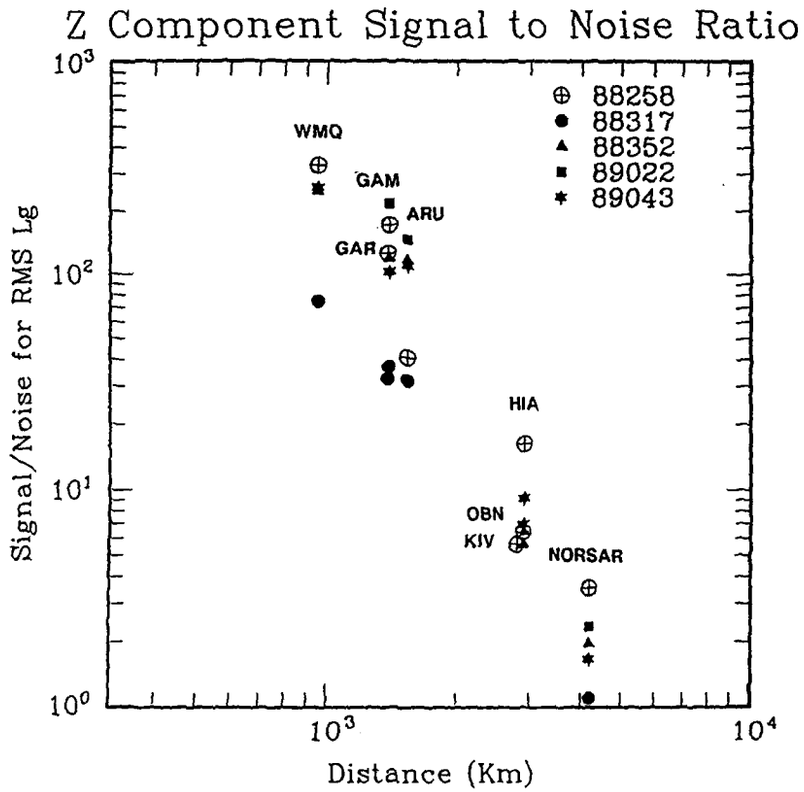

Fig. 7.2.6 Graph showing the variation of the signal-to-noise ratios (log RMS minus log RMS noise) among GAM, the four IRIS stations, the NORSAR array and the CDSN stations WMQ and HIA. Epicentral distance to the test site is plotted along the horizontal axis.

7.3 Wavefield decomposition for three-component seismograms

Seismograms at regional ranges are built up from a complex mixture of seismic propagation phenomena involving multiple reflections and guided waves in the crust (e.g. the phases Pg, Lg) and waves returned from the uppermost mantle (Pn, Sn). In order to detect and locate events as well as to assess the nature of the seismic source and propagation path, it is necessary to be able to recognize and characterize different parts of the seismic wavefield. Both phased array techniques for single component sensors and vectorial analysis of 3-component recordings can provide estimates of the azimuth and slowness of seismic phases. Although it has been shown that the accuracy of the 3-component estimates of slowness and azimuth is generally lower than from an array, especially for S waves, a combination of these approaches provides a more powerful tool to estimate the propagation characteristics of different seismic phases at regional distances.

Most methods of using three-component data rely on polarization parameters as their main device for characterizing different features on a seismic wavetrain. Recently Jepsen and Kennett (1990) have shown how it is possible to extract estimates of the relative amplitudes of the three incident wavetypes (P, SV, SH) from three-component records under the assumption that the dominant arrival at any given time is a single plane wave described by its slowness and azimuth. This procedure depends on modelling the interaction of the wavefield with near-receiver structure. The main contribution, at hard rock sites such as NORESS and ARCESS, comes from the interaction of the wavefield with the free surface.

If the slowness and azimuth of the incoming wavefield are known, then the free surface effect on an incident plane wave is frequency independent, but may involve phase shifts. The extraction of the wavefield components requires the inversion of the matrix of interaction imposed by the free surface together with rotation in a horizontal plane. For a three-component station situated at an array such as ARCESS, beamforming over the vertical component sensors can be used to estimate the slowness and azimuth as a function of time. These array beam parameters may then be used to produce estimates of the P, SV and SH contributions to the wavefield as a function of time. This process is illustrated in Fig. 7.3.1 for the 3-component station C7 at the ARCESS array for an event close to the array. The array beam estimates were generated by using the broadband f-k procedure on a sliding 2 sec window.

This decomposition of the seismic wavefield by wavetype as a function of time not only has considerable benefits for the recognition of seismic phases, but also provides a domain in which the relative proportions of P, SV, and SH can be compared directly, because free-surface amplification effects have been removed. This information on the current proportions of different wavetypes

summarizes much of the propagation processes between source and receiver and therefore can help to provide specific measures of wavefield character which can be beneficial in attempts to discriminate between different source types.

For an individual 3-component station, the estimation of apparent azimuth is usually more reliable than slowness. However, for regional phases, it proves quite effective to use the wavefield decomposition procedure with a number of fixed slownesses designed to enhance different features of the wavefield arriving at different times. A slowness of 0.12 sec/km gives very good resolution of the early P wave energy (see Fig. 7.3.2) while suppressing later SV energy. P is usually accompanied by a small S component which can be reduced by optimal estimates of slowness.

An S wave slowness of 0.22 (see Fig. 7.3.3) enables a clear identification of the SV contribution to Lg. Even though the wavefield decomposition procedure removes the phase shift from free surface reflection imposed on SV at large slownesses, there is commonly no close correspondence between the SV and SH components. Rg waves are evident by the presence of coupled P and S energy.

An interesting by-product of a high slowness decomposition is an amplification of the P arrivals occurring in the notional SV trace. This occurs without significant amplification of the background noise and can lead to a definite improvement in the signal-to-noise ratio. The SV trace for high slowness can therefore be investigated as a possible detector for the P onset.

The wavefield decomposition procedure depends on the specification of the near surface velocities, but fortunately in general the main results are not very sensitive to the values of the velocities. The exception is for slownesses close to the reciprocal of the surface P wave velocity (around 0.17 km/s at ARCESS) where the inverse of the free surface response is a rapidly varying function of slowness. Also an error of around 10° in azimuth can be tolerated, the main effect is on the SH component.

Although slowness and azimuth estimates from the array are most stable for a particular frequency band (typically 3–5 Hz), the f-k estimates can be applied quite successfully to unfiltered data or to particular filtered components.

Further examination of this class of 3-component analysis procedures will involve the implementation and testing of the classification schemes of Jepsen and Kennett (1990). Such schemes categorize the stability, rectilinearity, planarity, etc. of the wavefield and use a set of rules for classifying a particular wavetype (i.e. elliptical P and S, rectilinear P and S, rectilinear SH, Rayleigh, etc.).

B.L.N. Kennett & D.C. Jepsen, Research School of Earth Sciences
Australian National University
R.A. Hansen, NORSAR

References

Jepsen, D.C. and B.L.N. Kennett (1990): Three-component array analysis of regional seismograms. Manuscript accepted for publication in *Bull. Seism. Soc. Am.*.

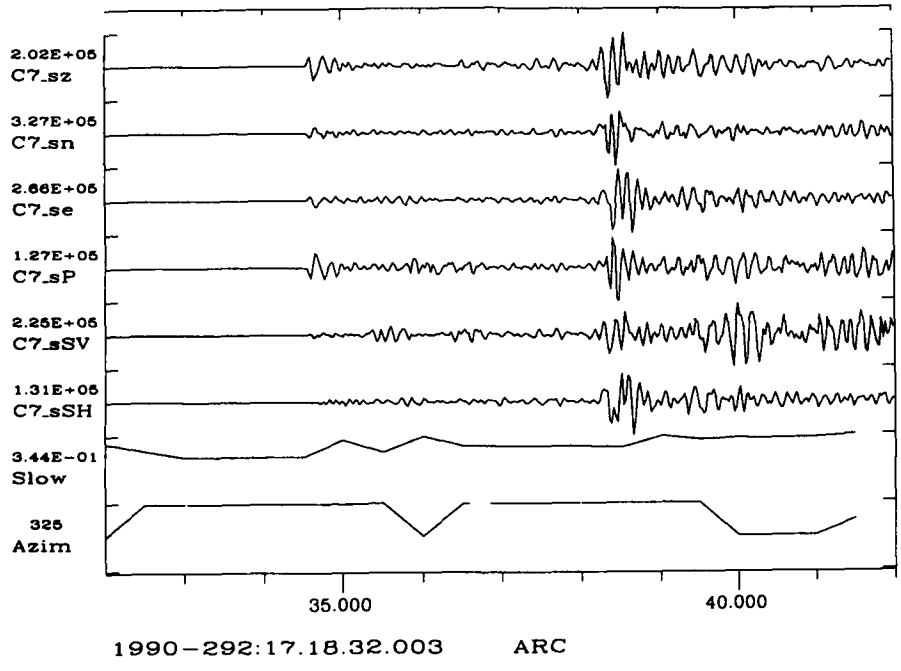

Fig. 7.3.1. This figure illustrates the decomposition of a three component seismogram into the relative components of P, SV and SH. The top three traces are the original three-component time series, the next three traces are for P, SV, and SH respectively, and the bottom two traces show the values, as a function of time, of slowness and azimuth used in computing the P, SV, and SH contributions. The slowness and azimuth were computed from a 2 second sliding window using the entire array of vertical sensors and a broad band f-k analysis.

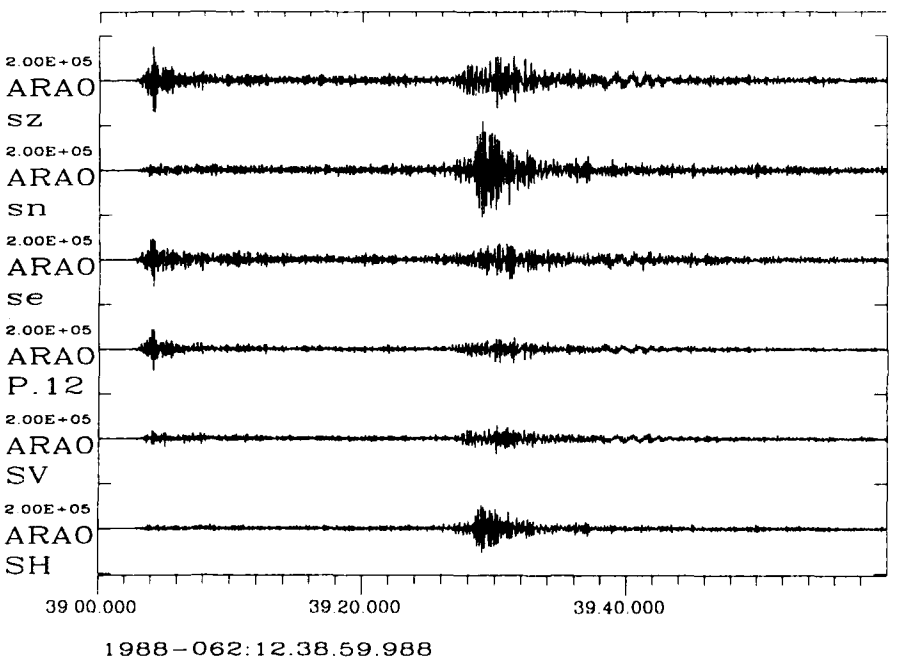

Fig. 7.3.2. This figure illustrates the decomposition of a three component seismogram into the relative components of P, SV and SH with a fixed slowness of .12 sec/km and azimuth of 92. The top three traces are the original three-component time series and the bottom three traces are for P, SV, and SH respectively.

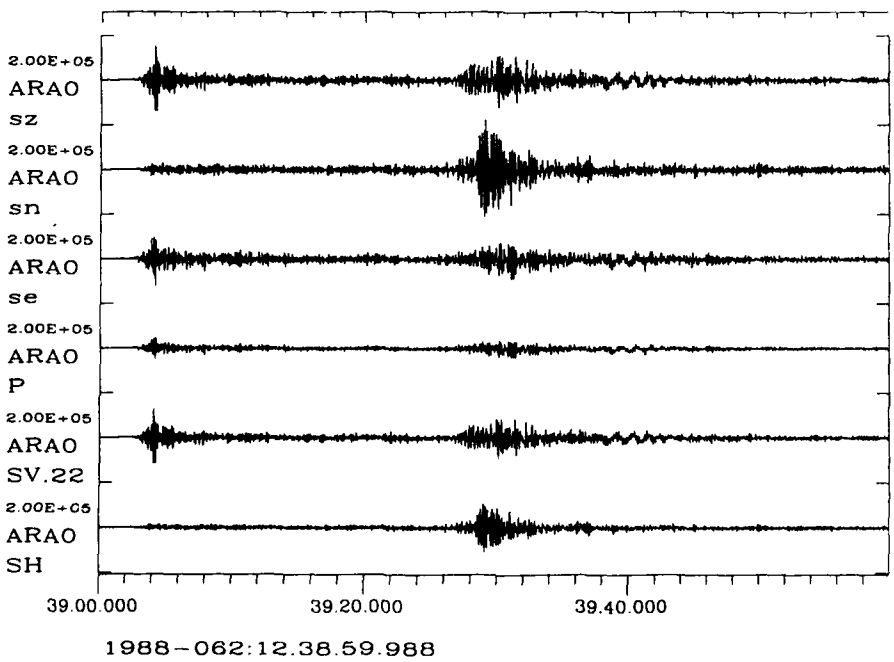

Fig. 7.3.3. This figure illustrates the decomposition of a three component seismogram into the relative components of P, SV and SH with a fixed slowness of .22 sec/km and azimuth of 92. The top three traces are the original three-component time series and the bottom three traces are for P, SV, and SH respectively.

7.4 Ray-based interpretation of Lg azimuth anomalies at NORESS

Introduction

In a recent paper, Bostock and Kennett (1990) introduced a method for predicting the propagation characteristics of the Lg phase in areas of complex crustal structure in a semiquantitative manner. The method relies on the interpretation of Lg as constructively interfering S waves multiply reflected within the earth's crust. A set of rays is traced outwards from a point source within a crustal waveguide of variable thickness. The geometrical characteristics of the rays are modified upon reflection from the crust-mantle boundary and the free surface according to Snell's law, and can then be monitored in plan view by the horizontal projection of the rays and the location of mantle reflection points. This approach allows a qualitative description of a variety of complex propagation processes including mode coupling, wavetype conversion, and lateral waveguiding for situations which, because of difficulties in handling boundary conditions, cannot be adequately described by current quantitative, modal descriptions of the Lg phase (see, e.g., Kennett, 1989). More specifically, it is possible to associate changes in the separation of S-wave reflection points with a change in the character of the wavefield viewed as a sum of higher mode surface waves since the angle a ray makes with the vertical may be related to an equivalent phase velocity. In addition, the polarization of the S waves may be used as a measure of the conversion between Love and Rayleigh waves.

Although the method has been used to explain the observed patterns of Lg propagation in central Asia (Bostock and Kennett, 1990) and the southwestern United States (Kennett *et al*, 1990), its success is highly dependent upon the knowledge of crustal model. In these previous studies, variation in crustal thickness was considered the dominant factor influencing the character of Lg on seismograms, and crustal models based on varying degrees of isostatic compensation were adopted in accordance with published geophysical and tectonic evidence. However, there are a number of other factors which may become significant in general applications. For instance, in areas of thick sedimentary cover it may be advisable to consider that portion of the crust comprising basement alone. In general, the effects of vertical velocity structure and systematic lateral variations therein will generally be insignificant at all but the lowest phase velocities, however abrupt lateral heterogeneity in physical properties will undoubtedly play an important role in distorting the observed wavefield. A truly quantitative representation of Lg propagation using the ray method is only possible when comprehensive information on all contributing factors is incorporated in the construction of our crustal models. Notwithstanding, in many cases valuable insight may be gained by considering simply the variation in crustal thickness, in which case an accurate knowledge

of the depth to Moho is essential since fluctuations in this lower boundary are, in general, more pronounced than those at the free surface.

Scandinavia crustal model

Our objective in this study is to employ the ray method as a tool in assessing the effects of gross crustal structure on Lg propagation in Scandinavia and adjacent areas to the east, and relating the predicted behavior to azimuth anomalies observed at the small-aperture NORESS array. We will therefore consider a single-layer crustal model over the area 0°–35°E, 55°–75°N comprising all of Scandinavia and Finland and parts of the Soviet Baltic states. The modelled free surface boundary is a smoothed (81 point average) version of relief data from the ETOPO5 world topography data base at 5' intervals. The crust-mantle boundary was constructed by interpolating the Moho map of Ruud (pers. comm.) which combines information from a variety of geophysical studies (seismic reflection, refraction, gravity, etc.) and is thought to be an accurate representation of the main low-wavelength structure over the region. The main topographic feature is the Caledonide Range paralleling the coast of Norway, which rises to an elevation of 2000+ m over a considerable area. The Moho map shown in Fig. 7.4.1 presents a slightly more complicated picture. The mean sea level depth to Moho decreases rapidly off the Norwegian coast to typical values for oceanic crust ($\sim$ 10 km). Interestingly, the Caledonides are not mirrored by any significant root on the Moho; rather, crustal thicknesses generally increase steadily as one approaches the center of the Baltic Shield. There are several areas of increased crustal thickness (> 50 km); notably along the central and northern portions of the Soviet-Finnish border, and a saddle-shaped structure straddling the eastern coast of Sweden. Moho depths tend to decrease further south and east approaching the Russian platform.

Ray analysis

Mykkeltveit *et al* (1989) have assembled a data base of Lg azimuth anomalies observed at NORESS from a variety of sources at distances from 100 to 1000 km which indicates that in some regions there is extreme variability in the magnitude and sign of azimuth anomalies with even minor changes in source position. We will examine possible causes for this anomaly distribution using the ray technique discussed above.

Perhaps the most interesting region in terms of anomalous behavior is located along the southern coast of Finland on the Gulf of Bothnia. Here Lg waves from sources separated by distances as small as 2°–3° in latitude exhibit strikingly different azimuthal anomalies. To investigate this behavior, we present ray diagrams generated for i) different phase velocities at a single

source location (21°E, 60°N) in Fig. 7.4.2, and ii) different source locations in this general area (21°E, 59.0°–62.0°N) at constant phase velocity (4.0 km/s) in Fig. 7.4.3.

We first describe the variable phase velocity diagrams shown in Fig. 7.4.2. For lower phase velocities (e.g., 3.8 km/s — Fig. 7.4.2a) guided wave propagation is generally less affected by lateral variation in crustal thickness as an individual ray undergoes fewer bounces over a given distance. The figure also indicates that a large proportion of the rays undergo reflection at the continental margin off western Norway accompanied by conversion to Sn mantle phases into the oceanic crust (denoted by solid diamonds). Of specific relevance is the saddle-shaped low in Moho relief centered roughly midway between NORESS and the source, and occupying a significant portion of the total path (see also Fig. 7.4.1). Note that the axis of the ridge separating the two pockets is roughly colinear with a line joining NORESS and the source. We recall that zones of increased crustal thickness tend to behave as attractors, pulling rays inward in much the same fashion as high velocity zones in conventional body wave raytracing. Hence as a general observation, rays launched at all 3 phase velocities tend to be drawn away from the Moho ridge leaving windows through which fewer rays pass. These windows overlap for the three ray diagrams (Figs. 7.4.2a, b, c) but do not exactly coincide since the phase velocity dictates the exact location of the basement reflection points for a given ray and their resulting ray curvature. The position of NORESS relative to these alternate low and high ray density windows is therefore a function of phase velocity, and we might accordingly expect the azimuth of the observed wavetrain to vary considerably with time as the individual phase velocity components arrive at different group velocities. In addition, observed azimuths are likely to depend significantly on the frequency characteristics of the particular source-excitation function.

We now consider the effect of shifting the source by 1° increments along the 21° E meridian on ray diagrams generated at a fixed phase velocity of 4.0 km/s as shown in Fig. 7.4.3. Note that even small changes in source position can significantly alter the source-heterogeneity-receiver geometry. The ray diagrams reflect this fact by exhibiting considerable variation in ray density west of the main heterogeneity: the saddle-shaped low in Moho relief behaves as a lens which focuses and defocuses ray bundles in a way that is strongly dependent on the location of the illuminating source.

Finally we examine a more distant source at the head of the Gulf of Estonia. The ray diagram in Fig. 7.4.4 indicates that the absence of major heterogeniety along the initial part of the ray paths results in a ray pattern which remains quite coherent into eastern Sweden. Rays in the vicinity of the heterogeneity are more nearly parallel than those from closer sources (as in Figs. 7.4.2 and 7.4.3) and tend not to diverge as markedly upon transmission. Nevertheless,

the effects of the Moho saddle are still manifest in a focusing and defocusing of rays which, for the particular phase velocity employed, leaves NORESS in a region of low ray density.

Discussion

Initial attempts to relate ray-calculated and observed azimuth anomalies yielded somewhat inconsistent results, but upon careful examination of the ray behavior it becomes evident that the nature of the Moho heterogeneity in the vicinity of NORESS is probably largely responsible. In areas of broader scale heterogeneity, ray diagrams are characterized by more systematic and gradual changes in ray pattern with respect to both source location and phase velocity (see for example Bostock and Kennett, 1990). The complexity of the Moho saddle east of NORESS, its comparatively complicated geometry over a region of restricted spatial extent, results however in ray diagrams which are considerably more sensitive to these two parameters. The observations made above would appear to bear important implications to the analysis of crust and upper mantle phases originating from parts east of the array, especially for more proximal sources. The study suggests that the Moho saddle, a feature which appears to be well defined and documented in a number of independent investigations, will play a significant role in distorting the wavefield and is probably responsible in large part for the Lg azimuth anomalies observed at NORESS from sources to the east.

M.G. Bostock & B.L.N. Kennett, Research School of Earth Sciences
Australian National University, Canberra
S. Mykkeltveit, NORSAR

References

Bostock, M.G. and B.L.N. Kennett (1990): Lg propagation patterns in three dimensional heterogeneity, *Geophys. J. Intl.*, in press.

Kennett, B.L.N. (1989): Lg waves in heterogeneous media, *Bull. Seism. Soc. Am.*, **79**, 860–872.

Kennett, B.L.N., M.G. Bostock and J.-K. Xie (1990): Guided-wave tracking in 3-D — a tool for interpreting complex regional seismograms, *Bull. Seism. Soc. Am.*, in press.

Mykkeltveit, S., S. Kibsgaard and T. Kværna (1989): Region-specific knowledge derived from analysis of NORESS data, in *NORSAR Basic Seismological Research, 1 January - 30 September 1989, Annual Technical Report, Contract No. F49620-89-C-0038*, ed. S. Mykkeltveit.

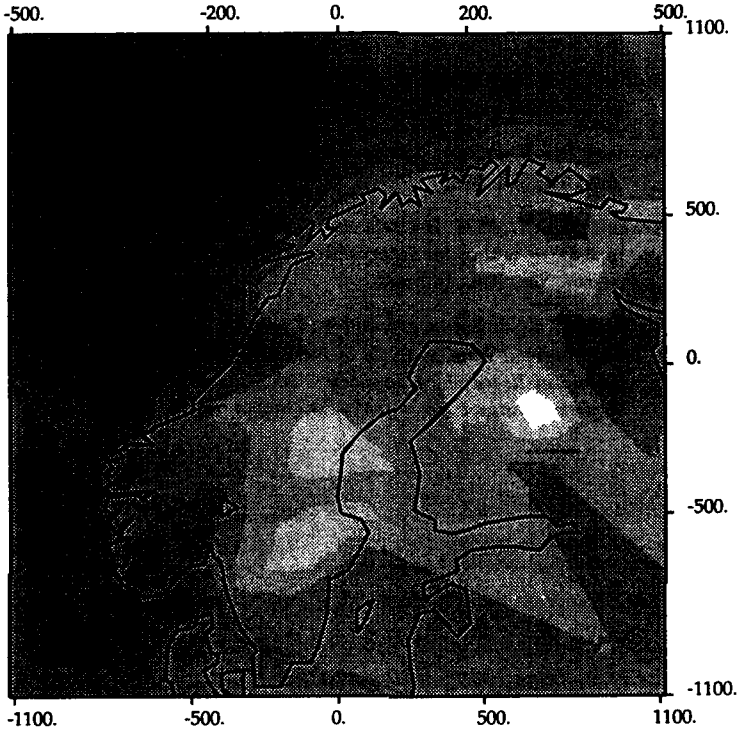

Fig. 7.4.1. Moho relief over Scandinavia, Finland and the Soviet Baltic states after Ruud (pers. comm.); lighter shades indicate increased Moho depths. The location of the NORESS array is marked by a triangle.

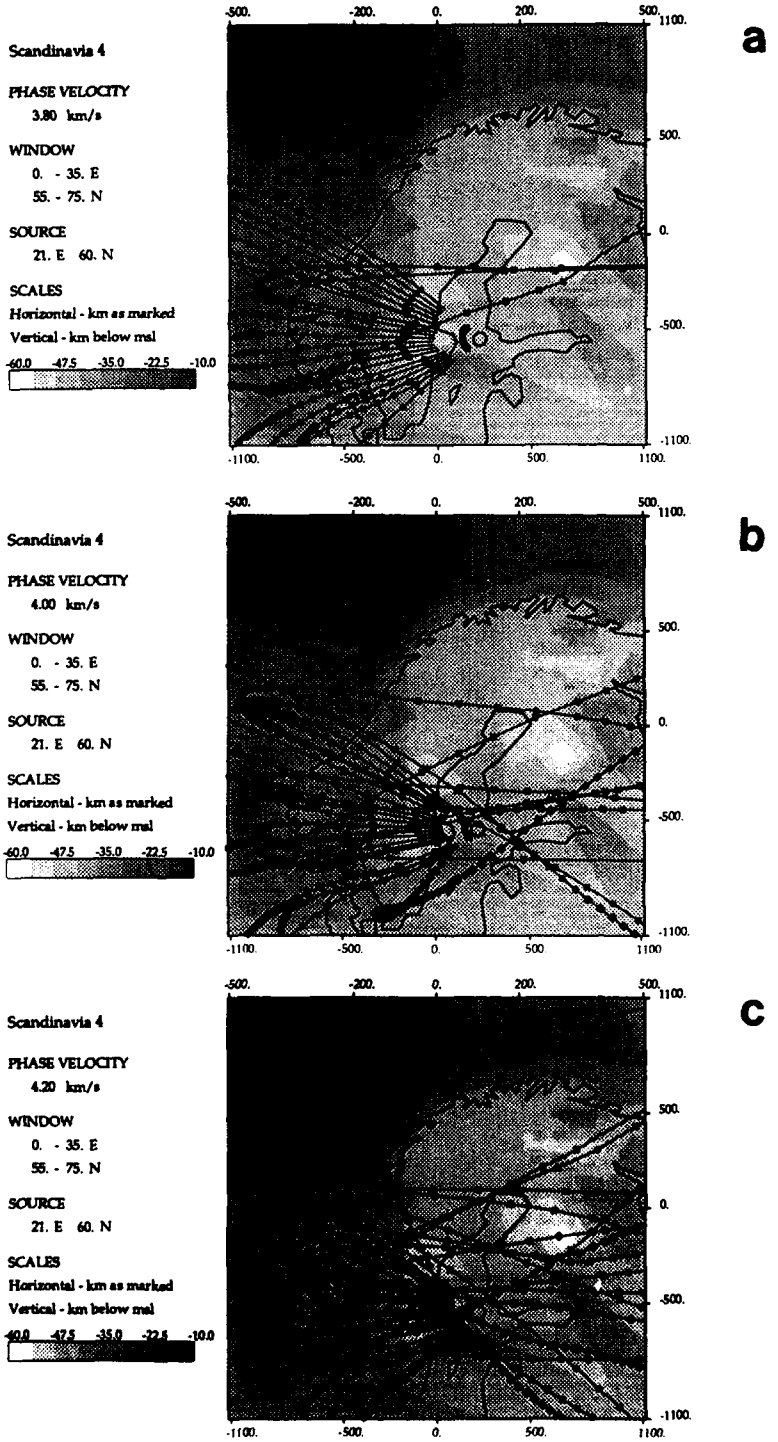

Fig. 7.4.2. Ray diagrams for a source located at 21°E, 60°N at three phase velocities a) 3.8 km/s, b) 4.0 km/s and c) 4.2 km/s. Note alternating high and low ray-density windows resulting from Moho saddle east of NORESS.

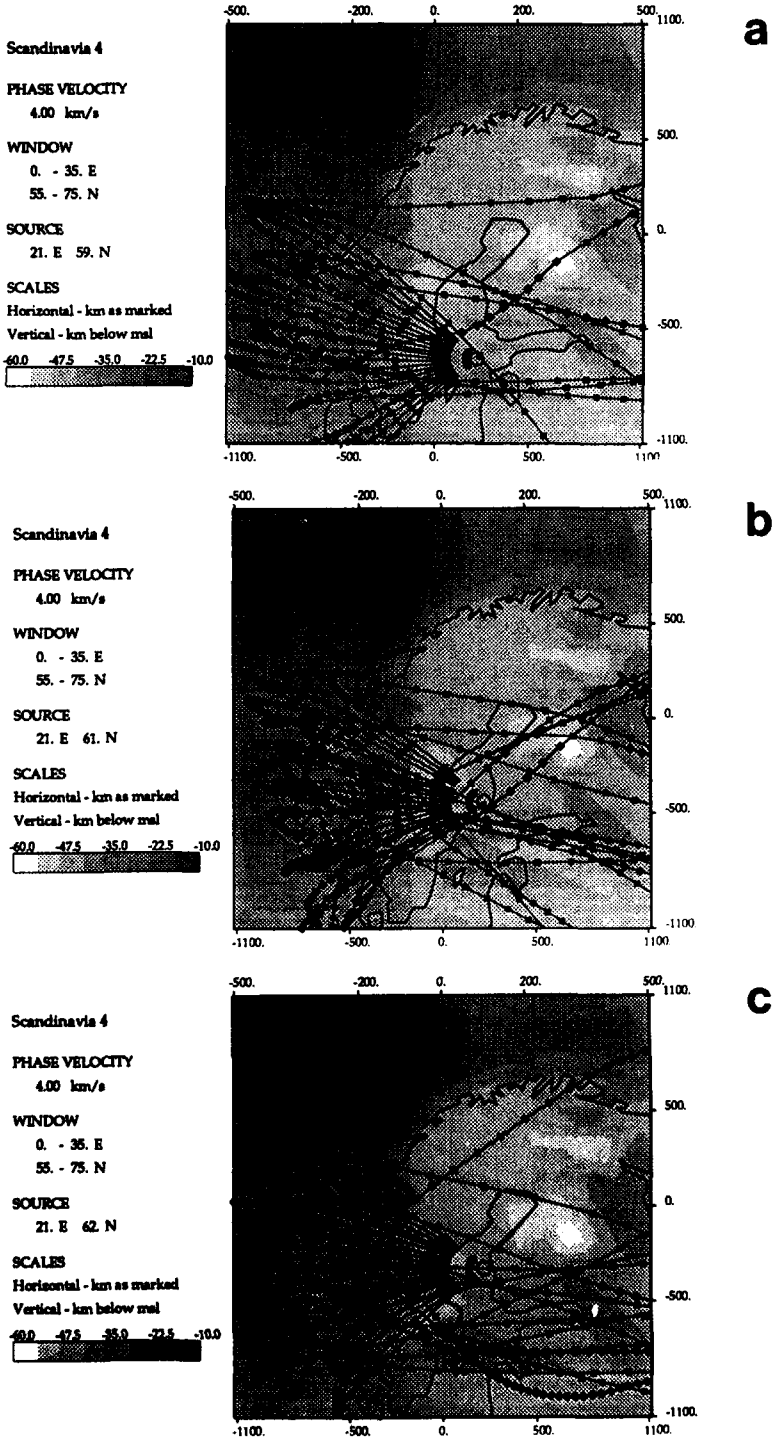

Fig. 7.4.3. Ray diagrams for 3 sources located at a) 21°E, 59°N, b) 21°E, 61°N and c) 21°E, 62°N at a phase velocity of 4.0 km/s. Note variability of ray patterns with source location.

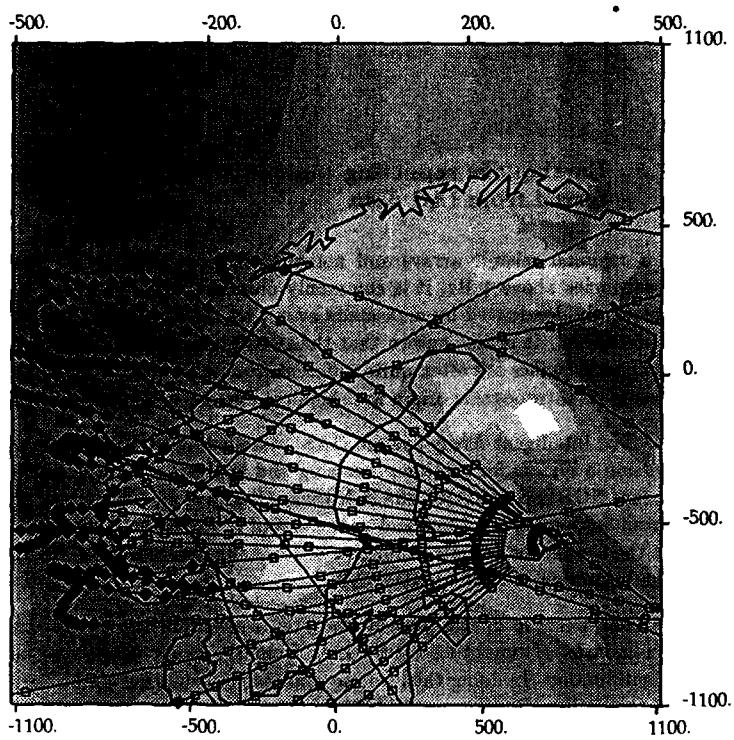

Gulf of Estonia 2

PHASE VELOCITY

4.00 km/s

WINDOW

0. - 35. E

55. - 75. N

SOURCE

29. E 60. N

SCALES

Horizontal - km as marked

Vertical - km below msl

-60.0 -47.5 -35.0 -22.5 -10.0

Fig. 7.4.4. Ray diagram for a source in the eastern Gulf of Estonia at a phase velocity of 4.0 km/s. Note the relative coherence in the ray pattern east of the Swedish coast.

7.5 Earthquake reporting capabilities in Fennoscandia as inferred from IAS data

For regional seismic arrays and networks in populated areas, operating at frequencies above 1 Hz, it is commonly observed that detections become increasingly dominated by man-made events as the signal-to-noise ratio (SNR) is decreased. It is also known that the spatio-temporal characteristics of natural earthquakes are often quite different from man-made events. Most of the events of antropogenic origin are chemical explosions of some sort.

The Intelligent Array System (IAS) installed at NORSAR is in its present version a system for routine processing and analysis of data from the regional arrays NORESS and ARCESS in Norway (Bache *et al*, 1990; Bratt *et al*, 1990). From September 29, 1989, and to the end of the year the system was operated at the Center for Seismic Studies (CSS) in Arlington, Virginia, USA, and from the beginning of 1990 at NORSAR.

The purpose of the present study is to evaluate the data from the first six months of operation of the IAS, from the point of view of earthquake identification. In doing this, we use available information about the seismicity of the region (Bungum *et al*, 1990), but with no prior assumptions otherwise about where to expect the man-made event.

Data and data analysis

The IAS system is fully automatic, but also supplemented by a thorough analyst review and evaluation. During the 6 months analyzed here, a total of 3813 located events were accepted by the analysts, who refined in one way or another the solutions for all but 669 of these. To further improve the quality of the event locations selected for the present analysis, we have accepted only solutions where the standard error of one observation (sdobs) is less than 3 seconds and where the standard error in time (stt) is less than 10 seconds (Bratt and Bache, 1988). This reduced the number of events to 2454, of which all but 9 are located within the greater Fennoscandian region of 54–76°N, 0–40°E.

The spatial distribution of these events is shown in Figs. 7.5.1a-c, revealing a pattern quite different from the known seismicity in the area, and with a non-uniform time-of-day (TOD) distribution as shown in Fig. 7.5.1d. This distribution contrasts strongly to that expected for earthquakes, with no dependence on time-of-day. There are two prominent peaks in the distribution, right ahter noon and around midnight. In fact, the amount of man-made events (explosions) in the data base is larger than what is indicated by Fig. 7.5.1d, since different areas should be expected to have their explosions peaks at different times of the day, thereby cancelling each other to some extent.

Our aim in the present study has been to identify areas with a significant number of explosions, and to flag these events in the data base. Our approach in this respect has been first to identify epicentral areas where the events are concentrated or clustered. A non-uniform TOD distribution and/or a non-exponential magnitude-frequency (MF) distribution then indicates the presence of man-made events within that area. The best way to do this analysis is to start with large areas or regions, and then to zoom in on smaller areas later.

For areas thus identified to contain a certain amount of explosions, we define one or more hourly intervals within which all events below a certain magnitude should be flagged as explosions in the data base. These hourly intervals coincide with peaks in the TOD distributions, while the magnitude thresholds depend on the character of the MF distributions within as well as outside of these intervals. The parameters should be tuned in such a way as to yield (after flagging of explosions) both TOD and MF distributions for the remaining events that are compatible with what should be expected for earthquakes.

After screening or filtering the entire data base in this way, we evaluate what this filtering represents in terms of magnitude thresholds for accepting events (as natural earthquakes) from particular areas, at different times of the day. These thresholds reflect in the present context the capabilities for reporting natural earthquakes, limited by a noise level which in this case is determined by the occurrence of man-made events.

The actual analysis for the IAS data base involved the testing of a large number of spatial windows, in order to identify areas with non-uniform TOD distributions and non-exponential MF distributions. The result of this analysis for the present data base of 2454 Fennoscandian event locations are the 52 TOD filters defined in Table 7.5.1. The spatial windows are shown also in Figs. 7.5.1a-c, and the TOD distributions for a selection of these windows are shown in Table 7.5.2.

In some cases, a spatial window is defined entirely within the area covered by another window. In that case, the smaller window has a higher magnitude threshold. In other cases, one window has two different hourly intervals connected to it, which is done by defining two different windows. After the first 47 windows were defined (only those are shown in Figs. 7.5.1a-c), it was found necessary to define also four larger regional windows (No 48–51), but with magnitude limits below the smaller windows covered inside. In addition, the last window (No 52) covers the entire area under analysis, for the purpose of defining a lower magnitude limit for all the events (here set to 0.5). From Table 7.5.1 it is seen that the other windows have magnitude limits ranging from 1.5 to 3.3.

After TOD filtering, there are 75 events remaining of the original 2454, or about 3%. These events are plotted in Fig. 7.5.2, with TOD distributions as shown in Fig. 7.5.1d and in in the last column of Table 7.5.2. It is likely, when studying the TOD distribution and also when comparing with earlier seismicity maps, that some explosions still remain in the data base. This is because they occur in areas with few other events, because they occur at TODs shared by few other events from the same area, or because they have magnitudes above other events from the same area and with the same TODs.

While it is likely that the TOD filtering has not removed all of the explosions, it is even more certain that some natural earthquakes have been removed. The latter is evident from the fact that what we have done is simply to remove all of the events below a certain threshold magnitude, a threshold which has been made dependent on region and TOD. In the cases when natural earthquakes occur within these spatio-temporal-magnitude windows, they will of course be flagged as explosions.

Earthquake reporting capabilities

The results of the above analysis for six months of available IAS data determines a threshold for the reporting of natural earthquakes, provided that no discrimination analysis of individual events has been performed. The key to this threshold, and the way in which it varies in time and space, is found in the definition of the TOD filters (Table 7.5.1).

We have developed a procedure for time dependent spatial contouring of this threshold by defining first an hourly time interval and a regular spatial grid. For each grid point, we loop through all TOD filters in order to identify those that contain the point, and a hit is declaired if there is some overlap between the selected hourly interval and the filter's hourly interval. The magnitude threshold for the selected grid point is then taken from the filter with the highest threshold. This procedure is repeated for all points in the grid, all of which are associated with a threshold magnitude applicable within the selected TOD interval. A threshold contouring can then be performed on this basis.

In the present case, we have defined a grid with steps 0.5° in latitude and 1° in longitude. The resulting contours (with some spatial smoothing) is shown in Fig. 7.5.2a-b for a time period (1030–1430 UTC) during the peak of the working hours, and in Fig. 7.5.2c-d for a time period (0030–1430 UTC) during the most quiet part of the night. The difference between the two is very significant: while the noise level (reporting threshold) at night time extends up to 1.5 in magnitude only in very few areas, the level in the middle of the day extends up to 2.5 over fairly large areas.

Discussion and conclusions

The hourly time period used in the examples above is somewhat arbitrarily set to 4 hours. The length of the time interval should reflect the particular purpose of the analysis, but it should also reflect the time resolution assumed in the definition of the TOD filters. A similar resolution consideration applies also to the determination of the grid size, which should reflect the purpose of the analysis as well as the resolution assumed in the definition of the TOD filters.

One of the limitations with the present data base is that it is based on observed data from only two regional arrays. However, even if this leads to a certain variation in both detection thresholds and location precisions over the area covered in this study, it should not affect the results significantly. The reason for this is partly that the poorest locations have been removed prior to the analysis, but first of all that a substantial amount of the explosions are in fact located more or less randomly outside of the main known explosion sites. Better locations should therefore only be expected to lead to minor changes in the space-time organization of the data.

The spatial windows as defined in this study are very simple, reflecting to some extent the limitations in location precisions. A natural refinement here would be to define windows in terms of polygones, an option which in fact is available in the sorting program used in this study. In the present first order approach, however, simple rectangular spatial windows are considered satisfactory.

Another natural refinement of the window definitions would be to include weekly and seasonal variations, both of which are known to be considerable. The weekly variation shows for most of the areas a stable weekend minimum (Bratt *et al*, 1990), while the seasonal variations probably are more complicated. An inclusion in the filter definitions of such variations is quite straightforward, however.

The explosion filters and associated noise levels defined in this work are of course applicable in general only for the time period for which they has been derived. However, only minor adjustments should normally be expected to be necessary in order to apply the present results to other time periods. It would be desirable to combine such an extention with the refinements discussed above. Similarly, the approach taken here should also be easy to apply to any new area from which event location data of similar nature are available.

What has been shown here is that the detectability now possible through a network of regional arrays cannot be fully utilized unless a substantial effort is being directed into the problem of event identification and discrimination. Being interested in earthquakes or explosions are two sides of the same ques-

tion in this respect, pursuable through the same approaches, methods and algorithms.

To be most useful, the discrimination algorithms, whether they are based on focal depth, spectral features, spectral ratios, etc. (e.g. Hedlin *et al*, 1990), should to the largest possible extent be included in the routine analysis of the events, with options for refinements and improvements as part of the analyst reviews as well as in subsequent offline analyses. These results should follow the events into the data base and be expressed in ways that could facilitate the computation of probabilities for the events being natural earthquakes or not.

In conclusion, we have found through a regionalized time-of-day analysis of six months of IAS data from the regional arrays NORESS and ARCESS shows that about 97% of the more well-located events probably are of man-made origin. Based on the derived information about where and when the man-made events occur, contour maps (in magnitude) of associated capabilities for reporting natural earthquakes are provided, for different times or hourly intervals of the day. The magnitude limits vary from about 3.0 as a maximum in some mining areas and down to less than 1.0 for western and northern Norway offshore areas, where most of the man-made disturbances are still below the detection level.

These results call for a dedicated effort into event discrimination work, with algorithms to be included preferably already in the routine analysis of the data.

Acknowledgements

This work was done while the author was a visiting scientist at Science Applications International Corporation (SAIC) in San Diego, CA.

H. Bungum

References

Bache, T.C., S.R. Bratt, J. Wang, R.M. Fung, C. Kobryn and J. Given (1990): The Intelligent Monitoring System, Accepted for publication in *Bull. Seism. Soc. Am.*.

Bratt, S.R. and T.C. Bache (1988): Locating events with a sparse network of regional arrays, *Bull. Seism. Soc. Am.*, 78, 780–798.

Bratt, S.R., H.J. Swanger, R.J. Stead, F. Ryall and T.C. Bache (1990): Initial results from the Intelligent Monitoring System, Accepted for publication in *Bull. Seism. Soc. Am.*.

Bungum, H., A. Alsaker, L.B. Kvamme and R.A. Hansen (1990): Seismicity and seismotectonics of Norway and nearby Continental Shelf areas, Submitted for publication.

Hedlin, M.A.H., J.B. Minster and J.A. Orcutt (1990): An automatic means to discriminate between earthquakes and quarry blasts. Accepted for publication in *Bull. Seism. Soc. Am.*.

No	La1	La2	Lo1	Lo2	M_L	H1	H2	No	La1	La2	Lo1	Lo2	M_L	H1	H2
1	59.6	61.0	4.8	6.0	1.6	9	17	27	59.0	60.0	26.0	30.3	3.0	8	15
2	61.6	62.8	5.2	8.0	1.6	9	17	28	62.9	63.4	27.0	29.2	2.5	11	12
3	58.0	59.1	5.3	7.8	1.6	13	17	29	60.0	61.5	27.5	30.3	2.6	9	15
4	59.1	60.3	6.0	7.3	1.6	10	17	30	60.6	61.4	28.5	29.8	3.0	12	13
5	60.3	61.2	6.0	7.5	1.6	9	17	31	60.8	62.2	30.3	32.0	2.7	9	15
6	56.5	58.0	7.0	11.0	1.6	10	12	32	59.3	60.1	33.0	35.0	2.9	8	12
7	62.0	62.7	8.6	10.0	1.6	10	19	33	61.2	63.2	34.0	37.0	2.8	9	14
8	58.7	60.2	9.0	12.0	1.6	7	16	34	65.3	68.5	15.0	19.5	1.8	0	24
9	57.5	58.7	11.5	14.4	1.6	9	15	35	68.5	70.0	18.2	22.4	1.5	8	19
10	58.7	60.0	12.0	14.2	1.6	10	17	36	66.5	68.2	19.5	22.8	1.6	0	15
11	54.0	56.0	12.5	17.5	2.5	6	16	37	66.5	68.2	19.5	22.8	2.4	16	24
12	54.6	55.9	15.8	17.0	2.9	0	24	38	70.0	71.5	23.0	31.0	1.6	9	14
13	59.1	60.4	14.2	16.0	1.6	0	24	39	67.2	68.0	23.2	25.4	1.9	6	24
14	60.4	61.3	14.5	16.3	1.6	9	13	40	64.7	66.6	23.9	27.6	2.1	7	20
15	58.3	59.2	18.0	19.1	3.0	6	19	41	66.8	68.3	29.5	35.2	2.0	0	24
16	57.5	59.8	17.2	19.5	2.4	9	14	42	66.8	68.3	29.5	35.2	2.6	3	20
17	54.0	55.4	18.3	21.0	2.5	9	18	43	67.1	67.9	32.6	35.2	3.3	5	19
18	59.3	60.2	20.0	22.3	2.7	7	13	44	68.3	69.8	29.7	33.4	2.0	0	24
19	60.8	61.7	20.0	21.5	2.0	8	14	45	68.9	69.8	29.7	32.0	3.1	11	12
20	54.0	57.5	22.0	32.0	2.5	9	14	46	64.5	65.1	29.9	31.8	2.8	9	12
21	62.0	63.8	22.0	27.0	2.0	9	12	47	68.8	69.8	33.4	36.0	2.4	7	11
22	63.8	64.4	23.1	25.8	2.3	9	13	48	53.0	61.0	9.0	21.0	1.5	6	15
23	59.0	60.0	23.7	26.0	2.5	9	16	49	56.0	62.0	21.0	32.0	2.1	7	15
24	60.0	62.0	25.0	27.5	2.6	0	1	50	62.0	68.0	15.0	25.0	1.8	6	14
25	60.0	62.0	25.0	27.5	2.6	11	15	51	62.0	69.0	25.0	40.0	2.1	8	15
26	57.6	59.0	25.6	27.0	2.6	9	13	52	50.0	80.0	-10.	50.0	0.5	0	24

Table 7.5.1. Time-of-day (TOD) filters as developed in this study for the purpose of removing presumed explosions from the IAS data base of event locations in Fennoscandia. The columns are filter (spatio-temporal window) number, latitude and longitude limits, magnitude limit and time-of-day limits. The last of the filters (52) covers the entire region under analysis, thereby defining a lower magnitude threshold for accepting any event.

Window Hour	7	8	9	13	27	28	29	36	39	40	41	44	46	All	Final
0- 1	0	0	0	6	0	0	0	5	0	1	9	5	0	35	5
1- 2	0	1	0	5	0	0	0	7	0	0	12	4	0	39	3
2- 3	0	0	0	0	1	0	0	3	0	0	10	6	0	26	3
3- 4	0	0	0	0	0	0	0	4	0	0	13	15	0	40	2
4- 5	0	0	0	0	0	0	0	1	0	0	14	11	0	32	0
5- 6	0	0	0	1	0	0	0	9	0	0	13	1	0	29	2
6- 7	0	0	0	2	0	0	0	3	2	0	8	0	0	27	2
7- 8	0	2	1	8	0	0	0	9	2	2	11	11	0	53	1
8- 9	1	5	0	3	1	0	0	11	1	0	15	11	0	59	0
9-10	1	6	2	1	3	0	1	10	1	0	27	15	3	125	4
10-11	4	4	2	1	12	0	1	9	4	3	25	16	13	130	2
11-12	0	7	4	6	18	3	2	6	1	17	69	21	4	202	1
12-13	0	13	5	2	34	12	19	5	17	9	79	73	5	253	5
13-14	1	17	9	4	15	0	12	17	9	2	36	45	0	245	7
14-15	4	22	12	3	9	0	6	23	8	2	19	13	0	186	4
15-16	5	7	10	21	2	1	2	10	4	4	11	2	0	128	4
16-17	2	3	0	2	0	0	0	14	2	5	9	3	0	57	6
17-18	0	1	0	3	0	0	0	20	2	1	12	2	0	62	2
18-19	0	0	0	6	0	0	0	33	1	10	8	4	0	70	4
19-20	18	0	0	0	1	0	0	15	1	3	13	2	0	65	5
20-21	0	0	0	1	0	0	0	12	0	2	14	4	0	44	5
21-22	2	0	0	1	0	0	0	24	1	0	8	1	0	46	3
22-23	1	0	1	0	0	0	0	124	0	0	6	3	0	139	3
23-24	0	0	0	3	0	0	0	227	1	0	12	3	0	253	2

Table 7.5.2. Time-of-day (TOD) distributions for the spatio-temporal windows (filters) defined in Table 7.5.1 that have more than 10 events in any particular hourly interval. The two last columns (shown also if Fig. 7.5.1d) give the distribution in the original data base and in the filtered one, respectively.

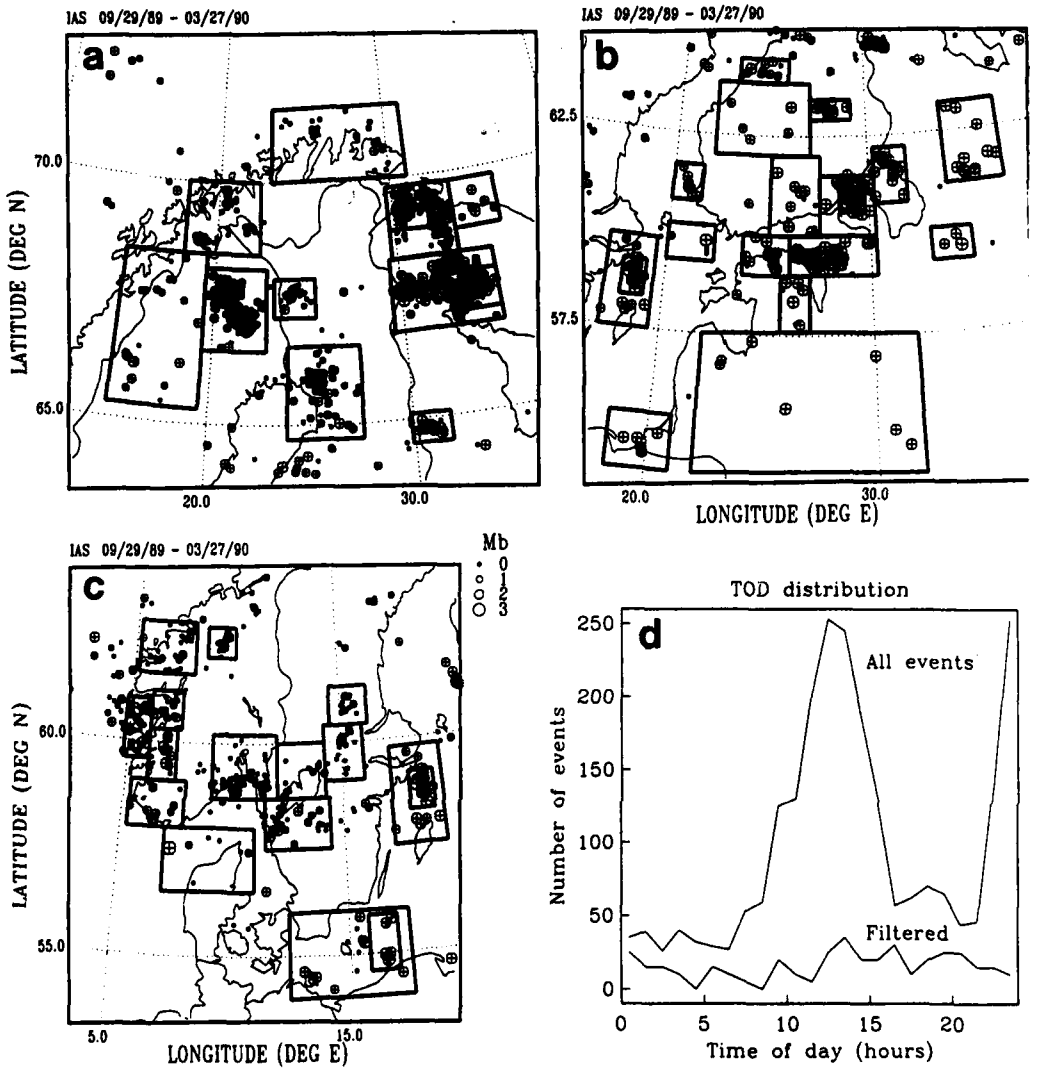

Fig. 7.5.1. Unfiltered IAS event locations for (a) northern, (b) eastern and (c) western Fennoscandia. The boxes are the spatial windows defined in Table 7.5.1, used in removing man-made events. In (d) is shown the time-of-day (TOD) distribution for the unfiltered data ('All events') together with the TOD distribution for the events remaining after application of the TOD filters ('Filtered'). The latter distribution has been scaled up by a factor of 5. The actual numbers for these two distributions are given in the last two columns of Table 7.5.2.

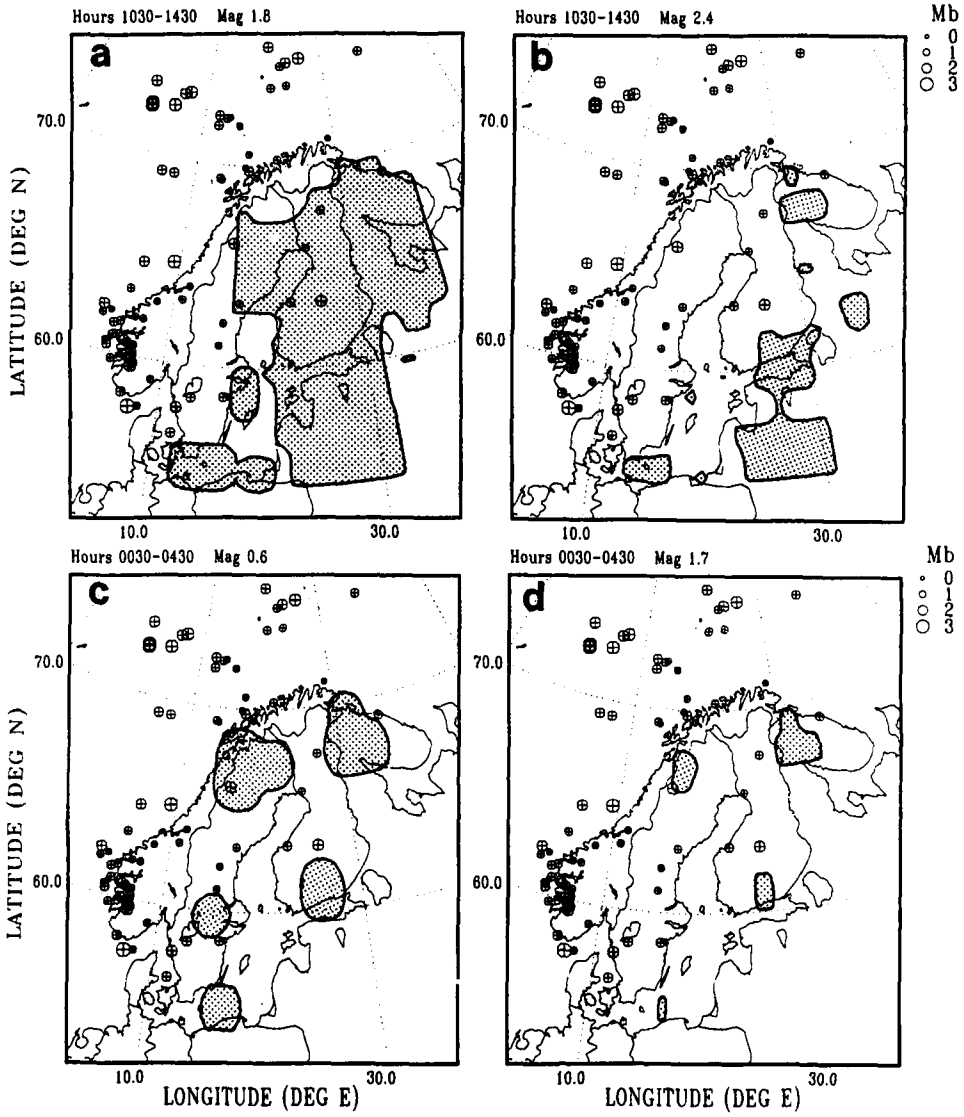

Fig. 7.5.2. Contour maps for the magnitude thresholds defined by the TOD filters developed in this study. The four maps correspond to (a) magnitude level of 1.8 for the hours between 1030 and 1430 UTC, (b) magnitude 2.4 for 1030–1430, (c) magnitude 0.6 for 0030–0430 and (d) magnitude 1.7 for 0030–0430. Under certain conditions, these contours indicate the day-time reporting capabilities for natural earthquakes.

7.6 Application of the threshold monitoring method

The concept of threshold monitoring was introduced by Ringdal and Kværna (1989) as a method of monitoring the seismic amplitude levels for the purpose of using this information to assess the largest size of events that might go undetected. In an effort to demonstrate the capabilities of this threshold monitoring concept, a preliminary version has been implemented into the Intelligent Monitoring System (IMS) (Bache *et al*, 1990). A demonstration of this implementation was given at the Symposium on Regional Seismic Arrays and Nuclear Test Ban Verification, held in Oslo in February 1990. In the following, we will present figures from that demonstration, as well as a brief description of the method.

Method description

The basic idea behind the threshold monitor is, for any given point in time, to infer the upper magnitude limit of a possible seismic event at a given geographical location. By combining observations of the amplitude of the seismic data at different arrays and/or single stations, we can apply the formalism developed by Ringdal and Kværna (1989) to compute an upper magnitude limit based on the network.

In order to apply this method the following procedure is required:

- For each location-station-phase combination, estimate continuously the seismic amplitude levels. If the station is an array, we use STA values of filtered beams to represent the amplitude levels. The steering parameters of the beams will then correspond to the apparent velocity and azimuth of the actual phase. The filter bands are chosen such that good SNR is ensured. If the observation unit is a single station, the STA values are computed from a filtered channel.

- When considering a potential event at a given time and location, measure the seismic amplitude levels at the expected arrival times for the relevant seismic phases. The travel times for each phase can be taken from standard travel time tables, or by processing events with known location and origin time.

- In order to relate the STA observations to actual magnitude estimates, apply the formula

$$m = log(STA) + b$$

  where b is a correction factor for each location-station-phase combination. The correction factors can be obtained by processing events with known magnitudes, or by using standard attenuation values.

- For assessing the significance of our magnitude estimates, assume that they are sampled from a normal distribution with a given standard deviation. Based on experience with signal amplitude variation across the NORSAR array, we have used a preliminary value of 0.2 for a small epicentral area.

- The magnitude limits computed by this algorithm are tied to a given confidence level, here set to 0.9. This means that the estimated limits represent the largest magnitude of a possible hidden event, in the sense that there is at least a 90 per cent probability that one or more of the observed amplitude values would be exceeded by the signals from an event with magnitude above these limits.

Interfering events

To illustrate the capability of the threshold monitor in the presence of an interfering event, we assume a situation as shown in Fig. 7.6.1. A teleseismic event is interfering with a local mining explosion, causing large amplitudes at the expected arrival time of Pn. We also assume that we are monitoring the source region of the actual mining explosion, using appropriate calibration values for the seismic phases considered.

If we now compute an upper magnitude limit only from the amplitude level at the time of the Pn arrival (where the interfering event is added), we will necessarily conclude that a relatively large explosion may have occurred. If we in addition bound the event magnitude by the undisturbed Lg amplitude, we will get a much lower value.

An actual interfering event situation may in fact be more complex than this, e.g. one station may be contaminated with high amplitudes for a long time period, or may even not record data. In such cases, amplitudes recorded at other stations may put strong constraints on the upper magnitude limit, and thereby exclude the possible occurence of a strong event.

Beamforming

The beamforming capability of regional arrays is efficiently exploited by the threshold monitor, both for P and S-phases. The STA traces used in the computation of the upper magnitude limits are derived from the amplitudes of filtered steered beams. At NORESS, we know that forming Pn beams will reduce the amplitude level of pure noise by about 14 dB (Kværna, 1989). For optimally steered Pn beams, the signal loss will be less than 3 dB for frequencies below 6 Hz. This will cause the calibration factors (b-values) to increase with the same amount, but we will still lower the upper magnitude limit by more than 10 dB (0.5 magnitude units).

For Lg, we expect the noise suppression to be somewhat less than for Pn, and we also expect a higher signal loss. Nevertheless, a reduction of the upper magnitude limit by more than 6 dB seems to be feasible for Lg.

Signals arriving from events outside the monitoring region may have their amplitudes significantly reduced by beamforming. The amount of amplitude reduction depend on the difference between the slowness vectors of the beam and the arriving signal, as well as on the beampattern of the array.

Implementation

In the present demonstration we use data from the three regional arrays in Fennoscandia: NORESS, ARCESS and FINESA. As target regions for threshold monitoring, we have chosen 10 active mining regions in Fennoscandia and Western USSR, as well as the Soviet nuclear test site at Shagan River (see Table 7.6.1).

For the 10 mining regions, the phases Pn and Lg at each array are being used to infer the upper magnitude limits. Calibration factors are found by processing events with magnitudes reported in the regional seismic bulletin of the University of Helsinki. Travel times and beamsteering parameters are obtained from the same processing. The filter bands for Pn and Lg are respectively 3–5 Hz and 1.5–3.5 Hz, and the STA sampling interval is set to 1 second. For Pn, the STA integration window is 2 seconds, and maximum STA is chosen within ± 2 seconds of the predicted arrival time. The reason why the amplitude level is represented by the maximum STA within a certain time tolerance, is that each target point represents a finite region, e.g. 10x10 km, and that phases from events occuring outside the center point will have somewhat different travel times. The STA integration window for Lg is 10 seconds, with maximum chosen within ± 3 seconds of the predicted arrival time. For distances less than 500 km, however, the integration window for Lg is reduced to 5 seconds.

For the Shagan River test site, calibration factors, travel times and beamsteering parameters for the phases P, PP and PcP were obtained from processing events with known magnitude and location. This was done for both ARCESS and NORESS, but as no observations were available for the FINESA array, the calibration factors were temporarily set to the same values as those of the ARCESS array. Travel times and apparent velocities are taken from standard tables, and the receiver-source azimuth is used. The STA integration windows are 2 seconds for P, and 5 seconds for PP and PcP. Time tolerances are 2 seconds for P and 3 seconds for PP and PcP.

The data processing flow can be outlined as follows:

- Compute filtered beams and STA traces for each array. The STA traces are stored on cyclic files, containing the last 5 days of data.
- Compute upper magnitude limits from the network of arrays, as well as from each array separately. The program reads the STA traces from the cyclic files, and stores the resulting magnitude traces on new cyclic files, also these containing the last 5 days of data. The total size of the files is altogether about 96 Mb.
- Analyze the magnitude traces by an interactive process within the IMS. Magnitude data are read from the cyclic files and displayed as continuous time series. The interactive processing is also attached to the IMS event data base, such that information on interesting events can be retrieved, e.g. by showing the location, origin time and estimated magnitude.

Examples from the demonstration

Fig. 7.6.2 shows the location of the 10 mining regions used as target areas for the threshold monitoring. In the following example, we will concentrate on the mine HC17. In addition to the upper magnitude limits derived from the network of arrays, upper magnitude limits were computed from each array separately. Fig. 7.6.3 shows these traces for Friday 02/03/90. The first 6 hours of the day are charcterized by low seismic noise levels, and any events at HC17 must have magnitudes well below 1.5. The low seismic activity is also illustrated by the V's on top of each curve, indicating origin times of events located by the IMS. An increase in the seismic amplitude level caused by an event shows up like spikes on the graphs. As expected, these occurrences are much more frequent during working hours (07-15 GMT). At NORESS, there is also a general increase in the background noise level during these hours. This is probabaly caused by nearby industrial activity (Fyen *et al*, 1990; Kværna, 1990).

From Fig. 7.6.2 we see that while the upper magnitude limits computed from each array separately indicate several time intervals where events with magnitudes greater that 2.0 may have occured at HC17, the network curve efficiently exclude all but two of these cases. The program allows us to expand the plots, so that interesting time intervals can be investigated. This is done in Figure 4, expanding Fig. 7.6.3 for a time interval around 12 GMT. The two interesting instances (called Event 1 and Event 2) are identified on the plot.

On Fig. 7.6.4 we see that the IMS has found events with origin times close to the peaks. By clicking on the V's with the mouse, the corresponding event location is sent to the map for display. Fig. 7.6.5 shows the map with

the locations of Event 1 and Event 2. Event 1 is in fact occuring at HC17, whereas Event 2 is located approximately 400 km further south.

These two events illustrate well some main features of the threshold monitoring technique, and we will comment upon them in some detail:

Event 1, located in the target region

In the case of Event 1, located at HC17, we note that this event was sufficiently large to have phase detections (both P and Lg) at all three arrays. The threshold monitor algorithm project the observations back to origin times at the target region, so with an event occuring at the target region, the corresponding peaks should line up for all four curves in Fig. 7.6.4. In addition, we expect the upper magnitude limits computed from each array separately, to approach the same value, provided that each array has peaks exceeding the background noise level. For Event 1, both of these features are clearly seen. In the IMS bulletin, the magnitude of the event is estimated to 1.6, whereas the Helsinki magnitude value is 2.2. This difference is attributed to different calibration factors, and it appears that the IMS in general gives lower magnitude values than Helsinki.

The network trace of Fig. 7.6.4 shows an "upper limit" value of 2.2 for Event 1. It is important to be aware that this value will be slightly underestimated (as a 90 per cent upper limit) in cases when several stations actually detect the event. The reason for this is the assumption that all observed phase magnitudes are less than or equal to the observed "*noise*" value. In case of phase detections acually attributed to the event, the term "less than or equal to" should be replaced by "equal to" for those phases, thus arriving at a standard maximum likelihood magnitude estimation formulation (Ringdal, 1976). In practice, this makes little difference for a network of the type we are considering, but it might become more significant for larger networks. We are currently looking into ways to correct for this bias.

Our conclusion from analyzing Event 1 is that an event actually occurring in the target region will have several readily identifiable features that can be used in visually confirming the event. The threshold monitor, when operated in conjunction with a network detector, will serve to point out such occurrences.

Event 2, located outside the target region

As seen from Fig. 7.6.4, the four peaks for Event 2 do not line up very well, indicating that the epicenter is not at the monitoring region. Note also that the upper magnitude limit inferred from the network of arrays is significantly smaller than the limits inferred from each array separately. From the map in Fig. 7.6.5, we see that the event is located well away from HC17. The

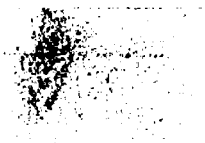

IMS bulletin report a magnitude of 2.6, while the Helsinki bulletin gives a magnitude value of 2.9. The upper magnitude limit for a hypothetical event at HC17 at the time considered is found to be between 1.9 and 2.0.

In this case, the upper limit represents a realistic 90 per cent confidence threshold for such a hypothetical event. Thus we note that the method serves to ensure that (at the given confidence level), a hypothetical event occurring at HC17 would be almost a magnitude unit smaller than the nearby interfering event.

An example of teleseismic monitoring

In an attempt to show the applicability of the threshold monitoring method to teleseismic distances, we have included the Shagan River test site as a target area (Fig. 7.6.6). The distances to the three arrays are in this case between 3400 and 4300 km. We know that the NORESS array has favorable signal focusing effects for P-phases from Shagan River, and that this will make NORESS the most valuable station for constraining the magnitudes. This is clearly illustrated in Fig. 7.6.7. The network upper magnitude limits are consistently below 3.5 for 02/02/90, and are only above 3.0 when interfering seismic signals are observed at NORESS.

We note that we do not have reliable magnitude calibration functions for FINESA at the present time, and the plots in Fig. 7.6.7 should therefore be interpreted with some caution.

Conclusions and future perspectives

The implementation of the threshold monitoring method in the IMS system has shown that the method can be used in real-time operation. The displays provided by the threshold monitor appear to be very valuable in pointing out time intervals of particular interest, thus aiding the analyst in his work. The interesting intervals can be examined by different processing techniques to locate and identify the events. Our examples have demonstrated that the method can be applied both at regional and teleseismic distances. We note however, that some additional research needs to be done to assess the potential bias in the upper magnitude limits when detected phases occur from events in the target region.

A natural extension of the implementation would be to include more arrays or single stations in the processing. This can be done in a straightforward manner, as the computing algorithm is fully parametrized. Larger geographical areas can be monitored if standard amplitude-distance relationships are used to derive the magnitudes. This will require careful positioning of the target points and some research on the tuning of the processing parameters.

Acknowlegements

This research was done while one of the authors (TK) was a visiting scientist at SAIC in San Diego. Jeff Given made an extensive contribution to this project through his cooperation and knowledge of the IMS.

T. Kværna
F. Ringdal

References

Bache, T.C., S.R. Bratt, J. Wang, R.M. Fung, C. Kobryn and J. Given(1990): The Intelligent Monitoring System, Acdepted for publication in *Bull. Seism. Soc. Am.*.

Fyen, J. (1990): Diurnal and seasonal variations in the microseismic noise level observed at the NORESS array. *Phys. Earth Planet. Int.*, in press.

Kværna, T. (1989): On exploitation of small-aperture NORESS type arrays for enhanced P-wave detectability. *Bull. Seism. Soc. Am.*, 79 888–900.

Kværna, T. (1990): Sources of short-term fluctuations in the seismic noise level at NORESS. *Phys. Earth Planet. Int.*, in press.

Ringdal, F. (1976). Maximum-likelihood estimation of seismic magnitude. *Bull. Seism. Soc. Am.*, 66, 789–802.

Ringdal, F. and T. Kværna (1989): A multichannel processing approach to real time network detection, phase association, and threshold monitoring. *Bull. Seism. Soc. Am.*, 79, 1927–1940.

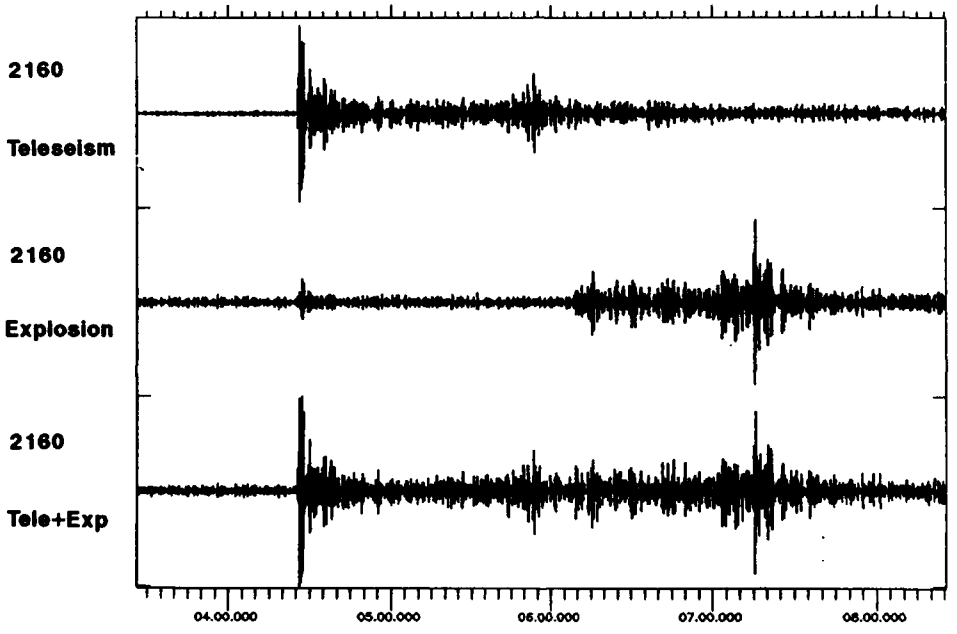

Fig. 7.6.1. Constructed example of a possible event interference, where a teleseismic P-phase is interfering with the Pn-phase of a regional event.

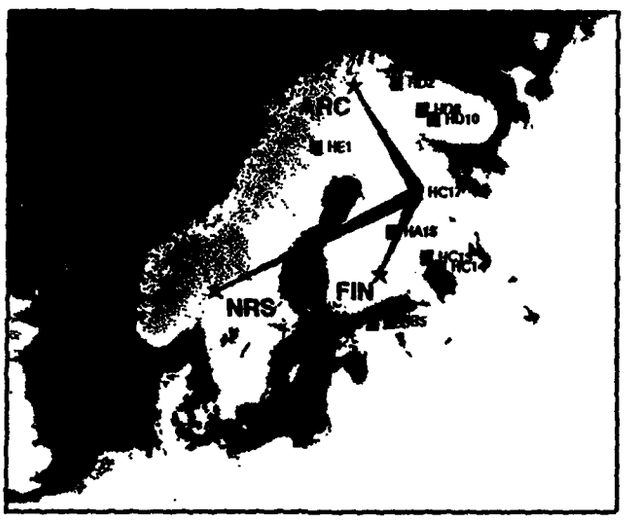

Fig. 7.6.2. The location of the mining regions subjected to threshold monitoring is shown by filled squares. The three regional arrays, NORESS, ARCESS and FINESA, are shown by stars. The filled sectors from each array to the mine HC17, serve to focus our interest to that particular mine location.

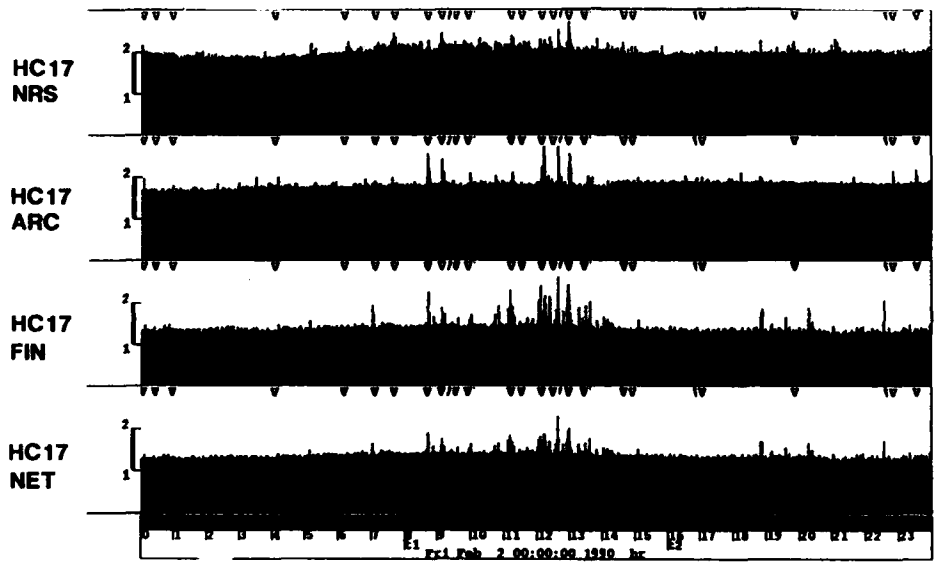

Fig. 7.6.3. The top three panels show the upper magnitude limits for mine HC17 for Friday 02/02/90, computed from the three regional arrays separately. The unit on the vertical axes is magnitude The lower panel shows the upper magnitude limit inferred from the network of arrays. The V's indicate origin times of events located by the IMS.

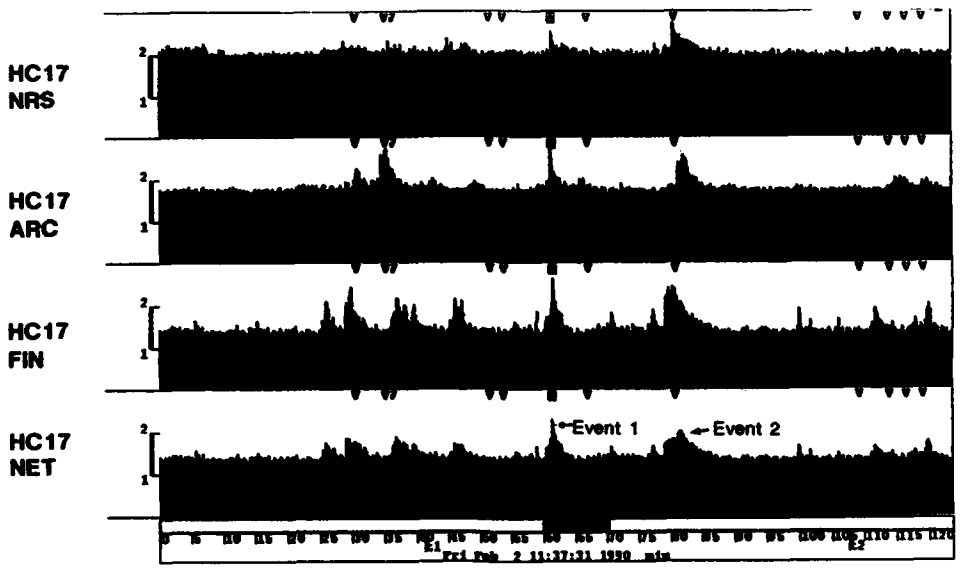

Fig. 7.6.4. This is a blowup of Fig. 7.6.3, with start time at 11.37.31. The length of the time interval is about 125 minutes. The two marked events are of special interest, since high upper magnitude limits are observed.

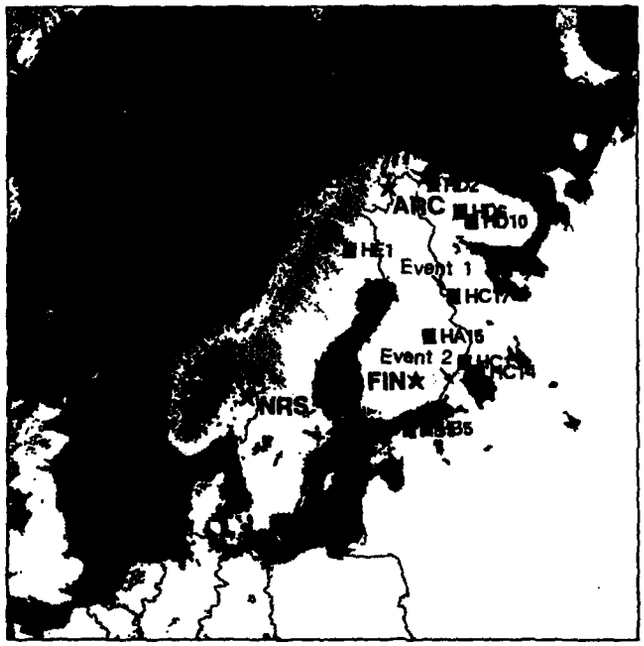

Fig. 7.6.5. Locations of the two events referred to in Fig. 7.6.4.

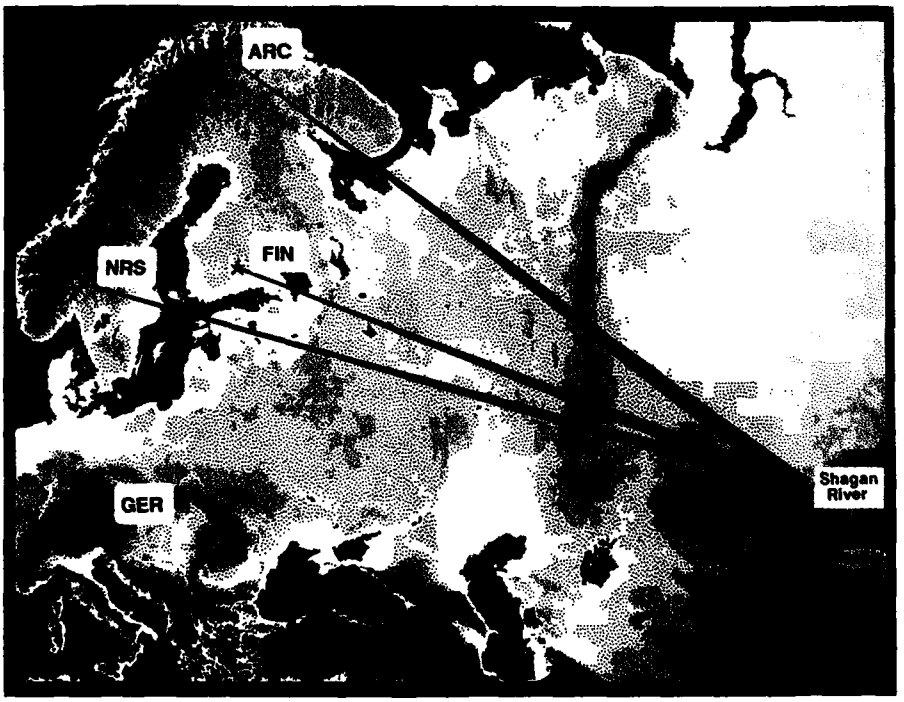

Fig. 7.6.6. This figure shows the location of the Shagan River test site, and also indicates the raypaths (approximated as straight lines) to NORESS, ARCESS and FINESA.

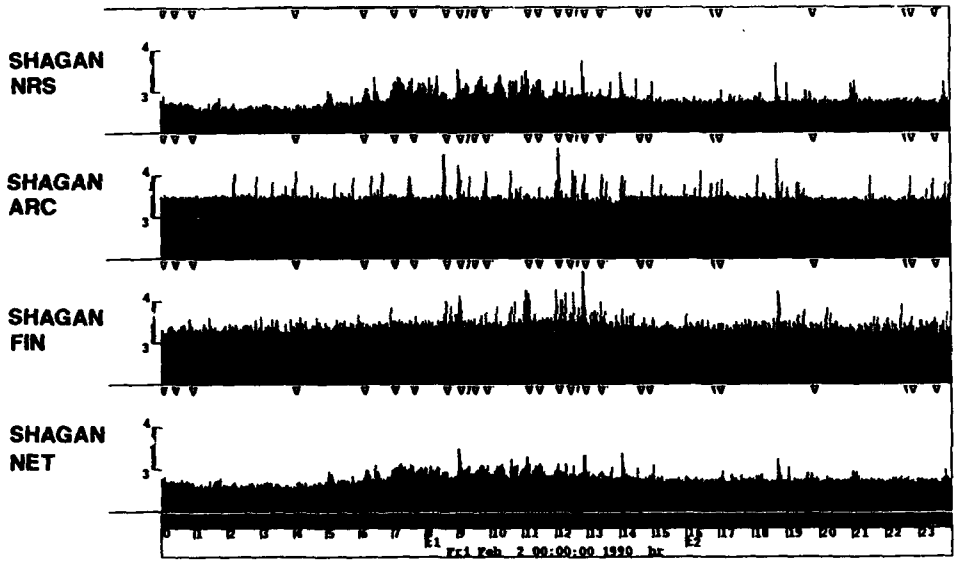

Fig. 7.6.7. Upper magnitude limits for the Shagan River test site for Friday 02/02/90. The panels are similar to those in Fig. 7.6.3, and the V's indicate origin times of events located by the IMS.